

Synthesis, Properties, and Reaction Behavior of Cobalt and Copper Organometallic Complexes with Chelating Ligands



TECHNISCHE
UNIVERSITÄT
DARMSTADT

Vom Fachbereich Chemie
der Technischen Universität Darmstadt

zur Erlangung des akademischen Grades eines

Doctor rerum naturalium (Dr. rer. nat.)

genehmigte
Dissertation

vorgelegt von

Baoxin Zhang, M.Sc.
aus Jinan

Referent: Prof. Dr. Jörg J. Schneider
Korreferent: Prof. Dr. Hans-Friedrich Klein
Tag der Einreichung: 11. März 2013
Tag der mündlichen Prüfung: 29. April 2013

Darmstadt 2013
D 17

Synthesis, Properties, and Reaction Behavior of Cobalt and Copper Organometallic
Complexes with Chelating Ligands

Vom Fachbereich Chemie der Technischen Universität Darmstadt

zur Erlangung des akademischen Grades eines

Doktors rerum naturalium (Dr. rer. nat.)

genehmigte Dissertation von M. Sc. Baoxin Zhang aus Jinan, V. R. China

1. Gutachten: Prof. Dr. Jörg J. Schneider

2. Gutachten: Prof. Dr. Hans-Friedrich Klein

Tag der Einreichung: 11. März 2013

Tag der mündlichen Prüfung: 29. April 2013

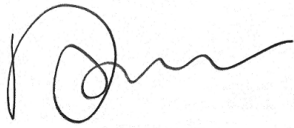
Darmstadt 2013

Die vorliegende Arbeit wurde am Eduard-Zintl-Institut für Anorganische und Physikalische Chemie der Technischen Universität Darmstadt unter der Leitung von Prof. Dr. Jörg J. Schneider in der Zeit von August 2008 bis Dezember 2012 erstellt.

Erklärung

Ich erkläre hiermit, daß ich meine Dissertation selbständig und nur mit den angegebenen Hilfsmitteln angefertigt habe.

Darmstadt, den 11. März 2013

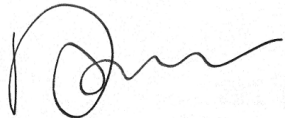


(B. Zhang)

Erklärung

Ich erkläre hiermit, noch keinen Promotionsversuch unternommen zu haben.

Darmstadt, den 11. März 2013



(B. Zhang)

to my dear parents
to my loving Xing

Contents

| | |
|--|-----------|
| I. Introduction | 14 |
| 1. Metal complexes with chelating ligands | 15 |
| 2. Poly(pyrazolyl)borate scorpionate ligands | 17 |
| 2.1. General description | 17 |
| 2.2. Nomenclature | 17 |
| 2.3. Coordinating features | 18 |
| 2.3.1. Different generations of Tp ^x ligands | 20 |
| 2.3.2. Cone angle of Tp ^x ligands | 20 |
| 2.3.3. Electron donating ability of Tp ^x ligands | 20 |
| 2.4. Applications | 21 |
| 2.4.1. Catalysis | 21 |
| 2.4.2. C-H bond activation | 23 |
| 2.4.3. Novel materials | 24 |
| 3. 2,5-Dihydroxy-1,4-benzoquinone metal complexes | 27 |
| 3.1. Oxidation states of 1,2-dioxolene and 1,2,4,5-tetraoxolene ligands | 27 |
| 3.2. Coordination modes of 2,5-dihydroxy-1,4-benzoquinone ligands | 29 |
| 3.3. Intramolecular electronic interaction of 2,5-dihydroxy-1,4-benzoquinone linked complexes | 29 |
| II. Objective and Aims | 33 |
| III. Results and Discussion | 35 |
| 4. Tris(pyrazolyl)borate Co complexes and their reactions | 36 |
| 4.1. Synthesis of cobalt tris(pyrazolyl)borate complexes | 36 |
| 4.1.1. Preparation of Potassium tris(pyrazolyl)borate (TpK) | 36 |
| 4.1.2. Synthesis of multinuclear bromo[tris(pyrazolyl)borato]cobalt com- plex | 38 |
| 4.1.2.1. IR investigation | 39 |

| | | |
|------------|---|------------|
| 4.1.2.2. | X-ray crystal structure determination | 40 |
| 4.1.2.3. | Discussion | 49 |
| 4.2. | Synthesis of cobalt tris(3,5-dimethyl-pyrazolyl)borate complexes | 51 |
| 4.2.1. | Synthesis of bromo[hydrotris(3,5-dimethyl-pyrazolyl)borato]cobalt | 52 |
| 4.2.1.1. | Spectroscopic characterization | 52 |
| 4.2.1.2. | X-ray crystal structure determination | 59 |
| 4.2.1.3. | Discussion | 66 |
| 4.2.2. | Reaction of bromo[tris(3,5-dimethyl-pyrazolyl)borato]cobalt with thiophenolate | 72 |
| 4.2.2.1. | IR spectroscopic investigation | 73 |
| 4.2.2.2. | X-ray crystal structure determination of (7) | 74 |
| 4.2.2.3. | Discussion | 75 |
| 4.2.3. | Reaction of bromo[tris(3,5-dimethyl-pyrazolyl)borato]cobalt with pyrazole | 77 |
| 4.2.3.1. | X-ray crystal structure determination | 79 |
| 4.2.3.2. | Spectroscopic characterization of complex (8) | 83 |
| 4.2.3.3. | Discussion | 84 |
| 5. | Linked multinuclear copper complexes | 86 |
| 5.1. | Synthesis of chloranilate bridged dinuclear copper complex | 86 |
| 5.1.1. | Preparation of [(dppf)Cu] ₂ (CA) | 87 |
| 5.1.2. | X-ray crystallographic determination of [(dppf)Cu] ₂ (CA) | 87 |
| 5.1.3. | IR spectroscopy of [(dppf)Cu] ₂ (CA) | 91 |
| 5.1.4. | NMR spectroscopy of [(dppf)Cu] ₂ (CA) | 91 |
| 5.1.5. | UV-vis spectroscopy of [(dppf)Cu] ₂ (CA) | 92 |
| 5.1.6. | Cyclic Voltammetry of [(dppf)Cu] ₂ (CA) | 94 |
| 5.1.7. | Discussion | 95 |
| 6. | Summary and conclusions | 103 |
| 6.1. | Complexes with tris(pyrazolyl)borate ligands | 103 |
| 6.2. | Cu(I) complex of the chloranilate dianion | 104 |
| IV. | Supplement | 106 |
| 7. | Experimental part | 107 |
| 7.1. | General description | 107 |
| 7.2. | Analytical methods | 107 |

| | |
|--|-----|
| 7.3. Preparation of starting materials | 108 |
| 7.3.1. Sodium 3,5-dimethylpyrazolide | 108 |
| 7.3.2. $[(\text{CH}_3\text{CN})_4\text{Cu}](\text{BF}_4)$ | 108 |
| 7.3.3. $[(\text{dppf})\text{Cu}(\text{NCCH}_3)_2](\text{BF}_4)$ | 108 |
| 7.4. Preparation of ligands | 108 |
| 7.4.1. Potassium hydrotris(pyrazolyl)borate (TpK) | 108 |
| 7.4.2. Potassium hydrotris(3,5-dimethyl-pyrazolyl)borate (Tp [*] K) | 109 |
| 7.5. Synthesis of new complexes | 109 |
| 7.5.1. $[\text{HB}(\text{pz})_3\text{Co}(\text{Hpz})]_2(\mu\text{-Br})_4\text{Co}$ (1) | 110 |
| 7.5.2. $\{[\text{HB}(\text{pz})_3]_2\text{Co}\}_2(\text{Co}_2\text{Br}_6)$ (2) | 111 |
| 7.5.3. $\text{HB}(\text{pz})_2(\text{Hpz})\text{CoBr}_2$ (3) | 113 |
| 7.5.4. $\text{HB}(3,5\text{-Me}_2\text{-pz})_3\text{CoBr}$ (4) | 114 |
| 7.5.5. $\text{HB}[(3,5\text{-Me}_2\text{-pz})_2\text{H}(3,5\text{-Me}_2\text{-pz})]\text{CoBr}_2$ (5) | 116 |
| 7.5.6. $\{[\text{HB}(3,5\text{-Me}_2\text{-pz})_3]_2\text{Co}\}[(3,5\text{-Me}_2\text{-pz})\text{CoBr}_3]$ (6) | 119 |
| 7.5.7. $\text{HB}(3,5\text{-Me}_2\text{-pz})_3\text{Co}(\text{SPh})$ (7) | 120 |
| 7.5.8. $[\text{HB}(3,5\text{-Me}_2\text{-pz})_3\text{Co}]_2(\mu\text{-pz})_2(\mu\text{-O}_2)$ (8) | 123 |
| 7.5.9. $(\text{dppf})_2\text{Cu}_2(\mu\text{-CA})$ (9) | 126 |

Nomenclature

| | |
|-------------------------|--|
| Δ | Ligand field splitting |
| δ | Chemical shift (NMR) and in-plane bending vibration (IR) |
| γ | Out-of-plane bending vibration |
| ν | Bond stretching vibration |
| <i>iPr</i> | Isopropyl |
| <i>ⁿBuLi</i> | n-Butyllithium |
| CA | Chloranilate |
| Cp | Cyclopentadienyl |
| CV | Cyclic voltammetry |
| DFT | Density functional theory |
| dhbq | 2,5-dihydroxyl-1,4-benzoquinone |
| DME | Dimethoxyethane |
| dppf | 1,1'-Bis(diphenylphosphino)ferrocene |
| EI-MS | Electron impact mass spectrometry |
| Et | Ethyl |
| et al. | et alia |
| EtOH | Ethanol |
| Fc | Ferrocene |
| h | hour |
| HOMO | Highest occupied molecular orbital |
| Hpz | Pyrazole |
| Hpz* | 3,5-Dimethyl-pyrazole |
| Hz | Hertz |
| i.e. | id est |
| IR | Infrared |
| KTp | Potassium tris(pyrazolyl)borate |

KTp* Potassium tris(3,5-dimethyl-pyrazolyl)borate

L Generalized ligand

LUMO Lowest unoccupied molecular orbital

M Generalized metal

m medium (IR); multiplet (NMR)

Me Methyl

MeCN Acetonitrile

min minute

MS Mass spectrometry

NMR Nuclear magnetic resonance

o ortho

Ph Phenyl

ppm parts per million

pz Pyrazolyl

pz* 3,5-Dimethyl-pyrazolyl

s strong (IR); singlet (NMR)

SOMO Singly occupied molecular orbital

THF Tetrahydrofuran

TMEDA N,N,N',N'-tetramethyl-1,2-ethylenediamine

TMS Tetramethylsilane

Tp Tris(pyrazolyl)borate

Tp* Tris(3,5-dimethyl-pyrazolyl)borate

UV Ultraviolet

V Volt

Vis Visible

vs very strong

w weak

Abstract

Several cobalt complexes with tripodal chelating ligands Tp and Tp* (Tp = tris(pyrazolyl)borate; Tp* = tris(3,5-dimethyl-pyrazolyl)borate) were synthesized by treating the homoscorpionates of the first generation with CoBr₂ under different conditions. These complexes were characterized with X-ray crystallographic determination as well as IR, NMR, MS, and UV-vis spectroscopies. Reaction of KTp with CoBr₂ in THF afforded an unprecedented trinuclear Co(II) complex [TpCo(Hpz)Br]₂(CoBr₂) (**1**) with Tp as terminal ligands, as well as an oxidized side-product (Tp₂Co)(Co₂Br₆) (**2**). The terminal Co(II) centers of (**1**) are octahedrally coordinated while the Co(II) in the bridging unit has a distorted tetrahedral geometry, holding a neighboring Co···Co distance of 3.472 Å. Reaction of KTp* with CoBr₂ afforded half-sandwich Tp*CoBr (**4**) with pseudotetrahedrally coordinated Co(II) center, which is accessible to other donors. Mononuclear Tp*CoSPh (**7**) and dinuclear (Tp*Co)₂O₂(pz)₂ (**8**) were prepared through ligand exchange reactions of LiSPh and Li(pz) with (**4**), respectively. (**8**) contains two octahedral Co(III) centers bridged by two pyrazolyl and a peroxide groups, in which the Co···Co distance is 3.591 Å.

Reaction of (dppf)Cu(NCMe) (dppf = 1,1'-bis(diphenylphosphino)ferrocene) with chloranilate dianion (CA²⁻) afforded tetranuclear complex (dppf)₂Cu₂(CA) (**9**). Single crystal X-ray diffraction revealed that the Cu(I) centers are coordinated by dppf and CA²⁻ in a distorted-tetrahedral manner. The two Cu(I) centers are located almost in the same plane of the bridging ligand with the Cu···Cu separation of 7.940 Å. In its UV-Vis spectrum, the π-π* and n-π* absorptions of CA²⁻ bridge are shown at 297.1 nm and 480.4 nm, respectively. Irreversible reduction waves were illustrated in the cyclic voltammogram of (**9**), which were attributed to an ECE process during the measurement.

Zusammenfassung

Diverse Kobaltkomplexe mit den tripodalen Chelatliganden Tp und Tp* (Tp = tris(pyrazolyl)borat; Tp* = tris(3,5-dimethyl-pyrazolyl)borat) wurden durch Umsetzung von Homoscorpionaten des ersten Generation mit CoBr₂ unter verschiedenen Bedingungen dargestellt. Diese Komplexe wurden sowohl kristallstrukturanalytisch als auch durch IR, NMR, MS, und UV-vis-Spektroskopie charakterisiert. In der Reaktion von KTp mit CoBr₂ in THF wurde der neue dreikernige Co(II)-Komplex [TpCo(Hpz)Br]₂(CoBr₂) (**1**) sowie das oxidierte Nebenprodukt (Tp₂Co)(Co₂Br₆) (**2**) erhalten. Während die terminalen Co(II)-Zentren in (**1**) oktaedrisch koordiniert sind, zeigt die verbrückende Co(II)-Einheit eine verzerrte tetraedrische Geometrie, wobei der Co···Co-Abstand 3.472 Å beträgt. In der Reaktion von KTp* mit CoBr₂ wurde dagegen der Halbsandwichkomplex Tp*CoBr (**4**) mit pseudotetraedrisch koordiniertem Co(II)-Zentrum erhalten, welches dem Angriff von anderen Donormolekülen zugänglich ist. So wurden der einkernige Komplex Tp*CoSPh (**7**) sowie der zweikernige Komplex (Tp*Co)₂O₂(pz)₂ (**8**) durch Ligandenaustauschreaktion von (**4**) mit LiSPh bzw. Li(pz) gebildet. (**8**) enthält zwei oktaedrisch koordinierte Co(III)-Zentren, die durch zwei Pyrazolyleinheiten und eine Peroxidgruppe verbrückt sind, wobei der Co···Co-Abstand 3.591 Å beträgt.

In der Reaktion von (dppf)Cu(NCMe) (dppf = 1,1'-bis(diphenylphosphino)ferrocen) mit dem Chloranilat-Dianion (CA²⁻) bildete sich der vierkernige Komplex (dppf)₂Cu₂(CA) (**9**). Eine Kristallstrukturanalyse zeigt, dass die Cu(I)-Zentren in (**9**) durch dppf und CA²⁻ verzerrt-tetraedrisch koordiniert sind. Die beiden Cu(I)-Zentren befinden sich nahezu in der Ebene des verbrückenden CA-Ligands, wobei der Cu···Cu-Abstand 7.940 Å beträgt. Im UV-vis-Spektrum wurden die den π – π* und n – π*-Übergängen der CA²⁻-Brücke zugeordneten Absorptionsmaxima bei 297.1 nm bzw. 480.4 nm registriert. Eine cyclovoltammetrische Analyse von (**9**) ergab lediglich irreversible Reduktionswellen, die ECE-Prozessen zugeordnet wurden.

Acknowledgments

I really appreciate **Prof. Dr. Jörg J. Schneider** for offering me the opportunity to work in his excellent group, who has kept enlightening me on my scientific researches with his sagacious instructions and constant inspirations in the last four years, especially for his helpful and constructive suggestions about the work in this thesis, from which I've gained invaluable knowledge and experience far beyond the scope of chemistry.

I'm extremely grateful to my dear friend and great teacher **Dr. Mathias Nowotny** for his patient and meticulous directions for the experimental work and instructive discussions with me on all the scientific problems I encountered, who is not only an outstanding advisor in the lab, but also an admirable chemist and a trustable friend. Without him this work wouldn't be finished.

I would like to express my profound gratitude to **Prof. Dr. Hans-Friedrich Klein**, for his kind revision of this piece of work, and the very irradiative remarks about the project during our discussion.

Special thanks are addressed to my dear friend **Dr. Jörg Engstler**, for his brilliant laboratorial management and technical support for all the instruments in the group that are essential to every result from my research; and to **Dipl.-Ing. Ildiko Balog** for her elaborate analytical work in NMR spectroscopy. I really appreciate **Prof. Dr. Christian W. Lehmann** and his colleagues from Max-Planck-Institut für Kohlenforschung in Mülheim an der Ruhr for the scrupulous measurement and analysis in the X-ray crystallography determination; and I would also like to thank **Ms. Sabine Foro** for her splendid contribution in the X-ray crystal structure analysis for this dissertation, and my excellent colleagues and good friends in the group: **Hermann Tempel, Dr. Ravi Joshi, Dr. Alexander Popp, Silvio Heinschke, Thorsten Heinlein, Deepu Babu, Emine Kayhan, Meike Naumann, Thobias Wombacher, Xiaoxiao Du, Dr. Mikhail Pashchanka, Sandeep Yadav, Julia Patzsch, and Shawn Sanctis**. The time I spent to work together with them will always be one of the most precious treasures in my life.

Finally, I thank my loving parents and wife for their incessant support during my stay in Germany, who are the reason I keep going forward for.

Part I.

Introduction

1 Metal complexes with chelating ligands

Coordination compounds, in which metal ions are bonded to organic frameworks, have been attracting great research interest recently along with increasing demands for new materials and biological studies. Due to rich electronic and magnetic properties of transition metals, which are crucial elements in consideration of designing modern functional materials, developing new structures of transition metal complexes with various functional organic ligands as well as determination of their unique electronic and/or magnetic behaviors within molecules have drawn more and more attentions in modern chemistry and materials research. Especially in the area of information technology, people are always seeking devices as small as possible in order to keep step with the explosive increase of information every day, so that developing new materials comprised of metal complexes which allows scientists to control the electronic and/or magnetic properties in molecular level is of particular importance that becomes nowadays a very popular research subject for chemists. For this purpose chelating ligands play an important role in developing process of novel functional metal complexes, because a larger molecular orbital overlap between neighboring metal ions and ligands could not only increase the coordinative stability, but also enable sufficient electronic and magnetic interactions among ligands and metal ions. Moreover, progress in bioinorganic chemistry has demonstrated that chelating metal complexes are essential to life process as they are included into a lot of proteins which are responsible for many important biochemical reactions.

Chelating ligands, especially those maintaining large valence electron conjugation, are suitable linkers or backbones for multinuclear complexes of mixed-valency. Since the discovery of Creutz-Taube ion [22], which is a pyrazine linked dinuclear ruthenium complex exhibiting unequivalent oxidation states of the metal centers, the research about mixed-valence complexes has become a very significant topic in inorganic chemistry. Two identical metal centers of the same chemical environment in a molecule could present different oxidation states if sufficient electronic interactions are enabled by large electron orbital delocalization within the molecule. The deviation in oxidation states from each of the metal ions to another results in different redox potentials of the two centers (Figure 1.1), and the stability of a mixed-valence species depends on

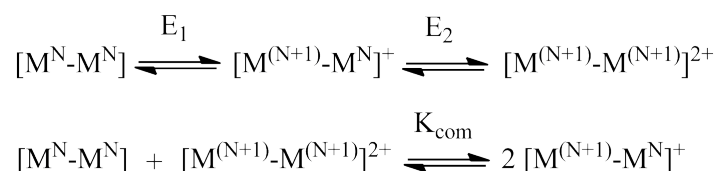


Figure 1.1.: Redox splitting of a mixed-valence compound.

the splitting of the two redox potentials that relates to the equilibrium constant of a comproportionation reaction (Equation 1.1).

$$RT \ln K_{com} = nF \Delta E \quad (1.1)$$

with $\Delta E = E_2 - E_1$. Applications of mixed-valence species are related to their intrinsic electronic properties that are determined by the extent of electron delocalization within each molecular framework. According to the Robin-Day classification [89], mixed-valence compounds are classified as follows:

Class I There is no electron delocalization within a bimetallic molecule; valence states of metals are trapped on a single site, and interactions of electrons from separated metal ions are obstructed by a such high level of energy that any communication is impossible.

Class II The energy barrier for moving of electrons from one site to another is lower than that in the class I compounds. Therefore, electronic interactions between metal centers can be triggered by appropriate activation energies introduced through e.g. thermal or UV-vis radiation. This brings about intense intervalence charge transfer.

Class III Electrons charge transfer within molecules are completely delocalized and the mixed valence states are indistinguishable by spectroscopic methods. This situation is often observed in complexes with ligands that contain highly conjugated electronic situations.

Compounds of class II and class III are of particular importance to development of molecular devices and new materials.

2 Poly(pyrazolyl)borate scorpionate ligands

2.1 General description

In 1966, S. Trofimenko (Central Research Department, DuPont Company) discovered and reported a new kind of ligands, in which more than one pyrazole rings are incorporated in one borane molecule via B-N bond and another nitrogen atom of pyrazole can offer an electron lone pair to the vacant orbital of metal ions. The construction of this ligand can be considered in a way that the hydrogen atoms of a boron hydride molecule are substituted by different pyrazolyl rings (Figure 2.1) to form a chelating ligand having multi-coordinating sites.

For this new kind of ligands the name “scorpionate” has been coined in consideration of the coordination mode which is just like a scorpion whose nippers are two nitrogens on each pyrazolyl ring clamping the metal ion and the third donor rotates forward above the ion ready to “sting” it as a scorpion tail (Figure 2.2). The scorpionate type ligands can coordinate to metal in either mono, bi or tri-dentate manner depending on the number of pyrazolyl substituents on boron atom and the coordination properties of metal ions. In the most common tripodal mode, a boron atom bears three pyrazolyl rings, of which the nitrogen atoms coordinate exclusively three facial sites of the metal that is usually referred to an analogue of the well-known cyclopentadienyl (Cp^x) ligands.

2.2 Nomenclature

Besides the well-known Tp [Hydrotris(pyrazolyl)borate] and Tp^* [Hydrotris(3,5-dimethylpyrazolyl)borate] abbreviations proposed by Curtis et. al., [25, 26] along with the development of the scorpionate chemistry, scientists have applied a special nomenclature

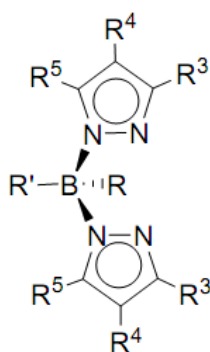


Figure 2.1.: General structure of poly(pyrazolyl)borate ligands. [85]

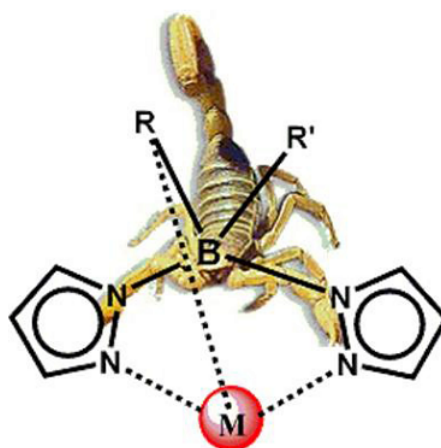


Figure 2.2.: The "Scorpionate". [85]

system for the polypyrazolylborate compounds in order to simplify the complexity of describing the usually long name, which has however already been accepted by chemists.

1. Any substitute in the 3-position of the pyrazolyl ring is denoted as a superscript of *Tp*. For example, hydrotris(3-*t*-butyl-pyrazolyl)borate is written as Tp^{tBu} .
2. Substitute in the 5-position besides the 3-substituent of the pyrazolyl ring is denoted by a superscript followed that of the 3-substitution and separated with a comma. So $Tp^{tBu,Me}$ is hydrotris(3-*t*-butyl-5-methyl-pyrazolyl)borate.
3. When the 3- and 5-substituents are identical the ligand is denoted by Tp^{R_2} .
4. The 4-substituent *R* of the pyrazolyl ring is represented by Tp^{4R} . For instance hydrotris(4-bromo-pyrazolyl)borate is written by Tp^{4Br} .
5. If the pyrazolyl ring is substituted in all the 3,4,5-position, their superscripts are separated with a comma in a sequence of 3-, 4-, and 5-substitution. Thus hydrotris(3-phenyl-4-Br-5-methyl)borate is $Tp^{Ph,4Br,Me}$.
6. The substitute on boron is presented preceding *Tp*. For instance phenyltris(3-isopropyl-pyrazolyl)borate is denoted by $PhTp^{iPr}$.

2.3 Coordinating features

For the structure shown in Figure 2.1, the boron atom is bonded to two identical pyrazolyl rings with various substitutes in the 3-, 4- and 5-position; and *R* and *R'* could be H, alkyl, aryl, and pyrazolyl group. A wide variety of substitutes allows the ligand to offer large structural flexibility that could affect its electronic, coordinating, and stereochemical properties causing this kind of compounds to have the potential of versatile applications in both practical and theoretical fields. The tunable structural features result in different coordinating behavior of the ligand. The ligand can coordinate to the

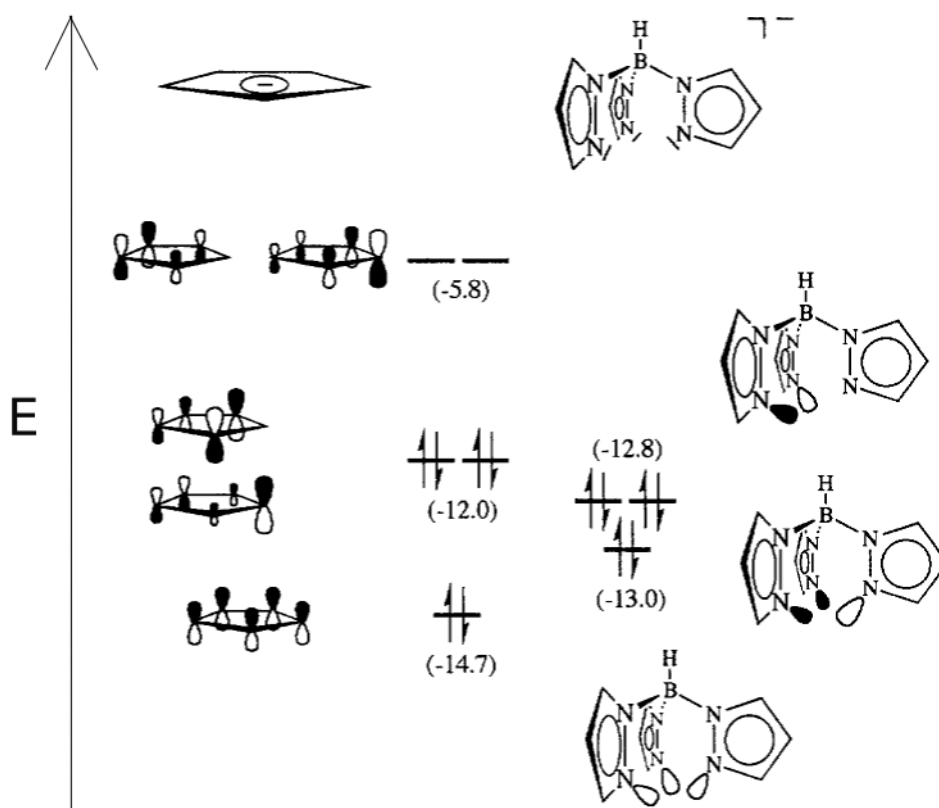


Figure 2.3.: Frontier orbital diagrams of Cp and Tp . (Energies in eV) [55]

metal in mono, bi, and tridentate modes depending on the properties of metals and the reaction conditions. In general, one calls the scorpionate ligands with R' identical to the other two pyrazolyl groups homoscorpionates, which are of great emphasis in this thesis; and those with R' different from the two pyrazolyl groups, heteroscorpionates.

The homoscorpionates, namely hydrotris(pyrazolyl)borates, are tripodal chelating ligands that coordinate three facial sites of a metal's coordination sphere, just like the cyclopentadienyl anions that bear one negative charge. However, they are two different types of ligands since they have disparate bonding natures: Tp^x is a σ -type ligand in which each nitrogen of pyrazole provides an electron lone pair to the metal center, while Cp^x is a soft π -donor ligand that could be much more easily polarized. That makes a considerable different behavior of scorpionates in affecting coordination geometry, molecular conformation, and electronic properties of the resulting complexes from that of cyclopentadienyl ligands. The frontier orbital diagram of the two classes of uni-negative ligand (Figure 2.3) shows that their occupied molecular orbitals have a similar energetic structure and symmetry as the Cp^x ligand but the σ -donating Tp ligand lacks empty π -acceptor orbitals which are available in the π -delocalized Cp ligand. [55] Moreover, including substitution on boron, Tp^x has in total ten positions allowing modifications of its steric and electronic properties while Cp^x has only five. And only R_5Cp type ligand can retain its original D_{5h} symmetry of Cp , whereas Tp^x has

more possibilities of substitution to leave its original C_{3v} symmetry unchanged such as Tp^{R_2} , Tp^R , Tp^{4R} , and RTp .

2.3.1 Different generations of Tp^x ligands

According to substituents on the pyrazolyl ring and boron, Tp^x ligands have been developed into three generations so far:

- First generation: hydrotris(pyrazolyl)borate (Tp) and hydrotris(3,5-dimethyl-pyrazolyl)borate (Tp^*).
 - Second generation: Tp^x with other bulky substitutes on pyrazolyl rings, for example $x = iPr, Ph, t-Bu, Br, Cl$, etc.
 - Third generation: substituents on boron atom, e.g. functional groups on the back side of Tp^x , for example $FcTp, PhTp$, etc.
-

2.3.2 Cone angle of Tp^x ligands

The cone angle is introduced to describe the size of a chelating ligand referring to its steric effects on the complex structure and the metal coordination trend. [105] For Tp^x ligands, it is defined by the solid angle of a cone of which the metal is on the vertex and the outermost hydrogen atoms of the substitutes in the pyrazolyl 3-position of Tp^x are on the perimeter taking into account their van der Waals radii. A large cone angle represents a highly space-demanding ligand which requires greater steric restriction while coordinating metal ions. This plays an important role in determining the final geometry of the complex and the coordination number of the metal center. Tp^x ligands with small cone angle, such as Tp and Tp^* , have a strong tendency toward the formation of Tp_2^xM complexes with a octahedrally coordinated metal ion, whereas those with large cone angle, for example Tp^{tBu} , prefer forming Tp^xML species in which the metal ion has a tetrahedral or pseudotetrahedral coordination geometry. The cone angles of some common Tp^x ligands are listed in Table 2.1.

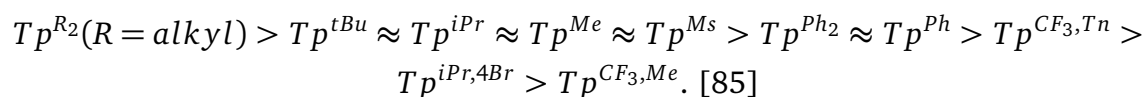
2.3.3 Electron donating ability of Tp^x ligands

The versatility of poly(pyrazolyl)borate ligand is manifested by its tunable structure in which amounts of functional groups can be introduced either on the pyrazolyl ring or the boron atom. These groups affect the properties of metal complexes such as reactivity and coordination geometry of their coordinated metal centers, solubility

| Complex | Cone angle | Wedge angle |
|--|------------|-------------|
| Tp | 183 | 70 |
| Tp ^{Cpr} | 223 | 68 |
| Tp ^{Cbu} | 234 | 51 |
| Tp ^{Br₃} | 234 | 60 |
| Tp ^{4Bo,3Me} | 235 | 68 |
| Tp ^{(CF₃)₂} | 237 | 49 |
| Tp [*] | 239 | 67 |
| Tp ^{<i>i</i>Pr,4Br} | 243 | 28 |
| Tp ^{<i>t</i>Bu,Me} | 243 | 31 |
| Tp ^{<i>t</i>Bu} | 251 | 29 |
| Tp ^{Cpe} | 253 | 46 |
| Tp ^{Cy,4Br} | 273 | 46 |
| Tp ^{3Bo,7<i>t</i>Bu} | 277 | 33 |
| Tp ^{Cy} | 281 | 53 |

Table 2.1.: Cone and wedge angles of common Tp^x ligands. [55]

towards organic solvents, as well as their electronic and magnetic properties. [85] Electronic properties of ligands related to electron donating/releasing ability of substituents are of great importance as they decide predominately the coordination environment of metal centers, which calls for a demand for a reliable electron donating sequence of various functional groups on Tp ligands. Kitajima and Tolman [63] described a way to discover this property by measuring CO vibration frequencies ν_{CO} for a series of metal-carbonyl $Tp^xM(CO)_nL$ complexes that only differ in their pyrazolyl substituents, such as $Tp^xCu(CO)$ [74, 62, 94, 12], $(\eta^2 - Tp^x)Rh(CO)_2$ [88], and $Tp^xMo(CO)_2(NO)$ [110, 109, 87]. Higher carbonyl stretching frequencies indicate lower electron density at the metal center, meaning that the substituents have less electron donating property. Thus a trend in electron donating ability for common Tp^x ligands has been derived:



2.4 Applications

2.4.1 Catalysis

Tris(pyrazolyl)borates are widely used for development of homogeneous catalysts because of their highly adaptable chelating ability and superb structural flexibility al-

lowing modification of various ligand positions to satisfy a specific steric and electronic requirement. Especially in the field of homo-catalyzed olefin polymerization and oligomerization, Tp^x complexes sometimes demonstrate better catalytic performance than organometallic Cp^x complexes if the activity of the latter is encumbered under certain circumstances. [8, 9, 117, 69, 58, 95, 98, 79, 32] Some lanthanide catalytic systems have proven to display advantages over their transition-metal analogues such as high stereo-selectivity, activity over wide temperature ranges, and lack of decomposition reactions. Long and Bianconi synthesized several Tp^* supported yttrium complexes $Tp^*YR_2(THF)_x$ ($R = Ph, CH_2SiMe_3$), which were found to be active in the catalytic polymerization of ethylene to linear, extremely high molecular weight polymers. [69] Tris(pyrazolyl)borates are also attractive candidates for ancillary ligands in catalytic systems containing early transition metal complexes, for their stable chelation to the metals as well as diverse variations on the pyrazolyl 3- and 5-substituents. The efficiency of catalysis is intensely concerned with substitutions of Tp^x . It is reported that some Tp^xTiCl_3/MAO catalysts with simple Tp and Tp^* ligands exhibit poor activity and produce polymers with broad molecular weight distribution doing ethylene polymerization; [81] however, a bulky substituted $HB(3\text{-mesitylpyrazolyl})_2(5\text{-mesitylpyrazolyl})^-$ (Tp^{Ms*}) and a supported $Tp^{Ms*}TiCl_3/MAO$ system have shown a high activity in linear polyethylene formation. [79] A similar trend of catalytic activities for phenylacetylene polymerization of a series of rhodium(I) complexes $Tp^{R2}Rh(cod)$ ($R = Me, Ph, i\text{-Pr}$) was discovered by Katayama et al., [58] who found that this kind of complexes could serve as effective catalyst for highly stereo-regular polymerization of phenylacetylene derivatives, and that with the most sterically demanding substituent ($i\text{-Pr}$), the Rh(I) complex exhibited the highest activity. This phenomenon was attributed to the preference of bulky substituents at the pyrazolyl 3-positions, for forming the κ^2 -isomer, which is one of the isomers in the $\kappa^2 - \kappa^3$ isomerism of $Tp^{R2}Rh(cod)$ (Figure 2.4). The κ^2 -isomer was believed to be vital for the catalytic reaction. These rhodium complexes with Tp and Tp^* ligands are also essential for catalyzing regioselective quinoline hydrogenation. [2] A molybdenum imido alkylidene complex stabilized by Tp , $TpMo(CHCMe_2Ph)(NAr)(OTf)$, and its alkylated derivative $TpMo(CHCMe_2Ph)(NAr)(CH_3)$, were able to catalyze the ring-opening metathesis polymerization (ROMP) of cyclooctene and norbornene and the oligomerization of 1,9-decadiene via acyclic diene metathesis polymerization (ADMET) in the presence of $AlCl_3$ [117]; and the air-stable high-valent tungsten analogues $Tp^*W(=CHCMe_3)(O)Cl$ and $TpW(=CHCMe_2Ph)(NAr)(OTf)$ could serve as precursors to ADMET and ROMP, respectively. [8, 9] Some ruthenium scorpionate compounds are also efficient in catalyzing olefin metathesis reactions. For example, $Tp(PCy_3)(Cl)Ru = CHPh$ was very active for olefin ring-closing metathesis if HCl,

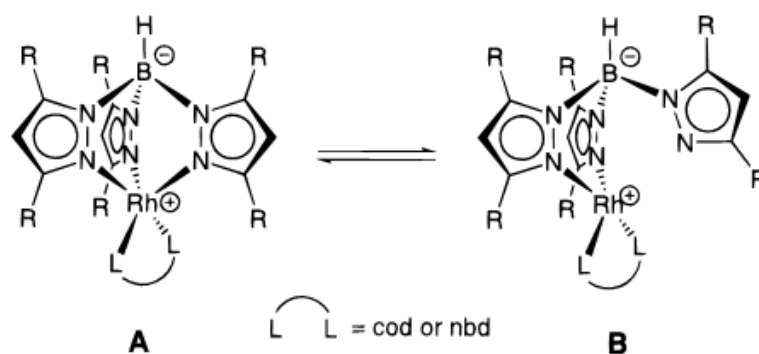


Figure 2.4.: $\kappa^3 - \kappa^2$ isomerism of $Tp^{R^2}Rh(cod)$. A: coordinatively saturated κ^3 form; B: coordinatively unsaturated κ^2 form. [58]

CuCl, and AlCl₃ were added as co-catalyst. [95] Stereo-selective cyclopropanation of α -olefins with ethyl diazoacetate could be realized under the condition that the copper(I) homoscorpionate catalyst $Tp^x Cu$ was generated in situ, during which the dipodal coordinating form of Tp^x played a substantial role in controlling the diastereoselectivity, as kinetic studies revealed. [32]

2.4.2 C-H bond activation

Mononuclear transition metal complexes supported by tris(pyrazolyl)borates often participate in stoichiometric and catalytic transformations of organic molecules. Especially in alkyne insertion reactions relating to acetylene and its substituted derivatives, some half-sandwich Tp complexes tend to activate the aliphatic $C - H$ bond through forming vinylidene metal complexes, which are crucial intermediates in these coupling reactions [99, 98] The significance of cyclopentadienyl vinylidene ruthenium complex for initiating carbon-carbon coupling in the condensation of terminal alkynes and allylic alcohols has been demonstrated by Trost et al. [112, 113, 114]; the organometallic intermediate was found to be vital for new bond forming and directing the stereoselectivity in this reaction. Analogously, neutral ruthenium complexes $TpRu(cod)Cl$, $TpRu(tmeda)Cl$, and $TpRu(py)_2Cl$ were able to catalyze the selective addition of benzoic acid to the terminal carbon atom of phenylacetylene, producing exclusively E- and Z-vinylesters in a certain stoichiometric ratio. A vinylidene-ruthenium intermediate was considered to play an important role in the $C - H$ bond activation and stereochemical regulation [42]. Such a Tp supported vinylidene metal complex was even isolated from a coupling reaction of terminal acetylenes with a coordinated P, N-ligand, featuring $C - H$ activation of a $-CH_2 - CH_2-$ group with concomitant $C - N$ bond cleavage [99]. The transformation of transition metal ethylene complexes into their hydride-vinyl isomers is one of the key processes involving $C - H$ bond activations inside

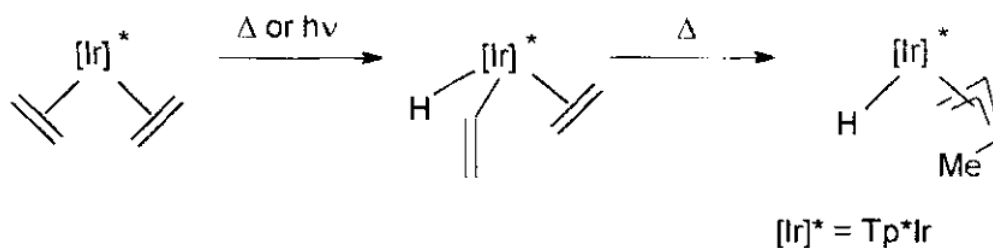


Figure 2.5.: Rearrangement of bis(ethylene) $[\text{Tp}^*\text{Ir}]$ complex. [1]

TpM moieties. This process could sometimes be triggered thermally and photochemically. Rearrangement of the bis(ethylene) complex $\text{Tp}^*\text{Ir}(\text{C}_2\text{H}_4)_2$ via the hydrido-vinyl form $\text{Tp}^*\text{IrH}(\text{C}_2\text{H}_3)(\text{C}_2\text{H}_4)$ finally to the hydrido-allyl complex $\text{Tp}^*\text{IrH}(\eta^3\text{-C}_3\text{H}_4\text{Me})$ took place under heating or irradiation in an experiment carried out in Alvarado's laboratory (Figure 2.5); the ethylene dimerization proceeded through sequential $\text{C} - \text{H}$ bond activation of the coordinated olefin and $\text{C} - \text{C}$ coupling between the resulting vinyl and ethylene moieties. [1] Similarly, under daylight or tungsten illumination, the rhodium complex $\text{Tp}^*\text{Rh}(\text{CO})_2$ was able to activate aromatic and saturated hydrocarbons at room temperature, generating $\text{Tp}^*\text{RhH}(\text{CO})\text{R}$ ($\text{R} = \text{Ph}, \text{Me}, \text{cyclohexyl}$) with high thermodynamic selectivity. [44] A hydrocarbon amination reaction involving the insertion of a nitrene group into aliphatic and aromatic $\text{C} - \text{H}$ bonds was reported to be initiated with $\text{Tp}^{\text{Br}3}\text{Cu}(\text{NCMe})$ in moderate to high yield. [31]

2.4.3 Novel materials

The possibility of modification on the boron site of tris(pyrazolyl)borates facilitates the development of oligonuclear coordinative aggregates and metal containing polymers if another coordinative entry is introduced by proper functional groups and thus becomes accessible on the boron center besides the tris-pyrazolyl donors of Tp^x moiety. For example, 1,1'-ferrocenediyl is able to combine two discrete Tp^x moieties into a bifunctional chelating reagent through substituting the hydrogen on boron of Tp^x with one of its Cp rings, respectively. The geometrically flexible cyclopentadienyl ring of the ferrocenediyl linker as well as its reversible redox activity enable this kind of ligand to be appropriate backbone for organometallic oligomers containing multiple metal centers, which were obtained in Wagner's laboratory [54, 34] (Figure 2.6). Developed from this idea, bifunctional cymantrenyl scorpionates and trifunctional cymantrenediyl-bridged scorpionates were successively prepared where two classes of coordinative ligands of different natures, cyclopentadienyl and tris(pyrazolyl)borates, were incorporated within one molecule [52, 65] (Figure 2.7). All these ligands and their resultant multinuclear complexes are ideal building blocks for metal containing oligomers

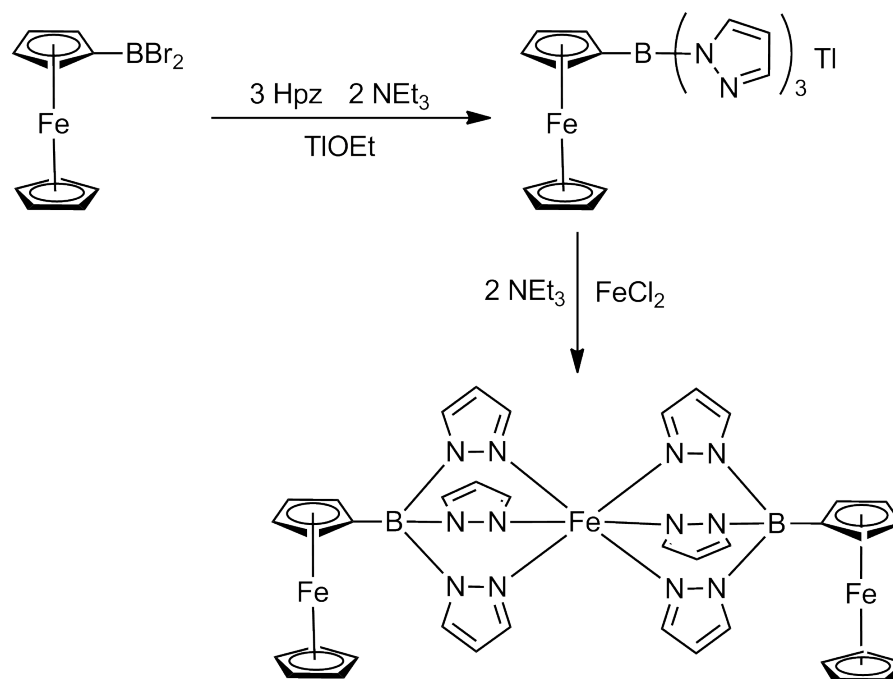


Figure 2.6.: Synthesis of the trinuclear Fe complex containing ferrocenyl tris(pyrazolyl)borate (FcTp) ligand [54].

and polymers that are of huge interest for novel materials. Moreover, mononuclear Tp-based complexes were found to be of remarkable importance in modern material science researching. For instance, lanthanide(III) monoporphyrate complexes stabilized by tris(pyrazolyl)borate with near-IR photoluminescent property prepared by Foley et al. [35], $TpLn(TPP)$ ($TPP = 5,10,15,20$ -tetraphenylporphyrinate), are suitable for molecules incorporated in the active layer of polymer light-emitting diodes (PLEDs) (Figure 2.8).

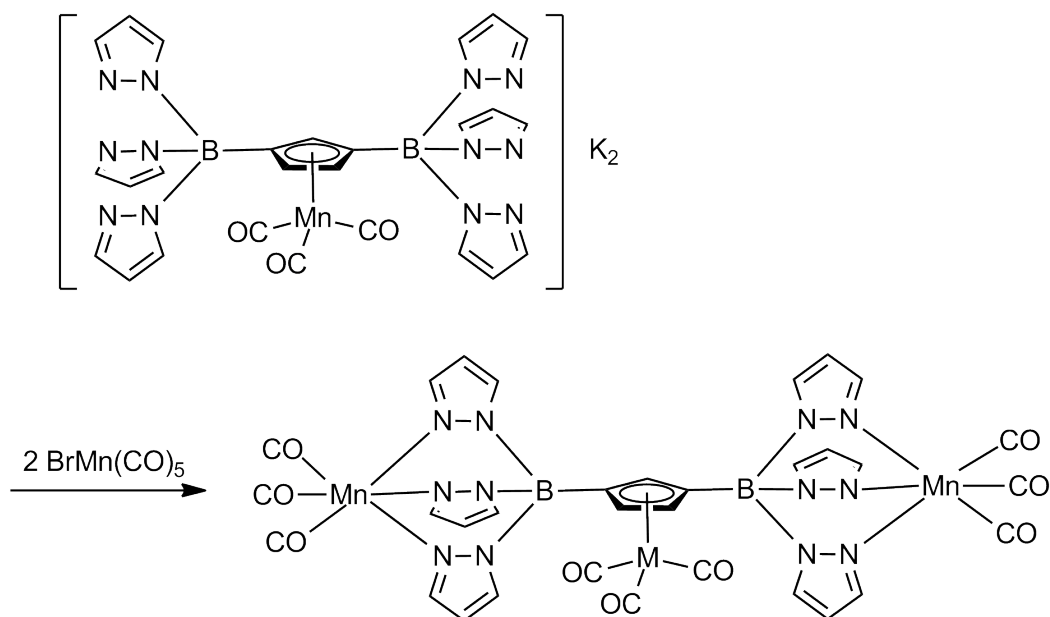


Figure 2.7.: Synthesis of a trifunctional cymantrenediyl-bridged trinuclear Mn complex with binding scorpionate ligands [65].

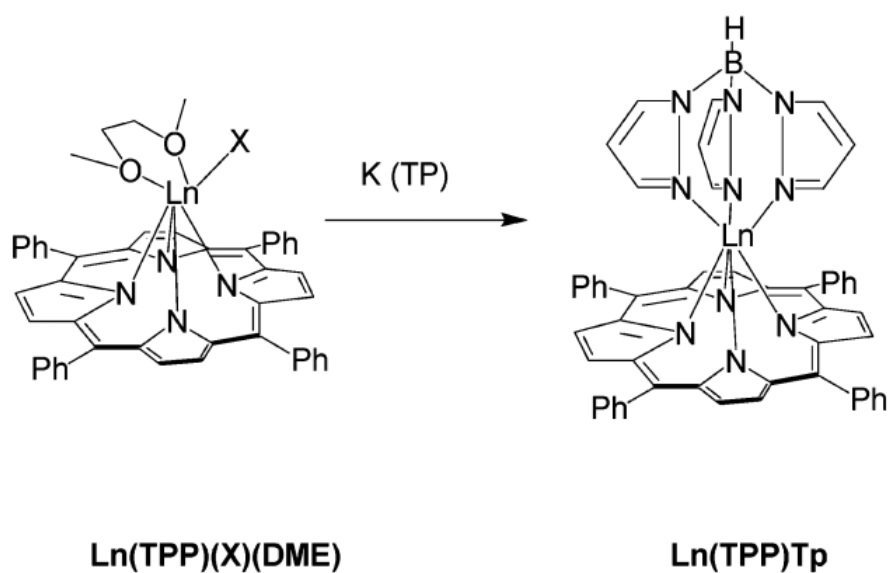


Figure 2.8.: $TpLn(TPP)$ ($TPP = 5,10,15,20$ -tetraphenylporphyrinate) [35].

3 2,5-Dihydroxy-1,4-benzoquinone metal complexes

Metal-quinone coordination compounds have become more and more noteworthy in inorganic chemistry research because of their interesting redox non-innocent property of ligand. [75] In quinoid metal coordination compounds, the ligand itself is redox active obtaining different electronic structures which allows interactions of unpaired electron in the metal d-orbital with ligand electrons in various modes to realize different electronic and magnetic communications. Quinone molecules can coordinate to metal ions in a variety of modes due to more than one coordination sites accessible for the metal ion. This often allows to form attendant hydrogen bonds to build supermolecular frameworks. The possibility of chemically controlling the oxidation state of the quinone ligand and the structural morphology of the corresponding compounds allows to manipulate specific electronic, magnetic, and optic properties of materials based on these metal-quinone complexes, which is the principal concept of molecular engineering in modern material science exploration.

3.1 Oxidation states of 1,2-dioxolene and 1,2,4,5-tetraoxolene ligands

An o-dioxolene metal complex has three degenerate states arising from three different redox states of the ligand, corresponding to catecholate (cat), semiquinone (sq), and quinone (q) (Figure 3.1). [30] The electron distribution depends on the nature of metal ion and environmental conditions such as temperature, solvent, pH etc.. [30] For a o-dioxolene complex with the same metal ion, delicate treatment of the compound would allow for a control of each state, bringing about a switching effect on the quinone ligand and a proper change in the oxidation state of the coordinated metal. Due to large charge delocalization above and below the molecular plane of the benzoquinone ligand, this kind of ligand is well appropriate as linker for multinuclear compounds in which communication between different metal centers could be studied. Thus dinuclear complexes with 2,5-dihydroxyl-1,4-benzoquinone as bridge and their derivatives have been extensively studied over the past 20 years. Like o-dioxolene ligands, tetraoxolenes are also redox active and, for the extended structure, obtain five states bearing different amount of valence electrons, which are illustrated in Figure 3.2 together with their resonance structures. [45]

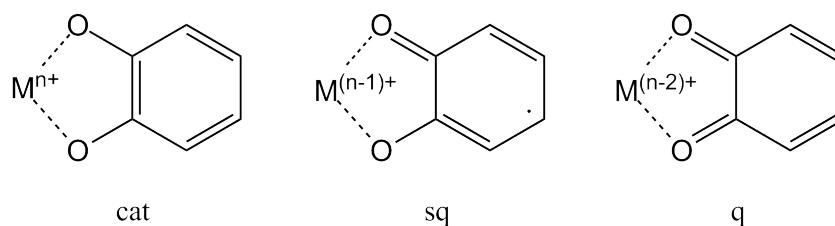


Figure 3.1.: Tautomers of o-dioxolene metal complexes, where the abbreviations “cat”, “sq”, and “q” represent catecholate, semiquinone, and quinone, respectively.

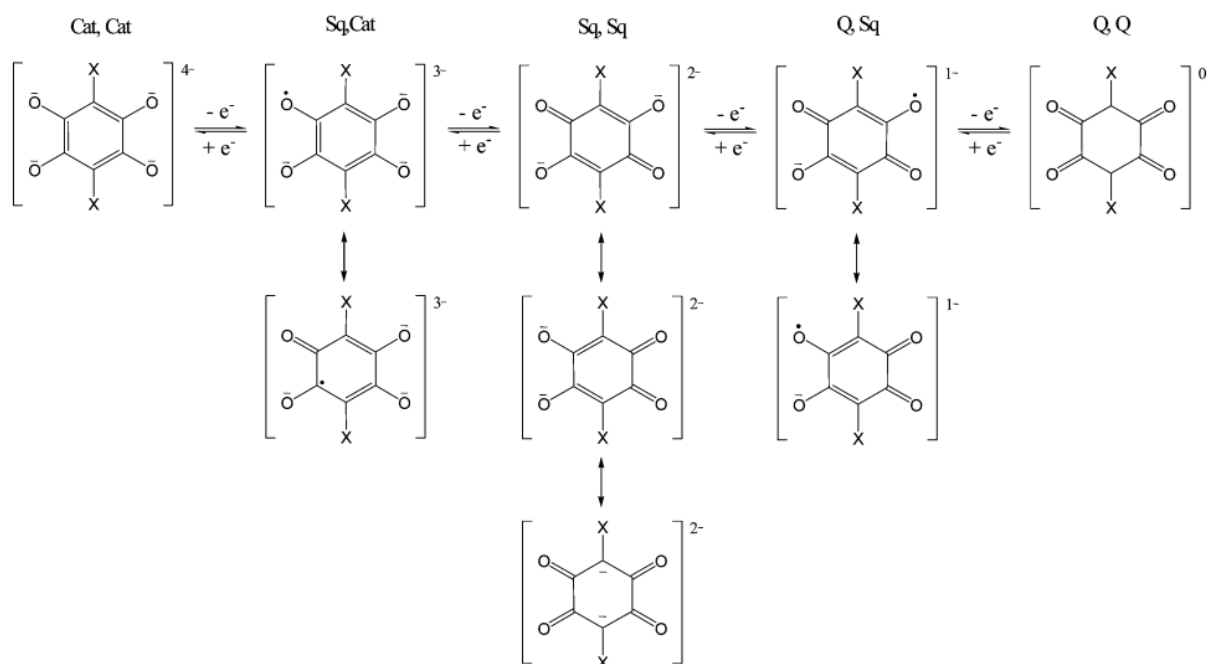


Figure 3.2.: Oxidation states of 2,5-dihydroxy-1,4-benzoquinone and their possible resonance structures, where the abbreviations “Cat”, “Sq”, and “Q” represent catecholate, semiquinone, and quinone, respectively. [45]

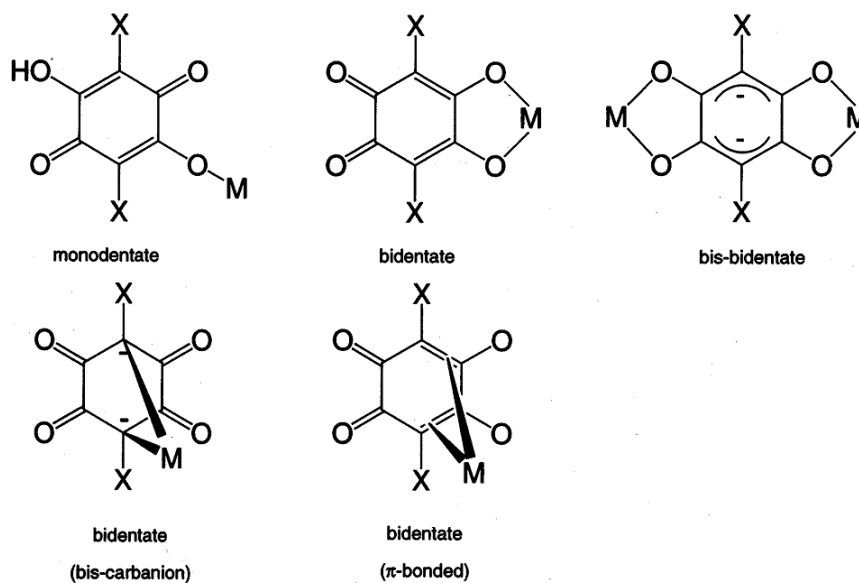


Figure 3.3.: Coordination modes of 2,5-dihydroxy-1,4-benzoquinones. [61]

3.2 Coordination modes of 2,5-dihydroxy-1,4-benzoquinone ligands

Four oxygen donors along with delocalized electron orbitals of the tetraoxolene enable the ligand to bind to metal ions in different coordination modes. The organic molecule can not only coordinate to metal ions via oxygen donors, but also through carbanions and π -bonding to bind metal ions to its carbon skeleton. In fact, there are five possible coordination modes for 2,5-dihydroxy-1,4-benzoquinone and its analogues which are shown in Figure 3.3. [61] With help of hydrogen bonding exerted by the ligand itself and some guest molecules, for instance water, coordination polymers with 1D, 2D, and 3D structures composed of mono or dinuclear complex unit are accessible [13, 60, 70, 61]. For mono-nuclear tetraoxolene complexes, electronic interaction takes place between metal ion and the ligand, resulting in tautomers among which the metal ion and ligand have different oxidation states respectively (see Figure 3.1). Nevertheless, in the dinuclear complexes with a bis-bidentate coordinating quinone, valence electrons of each metal center are able to communicate through the delocalized orbitals of the ligand, and of course, interact with electrons in the frontier orbitals of the ligand as well. [15, 29, 21, 46, 14, 118, 76, 77, 49]

3.3 Intramolecular electronic interaction of 2,5-dihydroxy-1,4-benzoquinone linked complexes

The various electronic states and the resulting metal-ligand bond types as well as the extent of valence electron delocalization of quinone tetraoxolene ligands are of particu-

lar interest for chemists, who intend to prepare versatile functional multi-nuclear complexes. Contrary to polypyridyl-based bridging ligands which are often used in synthesis of mixed-valence compounds, tetraoxolene-based linkers have orbitals of π symmetry which are relatively closer in energy to the metal $d(\pi)$ orbitals [118], bringing about even a larger orbital overlap between ligand and metal. Sufficient metal-ligand orbital overlap would be beneficial for both electronic communication and magnetic interaction between metal ions bridged. Mixed-valence compounds in which same metal ions of different oxidation states coexist in one molecule are therefore likely to be obtained if such ligands are applied as the bridging unit. Moreover, the nature of the metal ions could in turn affect the charge distribution in the bridging ligand; appropriate electronic configuration of tetraoxolenes, i.e. quinone or catecholate bond type, would therefore be present depending on the prerequisites introduced by the ions. [118]

The degree of electronic communication between metal ions within mixed-valence complexes depends on three main components: the bridging ligand, the supporting ligands, and the property of the metal ion itself. Although the electronic interaction appears to take place in the core moiety of a bridged complex, consisting of metal ions and linker ligand, the terminal supporting ligands play as well an important role in determining the electronic population by exerting steric and inductive effects. [101, 46, 15] Gupta et al. prepared a dinuclear chloranilate bridged Os complex with 2,2'-bipyridine as terminal ligand, $[Os(bpy)_2]_2(\mu - CA)(ClO_4)_2$, which represented two reversible redox processes for $Os^{II} \rightarrow Os^{III}$ with a peak separation $\Delta E = 430$ mV, demonstrating a high degree of electronic communication between Os ions through the CA^{2-} linker; whereas its analogous complex $[Os(PPh_3)(pap)]_2(\mu - CA)(ClO_4)_2$, ($pap = 2$ -(phenylazo)-pyridine), showed only one reversible $Os^{II} \rightarrow Os^{III}$ oxidation while the second step was irreversible, with a relatively smaller peak separation of 310 mV, just by replacing the bipyridine terminal ligand with triphenylphosphine and 2-(phenylazo)-pyridine. [46] A dinuclear Co complex bridged by deprotonated 2,5-dihydroxyl-1,4-benzoquinone ($dhbq$) was also obtained by Carbonera and co-workers. [15] The linked Co^{II} complex $[Co(cth)]_2(\mu - dhbq)(PF_6)_2$, where $cth = (dl)$ -5,7,7,12,14,14-hexamethyl-1,4,8,11-tetraazacyclotetradecane, was one-electron oxidized by $AgNO_3$ to afford $[(cth)Co^{II}(\mu - dhbq)^{sq,sq}Co^{III}(cth)]^{3+}$, which could undergo valence tautomerism between Co and the tetraoxolene ligand to become $[(cth)Co^{III}(\mu - dhbq)^{cat,sq}Co^{III}(cth)]^{3+}$ with two low spin Co(III) ions instead of a high spin Co(II) ion and a low spin Co(III), triggered by thermo- and UV-vis radiation. Similar results were attained by Tao and co-workers, [101] who prepared an analogous mixed-valence dinuclear Co complex $[(TPA)Co^{II}(\mu - dhbq)^{sq,sq}Co^{III}(TPA)(PF_6)_3$ that exhibited the thermo- and photoinduced valence tautomerism to $[(TPA)Co^{III}(\mu - dhbq)^{cat,sq}Co^{III}(TPA)](PF_6)_3$, and a thermal hysteresis loop at 13 K. Dei et al. proposed that this radical form of the tetraox-

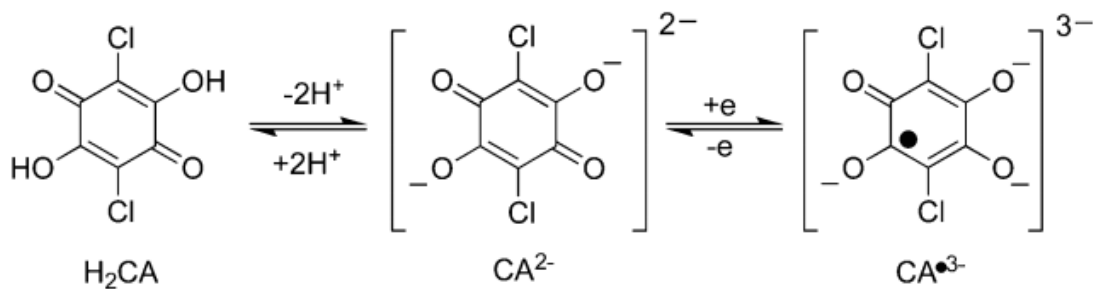


Figure 3.4.: Chloranilic acid and its anions.

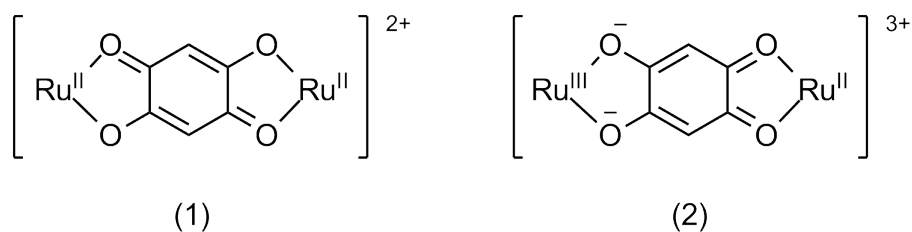


Figure 3.5.: A redistribution of electron density in the bridging ligand of linked Ru complex. [118]

olene ligand was likely to be stabilized using proper trivalent cations, such as Fe(III) and Cr(III). [29] The charge rearrangement in the tetraoxolene plane can be also expressed as shifting among different resonance forms. M. D. Ward discovered that the carbon-oxygen bond order could be altered by redistribution of the valence electrons from a conjugated bond order of 1.5 for $[(bipy)Ru^{II}(dmbq)Ru^{II}(bipy)]^{2+}$ ((1) of Figure 3.5) to unsymmetrical localized catecholate and quinone bonds for its one-electron oxidized product $[(bipy)Ru^{III}(dmbq)Ru^{II}(bipy)]^{3+}$, in which the Ru(III) center was bound to two catecholate oxygens, with a bond order of 1.0 ((2) of Figure 3.5). [118] Sometimes the oxidation of tetraoxolene ligands can be observed during electrochemical measurement; and in the cyclic voltammogram of $(cod)Rh^I(dmbq)Rh^I(cod)$ prepared by Calvo et al. two stepwise oxidation waves of the linker were recorded, which were attributed to the quinone-semiquinone and semiquinone-catecholate couples, respectively. [14]

Besides thermo- and photoradiation, the oxidation state of tetraoxolene ligand can be controlled chemically. For magnetically active bridged dinuclear complexes, the spin bearing radical form of $dmbq^{\bullet 3-}$, $CA^{\bullet 3-}$ and other tetraoxolene derivatives would significantly increase the magnetic coupling between metals, since direct spin exchange coupling would take place arising from the overlap of the π^* SOMO of $S = \frac{1}{2}$ radical linker and d orbitals of metal ion, contrary to the associated dianion form, in which magnetic coupling occurs via superexchange. [78, 76, 77, 45] (Figure 3.4) Min et al. successfully isolated radical bridged $(TPyA)Co^{III}(CA^{\bullet 3-})Co^{III}(TPyA)(BF_4)_3 \cdot 4MeCN$ through redox-induced

electron rearrangement (RIER). Under this mechanism CA^{2-} was reduced by an oxidant, not a reductant, from $[(TPyA)Co^{II}(CA^{2-})Co^{II}(TPyA)]^{2+}$ via a quick valence tautomerisation of Co(II) and CA^{2-} . [77] The $CA^{\bullet 3-}$ radical was stabilized by the electron withdrawing Cl group in contrast to $[(CTH)Co(dhbq^{\bullet 3-})Co(CTH)]^{3+}$ [15] and $[(TPyA)Co(dhbq^{\bullet 3-})Co(TPyA)]^{3+}$ [101] which undergo $Co^{III}(dhbq^{\bullet 3-})Co^{III} \leftrightarrow Co^{II}(dhbq^{2-})Co^{III}$ spin crossover. Temperature dependent magnetic susceptibility measurement showed the radical bridged Co(III) complex exhibited strong antiferromagnetic coupling, with the magnitude of J two orders larger than that for the dianion linked Co(II) complex. The property of spin exchange interaction of the paramagnetic metal center and the bridging radical was elucidated by Guo and McKusker [45], when synthesizing a series of metal complexes bridged by chloranilate ligand with various spin states, i.e. $CA^{sq,q-}$, $CA^{sq,sq^{2-}}$, $CA^{cat,sq^{3-}}$, and $CA^{cat,cat^{4-}}$. Antiferromagnetic interaction mediated by chloranilate occurring in multi-nuclear metal complexes has been intensely studied since 1980s. A lot of dinuclear chloranilate complexes with paramagnetic copper centers and various counterligands were synthesized, most of which contained CA^{2-} bridging ligand, and all of those were characterized to have $Cu \cdots Cu$ antiferromagnetic coupling over a long distance (5–8 Å) via superexchange interaction. [86, 104, 36, 37, 16, 40, 41] High spin iron(III) complex linked by tetraoxolene supported by salen (*salen*)₂Fe₂(μ -*dhbq*) was prepared and presented $Fe \cdots Fe$ antiferromagnetic coupling to be weaker than that for copper complex under same conditions, in which the bridging ligand was in the (sq, sq) dianion form as well. [68] Heinze et al. isolated the catecholate tetraanion linked complex $LCo^{III}(\mu - CA^{4-})Co^{III}L$, in which L is a tripodal phosphane ligand and CA^{4-} is in the completely reduced (cat, cat) form (Figure 3.2). [49] The tetraoxolene complexes could even self-assemble into polynuclear 2D or 3D motif connected with coordination and hydrogen bondings, exhibiting magnetic and electronic intermolecular interactions. [60, 70, 13]

These examples elucidate the versatility of electron distribution and the complexity of redox and magnetic behavior for the tetraoxolene-based complexes. It is further intriguing to conduct research into this area and type of ligands due to their potential in molecular engineering and bioinorganic studying. Therefore, my research interest in that field was focusing on the preparation of redox active multinuclear metal complexes bridged by chloranilate ligand.

Part II.

Objective and Aims

Multinuclear linked metal complexes are of particular importance in modern inorganic chemistry, metalorganic chemistry, as well as material science. These compounds own spectacular redox and magnetic properties allowing to develop new functional materials and discover new electronic interactions. Typically the electronic and magnetic characteristics of such molecules are dependent upon properties of the bridging and supporting ligands. In this thesis it was a central goal to develop novel di and polynuclear coordination compounds. It was expected to obtain novel mixed-valence properties based on their multinuclearity.

With respect to more complicated scorpionates, first generation homoscorpionates, e.g. hydrotris(pyrazolyl)borate (*Tp*) and hydrotris(3,5-dimethyl-pyrazolyl)borate (*Tp*^{*}), have been developed very scarcely; and only limited amount of metal complexes supported by *Tp* or *Tp*^{*} has been prepared up to now. Metal ions having *d*⁶ and *d*⁷ electronic configurations, such as *Fe*²⁺ and *Co*²⁺, usually possess a rich redox activity as well as magnetic properties, however only a small number of half-sandwich *Tp* or *Tp*^{*}-based complexes have been reported, which would be suitable as building blocks for assembling linked multinuclear complexes. I was aiming to prepare bridged coordination compounds with tris(pyrazolyl)borate ligands, in order to discover new complexes (M = Fe, Co) with mixed-valence functionalities.

For the same purpose, another interesting type of compounds containing metal complexes bridged via chloranilate dianions was studied. This bis-bidentate chelating ligand features rich redox properties, establishing itself as a very intensively studied non-innocent ligand, being able to build linked metal complexes that would exhibit intramolecular electronic interactions between metal centers as well as metal and ligand. The valence delocalization of these bridging ligands provides possibilities for electronic communication, making these coordination systems intriguing. The appealing prospect of future applications prompts me to address emphasis on preparing redox active linked multinuclear complexes bridged by the non-innocent chloranilate ligand, hoping to observe intra electronic communications in these coordination compounds.

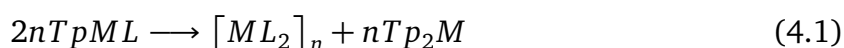
Part III.

Results and Discussion

4 Tris(pyrazolyl)borate Co complexes and their reactions

4.1 Synthesis of cobalt tris(pyrazolyl)borate complexes

Since the cone angle of unsubstituted Tp complexes is relatively small, formation of its half-sandwich divalent metal complex is mostly disturbed by a further ligand disproportionation reaction



to form Tp_2M , a sterically more stable octahedral complex, which renders $TpM(II)L$ type tetrahedral compounds considerably rare.

Bruce and Ostazewski [12] have succeeded to isolate a Copper(I) complex $TpCu(CO)$ which was crystallographically confirmed to have a tetrahedral geometry showing C_3 symmetry with O, C, Cu, and B lying along the $C_2(C_3)$ axis (Figure 4.1) [18]. Further heating of the compound under vacuum afforded neutral dimeric Cu(I) complex $[TpCu]_2$ [74] in which each Cu(I) atom is coordinated by four nitrogens from pyrazolyl ring of Tp in a distorted tetrahedral manner. Attempts to prepare the Cu(II) analogue containing an unsymmetrical coordination center were undertaken by Roundhill et al. [90], who obtained dimeric $[TpCuCl]_2$ by treating $TpNa$ with $CuCl_2$. The complex is proven to be a dimer in which two $TpCu$ subunits are linked by two chlorines each coordinating both copper centers (Figure 4.2).

Motivated by this idea, I tried as well the synthesis of half-sandwich $TpCo$ complex with Br as supporting ligand, and succeeded in obtaining a bromo linked trimeric Cobalt(II) complex for the first time.

4.1.1 Preparation of Potassium tris(pyrazolyl)borate (TpK)

The hydrotris(pyrazolyl)borate ligand (Tp) is usually introduced to metal ions in the form of its potassium salt, which can be prepared as described by Trofimenko's procedure [107]. Molten pyrazole and KBH_4 are heated together in a ratio of 4 to 1 until 3 equiv. of H_2 are released. White crystals of TpK can be isolated in 40 % yield. They are stable at room temperature in air for months and soluble in water, alcohol, and other common polar solvents.

Its IR spectrum has a single $B - H$ bond stretching vibration at 2436 cm^{-1} that is characteristic to tris-substituted borate anion. An aromatic $C - H$ bond stretch at 2900 cm^{-1}

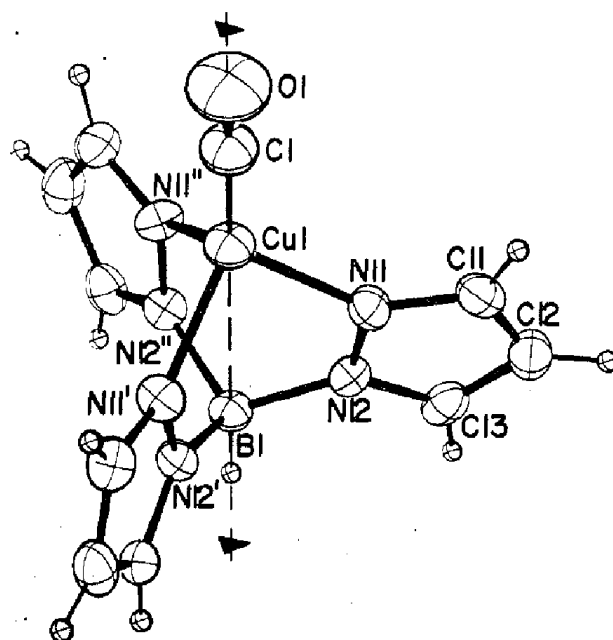


Figure 4.1.: Crystal structure of $TpCu(CO)$ (ORTEP diagram with 50 % probability envelopes for the thermal ellipsoids). [18]

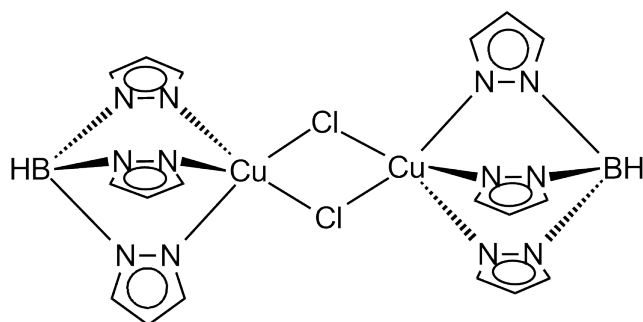


Figure 4.2.: Chemical structure of $[TpCuCl]_2$. [90]

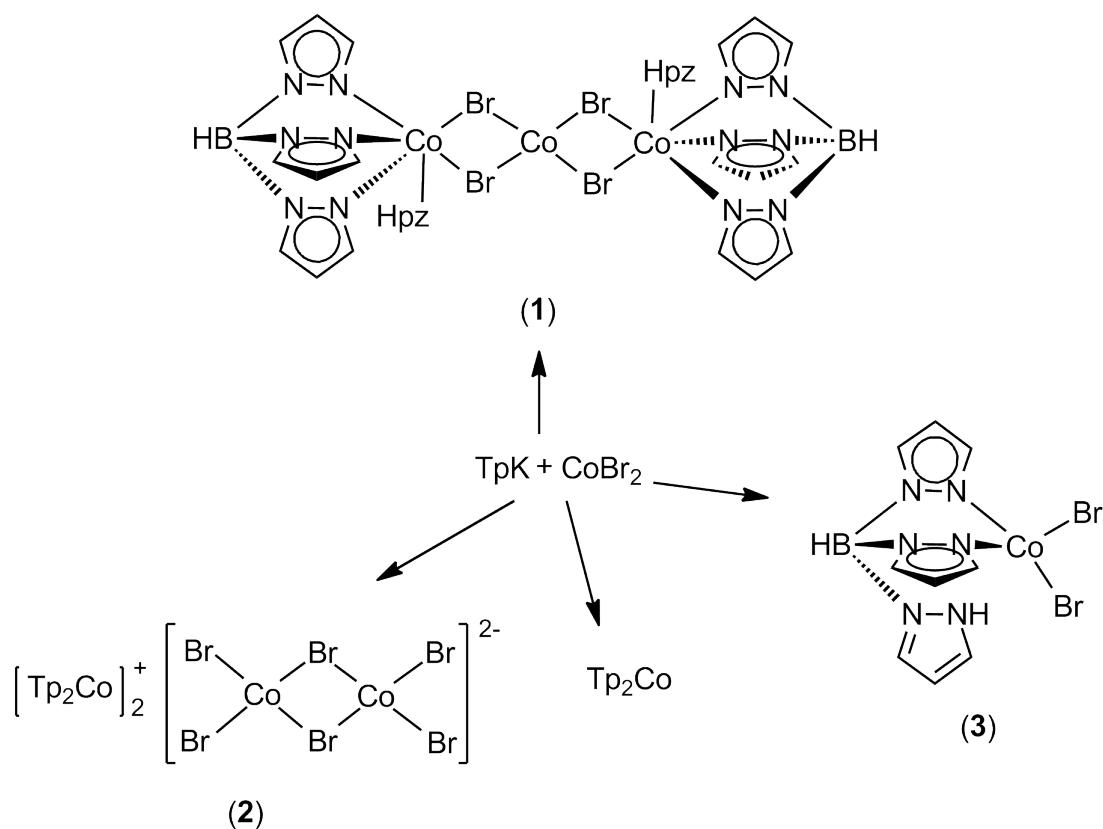


Figure 4.3.: Reaction of *TpK* and *CoBr₂* in THF.

corresponds to the three equivalent substituted pyrazolyl rings. Elemental analysis is consistent with the molecular constitute as well.

4.1.2 Synthesis of multinuclear bromo[tris(pyrazolyl)borato]cobalt complex

At room temperature, a *TpK* solution was dropped into the solution of anhydrous *CoBr₂* in THF. After stirring overnight, a mixture of products was collected. Recrystallization in dichloromethane layered by pentane gave four different types of crystals, which can be separated due to their different colors (Figure 4.3). As determined by X-ray crystallography three of those are new compounds containing *Tp* ligand: purple crystals of (1), [*TpCo(Hpz)*]₂*CoBr*₄, can be assigned to a trinuclear structure in which three cobalt(II) atoms reside in a framework consisting of two *Tp* ligands, four bromines, and two pyrazole molecules. Green crystals of (2), [*Tp*₂*Co*]₂[*Co*₂*Br*₆], have two Co(III)-positive charged cations [*Tp*₂*Co(III)*]⁺; and the counterion is [*Co(II)*₂*Br*₆]²⁻, hence two cobalt ions of different oxidation states coexist in the molecule. Finally blue crystals of (3), *HTpCoBr*₂, display the structure of a mono-nuclear half-sandwich complex with dipodal coordinated *Tp* ligand and two bromine ligands. In addition yellow crystals are *Tp*₂*Co* which is expected to be a side-product of this reaction.

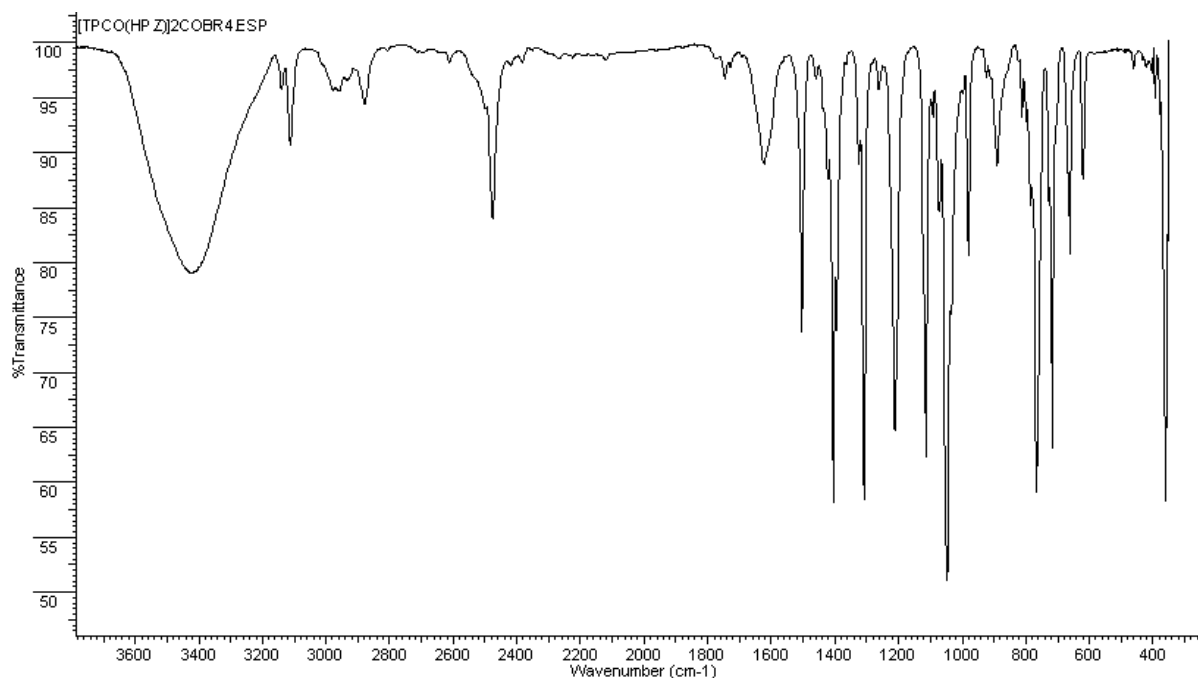


Figure 4.4.: IR spectrum of complex (1).

4.1.2.1 IR investigation

The IR spectrum of the trinuclear cobalt complex (1) is shown in Figure 4.4. A single $B-H$ stretching vibration appears unambiguously at 2477 cm^{-1} indicating the presence of Tp ligand, whose ring $C-H$ stretch is shown at signals around 3112 cm^{-1} . Bands at 1623 and 1503 cm^{-1} are assigned to $C=C$ bond stretch in pyrazolyl ring while the aromatic $C=N$ and $N=N$ stretching vibrations locate at 1405 , 1394 , and 1308 cm^{-1} as well as pyrazolyl ring breathing at 980 cm^{-1} . Two bands at 1212 and 1114 cm^{-1} are due to $C-H$ in-plane deformation, and its corresponding out-of-plane deformation appears at 766 and 716 cm^{-1} . A strong band at 1047 cm^{-1} probably arises from $B-N$ bond stretch, and the $Co-N$ or $Co-Br$ bond stretches are assigned to 461 and 393 cm^{-1} since in IR spectrum of TpK these two frequencies are present. The broad absorption at 3419 cm^{-1} is contributed by $N-H$ bond stretch of the two coordinated pyrazole molecules.

The IR spectrum of complex (2) (Figure 4.5) looks quite similar to that of complex (1). A dominating difference comes from the bond stretch of the $B-H$ band at 2532 cm^{-1} . As the central cobalt is in +3 state and coordinated by two Tp ligands, the electronic density of ligand is reasonably enhanced to make the $B-H$ and $B-N$ bond stronger. Hence the ν_{B-H} at 2532 cm^{-1} and ν_{B-N} at 1053 cm^{-1} are higher shifted by 55 cm^{-1} and 6 cm^{-1} , respectively. Besides, the $C-H$ stretch is assigned to frequencies around 3102 cm^{-1} ; and bands at 1623 , 1502 , 1410 , 1397 , 1326 , and 997 cm^{-1} are due to the pyrazolyl ring stretch. The $C-H$ in-plane and out-of-plane bends are displayed at 1223 ,

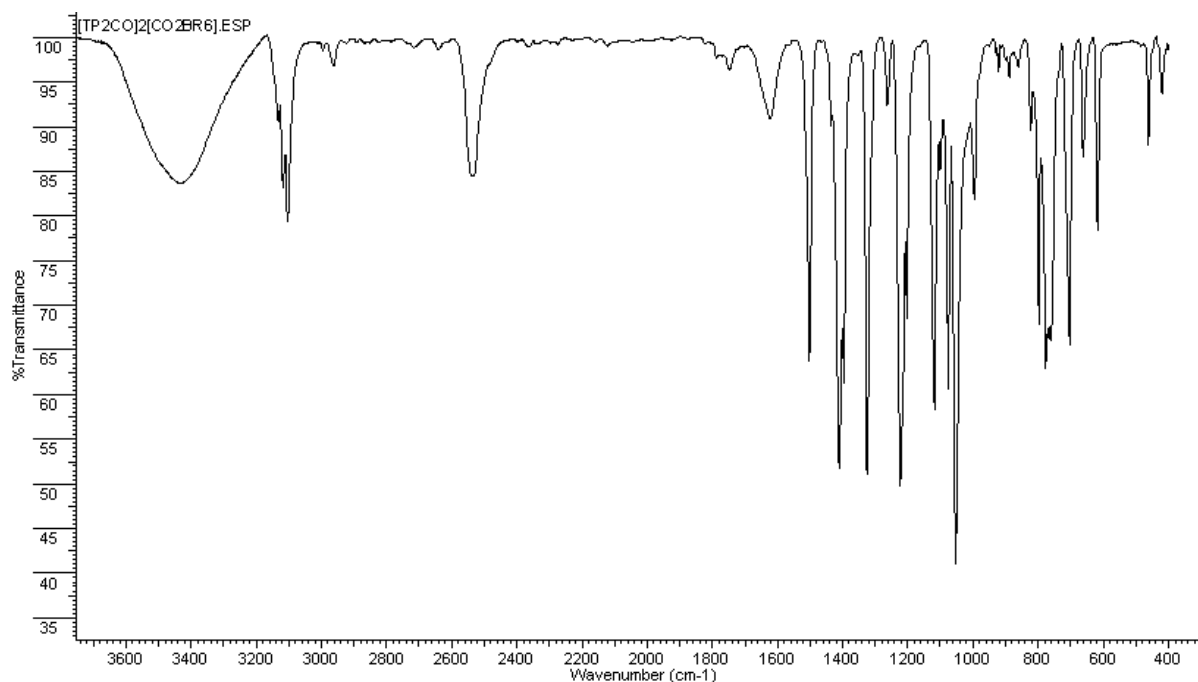


Figure 4.5.: IR spectrum of complex (2).

1119, 777, and 704 cm^{-1} . Finally, vibrations at 461 and 421 cm^{-1} from $\text{Co} - \text{N}$ bond stretch confirm coordination to cobalt.

4.1.2.2 X-ray crystal structure determination

Structure of $[\text{HB}(\text{pz})_3(\text{Hpz})\text{BrCo}]_2\text{CoBr}_2$ (1)

Single crystals of complex (1) were grown from a solution of (1) in dichloromethane layered by petroleum ether. The purple crystals obtained were studied by X-ray single crystal diffraction confirming a unit cell with $a = 13.249(1) \text{ \AA}$, $b = 15.438(1) \text{ \AA}$, $c = 19.379(2) \text{ \AA}$, and the volume of $3963.7(6) \text{ \AA}^3$ in the orthorhombic crystal system space group $Pbcn$. Half of the molecule was solved firstly and the left atoms were generated using symmetry transformations: $-x, y, -z + 1/2$. Some of its crystallographic parameters are summarized in Table 4.2. An ORTEP diagram of the molecular structure with specific atoms labeled is given in Figure 4.6. The molecule contains three cobalt(II) cations, two of which are octahedrally coordinated by a Tp , two bromides, and a separated pyrazole molecule, and another cobalt ion is coordinated by four bromides in a tetrahedral manner. The $\text{Co} \cdots \text{Co}$ distance of 3.472 \AA indicates that there is no direct bonding interaction between cobalt atoms. Tp offers three nitrogen donors coordinating facially with an average $\text{N} - \text{Co}$ bond length of $2.084(8) \text{ \AA}$, which is longer than that in Co(III) complex $[\text{Tp}_2\text{Co}][\text{PF}_6]$ (average $\text{N} - \text{Co}$ length $1.925(3) \text{ \AA}$) [48] and shorter than that in Tp_2Co (average $\text{N} - \text{Co}$ length $2.129(7) \text{ \AA}$) [19], and consistent with the value in similarly structured cobalt

complex $[CoBr(TPyEA)]_2(BPh_4)_2$ (average $N - Co$ length 2.13(2) Å) [116]. Notably the $N(3) - Co(1)$ distance (2.074(8) Å) is slightly shorter than the other two ($N(1) - Co(1) = 2.081(8)$ Å; $N(5) - Co(1) = 2.099(9)$ Å) bond lengths. This alteration is probably because the $N(3)$ pyrazolyl ring has less electrostatic repulsion with the neutral pyrazole and two bridging bromides than another two pyrazolyl rings of the same TP . The neutral pyrazole coordinates to Co with $N(7A) - Co(1) = 2.118(18)$ Å longer than those of TP , resulting from lack of the chelate effect. The $Br - Co$ distance is tremendously elongated ($Br(1) - Co(1) = 2.7026(17)$ Å; $Br(2) - Co(1) = 2.6777(17)$ Å) due to another bonded $Co(2)$ 3.472 Å away from the octahedrally coordinated center, which is also in agreement with the value of $[CoBr(TPyEA)]_2(BPh_4)_2$ (average $Br - Co = 2.682(3)$ Å). [116] The tetrahedral $Co(2)$ center is coordinated by the bridging bromides with a shorter bond length than the average $Br - Co(2) = 2.3945(17)$ Å. From the displayed bond angles one can see that the terminal $Co(1)$ ion is in a distorted octahedral geometry. The $Co(1) - N(3)$ bond is bent towards the boron atom with $N(3)Co(1)N(5) = 86.9(3)^\circ$ and $N(3)Co(1)N(1) = 87.5(3)^\circ$ with respect to the ideal angle of 90° . Steric restriction of TP plays an important role in the deformation. Interestingly, the $N - Co$ bond between the neutral pyrazole and Co , $N(7A) - Co(1)$, is bent towards $N(1)$ -pyrazolyl ring and $Br(1)$ with $N(7A)Co(1)Br(1) = 84.0(5)^\circ$ and $N(7A)Co(1)N(1) = 85.1(6)^\circ$ rather than staying centered perpendicular to the equatorial plane of the octahedron. This distortion may be due to packing forces in the crystal. The angle $Br(1)Co(1)Br(2) = 86.85(5)^\circ$ corresponds to the large $Co(1) - Co(2)$ distance and long $Br - Co(1)$ bridging bond. Atoms $Br(1)$, $Co(1)$, $N(5)$ are arranged almost linearly ($Br(1)Co(1)N(5) = 179.80^\circ$), while $N(1)$ is neither located along the axis determined by $Co(1)$ and $Br(2)$ forming an angle of $N(1)Co(1)Br(2) = 177.65^\circ$, nor resides in the equatorial plane. The atom $N(1)$ is bent 1.26° up to the equatorial plane $Co(1)Br(1)Br(2)$ towards the neutral pyrazole. The coordination geometry of the central $Co(2)$ is distorted due to the bridging bromine atoms displaying a pseudo-tetrahedron. The angle $Br(1)Co(2)Br(2) = 101.12(4)^\circ$ is therefore 8.4° smaller than that of an ideal tetrahedron.

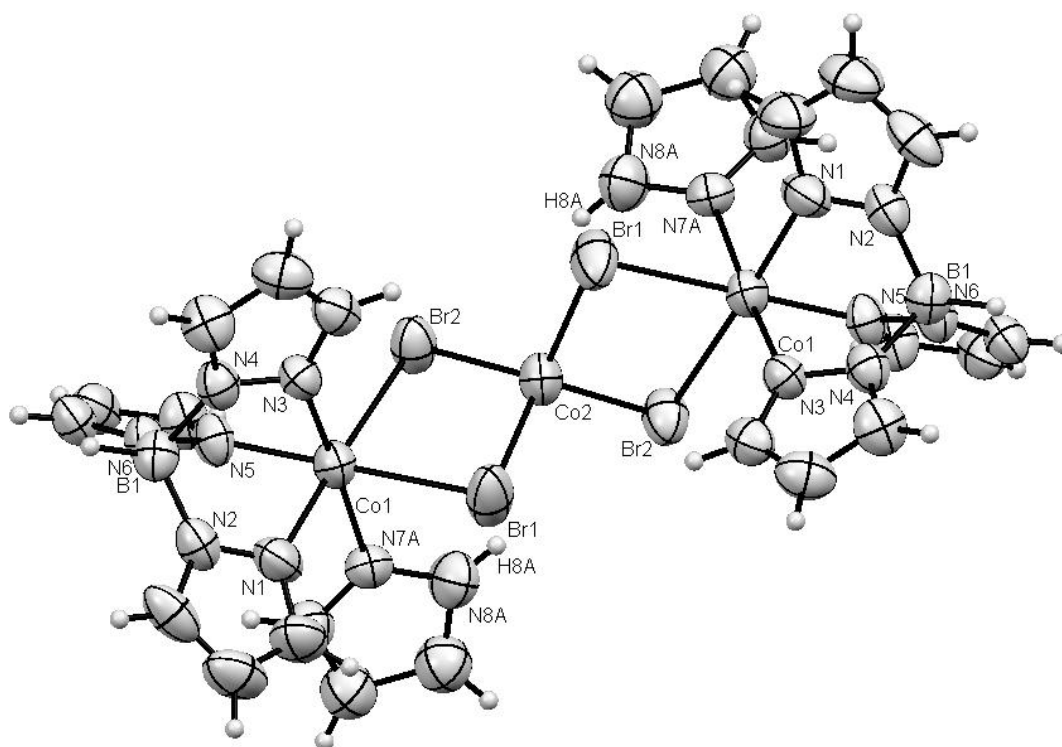


Figure 4.6.: ORTEP drawing of the crystal structure of complex (1) with selected atoms labeled. The thermal ellipsoids represent the probability level of 50 %.

| | |
|-----------------------------|--|
| Empirical formula | C ₂₄ H ₂₈ B ₂ Br ₄ Co ₃ N ₁₆ |
| Formula weight | 1058.67 |
| Temperature | 293(2) K |
| Wavelength | 0.71073 Å |
| Crystal system, space group | Orthorhombic, P b c n |
| Unit cell dimensions | a = 13.249(1) Å alpha = 90 deg. b = 15.438(1) Å beta = 90 deg. c = 19.379(2) Å gamma = 90 deg. |
| Volume | 3963.7(6) Å ³ |
| Final R indices [I > 2σ(I)] | R ₁ = 0.0741, wR ₂ = 0.1531 |
| R indices (all data) | R ₁ = 0.2033, wR ₂ = 0.2052 |

Table 4.2.: Selected crystallographic data for complex (1).

| Bonds | Bond lengths (Å) | Bonds | Bond lengths (Å) |
|-------------------|------------------|---------------------|------------------|
| Br(1)-Co(2) | 2.3968(17) | Co(1)-N(7A) | 2.118(18) |
| Br(1)-Co(1) | 2.7026(17) | Co(2)-Br(2)#1 | 2.3921(16) |
| Br(2)-Co(2) | 2.3921(16) | Co(2)-Br(1)#1 | 2.3968(17) |
| Br(2)-Co(1) | 2.6777(17) | N(2)-B(1) | 1.529(14) |
| Co(1)-N(3) | 2.074(8) | N(4)-B(1) | 1.544(13) |
| Co(1)-N(1) | 2.081(8) | N(6)-B(1) | 1.561(14) |
| Co(1)-N(5) | 2.099(9) | | |
| | Angles (deg) | | Angles (deg) |
| Co(2)-Br(1)-Co(1) | 85.59(5) | N(1)-Co(1)-Br(2) | 177.7(3) |
| Co(2)-Br(2)-Co(1) | 86.24(5) | N(5)-Co(1)-Br(2) | 93.1(2) |
| N(3)-Co(1)-N(1) | 87.5(3) | N(7A)-Co(1)-Br(2) | 93.7(5) |
| N(3)-Co(1)-N(5) | 86.9(3) | N(7B)-Co(1)-Br(2) | 82.3(5) |
| N(1)-Co(1)-N(5) | 89.0(3) | N(3)-Co(1)-Br(1) | 92.9(2) |
| N(3)-Co(1)-N(7A) | 171.9(6) | N(1)-Co(1)-Br(1) | 91.1(3) |
| N(1)-Co(1)-N(7A) | 85.1(6) | N(5)-Co(1)-Br(1) | 179.8(2) |
| N(5)-Co(1)-N(7A) | 96.3(6) | N(7A)-Co(1)-Br(1) | 84.0(5) |
| N(3)-Co(1)-N(7B) | 172.5(6) | Br(2)-Co(1)-Br(1) | 86.85(5) |
| N(1)-Co(1)-N(7B) | 96.8(5) | Br(2)-Co(2)-Br(2)#1 | 116.31(10) |
| N(5)-Co(1)-N(7B) | 87.0(5) | Br(2)-Co(2)-Br(1)#1 | 112.83(4) |
| N(7A)-Co(1)-N(7B) | 15.1(7) | Br(2)-Co(2)-Br(1) | 101.12(4) |
| N(3)-Co(1)-Br(2) | 93.6(2) | Br(1)#1-Co(2)-Br(1) | 113.20(12) |

Table 4.4.: Selected bond lengths (Å) and angles (deg) for complex (1).

Structure of $\{[\text{HB}(\text{pz})_3]_2\text{Co}\}_2[\text{Co}_2\text{Br}_6]^{2-}$ (2)

The molecule of complex (2) is composed of two $[\text{Tp}_2\text{Co}]^+$ cations and a $[\text{Co}_2\text{Br}_6]^{2-}$ anion crystallized in the triclinic crystal system, space group $P-1$, with the unit cell dimensions of $a = 10.530(1) \text{ \AA}$, $b = 11.356(1) \text{ \AA}$, $c = 13.728(1) \text{ \AA}$; $\alpha = 101.207(9)^\circ$, $\beta = 93.387(7)^\circ$, $\gamma = 99.085(8)^\circ$. The structure is illustrated in Figure 4.7. Cobalt in the $[\text{Tp}_2\text{Co}]^+$ cation is octahedrally coordinated by two Tp s possessing C_3 symmetry along $B - \text{Co}$ axis and a center of inversion at the Co atom. The average $N - \text{Co}$ bond length for Co(1) is $1.928(4) \text{ \AA}$, and the two $N(1) - \text{Co}(1)$ bonds are relatively longer than the other four of the complex cation by 0.012 \AA ; whereas for Co(2) it has a shorter bond length for $N - \text{Co}$ of average $1.924(4) \text{ \AA}$. Both are in accordance with values observed in $[\text{Tp}_2\text{Co}][\text{PF}_6]$ (av. $1.925(3) \text{ \AA}$) [48] and $[\text{Tp}_2\text{Co}][\text{Sn}_2\text{Co}_5\text{Cl}_2(\text{CO})_{19}]$ (av. 1.918 \AA) [23] Although the $\text{Co} - \text{N}$ distance is distinctly shortened due to the higher oxidation state of Co with respect to those in Tp_2Co (av. $2.129(7) \text{ \AA}$), their average $B - \text{N}$ distances of Tp do not alter significantly ($1.544(21) \text{ \AA}$ for Tp_2Co ; $1.535(7) \text{ \AA}$ for $[\text{Tp}_2\text{Co}]^+$). [19] That means one more positive charge on Co enhances the ligand field of Tp but doesn't influence its $B - \text{N}$ bond length. However, the Tp ligand is compressed because of the shortened $N - \text{Co}$ bond, and the average NBN in $[\text{Tp}_2\text{Co}]^+$ is decreased to 106.4° comparing with 108.9° in Tp_2Co . The coordination geometry of the Co(III) cation is almost a regular octahedron with all $N - \text{Co} - \text{N}$ angles close to 90° while that of Tp_2Co is relatively elongated along the $B - \text{Co} - \text{B}$ axis to give $N - \text{Co} - \text{N}$ angles of ca. 85° , which is another evidence of stronger octahedral ligand field around Co(III) atom. Both cobalt atoms in $[\text{Co}_2\text{Br}_6]^{2-}$ are surrounded by four bromides in distorted tetrahedral geometry. The anion contains three C_2 axes, two of them intersecting the two cobalt atoms and two bridging bromides respectively, and the third one perpendicular with all of them going through a center of inversion. The $\text{Co} \cdots \text{Co}$ distance is 3.374 \AA about 0.1 \AA shorter than that in complex (1), but still too far away to form a direct $\text{Co} - \text{Co}$ bond. The cobalt atoms are bridged by two bromides with an average bond length of $2.4745(8) \text{ \AA}$, which is significantly shorter than the respective distances of ca. 2.69 \AA in complex (1). The terminal $\text{Br} - \text{Co}$ bonds have an even shorter average bond length of $2.3669(9) \text{ \AA}$, meaning that the tetrahedral coordination geometry is stretched on account of the repulsion between the two neighboring cobalts, which is also supported by the decreased $\text{Br} - \text{Co} - \text{Br}$ angle of $94.03(3)^\circ$ with respect to 109.5° for a regular tetrahedral geometry. Some crystallographic parameters and important bond lengths and angles are summarized in Table 4.6 and Table 4.8.

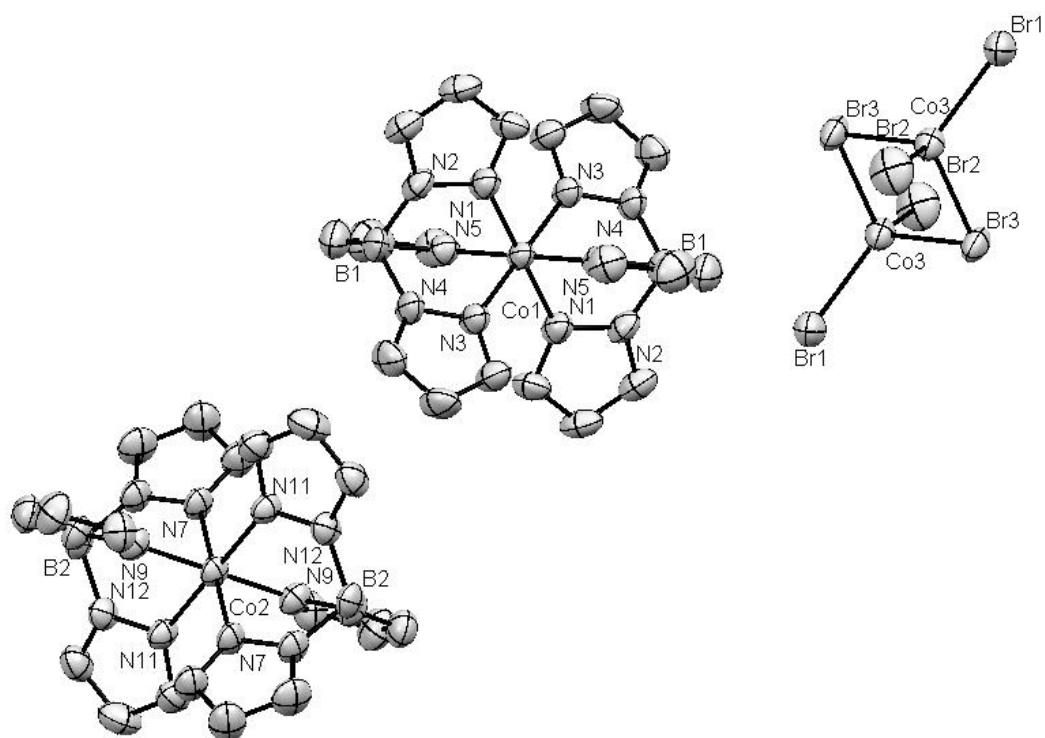


Figure 4.7.: ORTEP drawing of the crystal structure of complex **(2)** with selected atoms labeled. The thermal ellipsoids represent the probability level of 50 %. All H atoms are omitted for clarity.

| | |
|-------------------------------|--|
| Empirical formula | C19 H24 B2 Br3 Co2 N12 O2 |
| Formula weight | 831.71 |
| Temperature | 293(2) K |
| Wavelength | 0.71073 Å |
| Crystal system, space group | Triclinic, P -1 |
| Unit cell dimensions | a = 10.530(1) Å alpha = 101.207(9) deg. b = 11.356(1) Å beta = 93.387(7) deg. c = 13.728(1) Å gamma = 99.085(8) deg. |
| Volume | 1583.2(2) Å ³ |
| Final R indices [I>2sigma(I)] | R1 = 0.0406, wR2 = 0.1177 |
| R indices (all data) | R1 = 0.0624, wR2 = 0.1254 |

Table 4.6.: Selected crystallographic data for complex **(2)**.

| Bonds | Bond lengths (Å) | Bonds | Bond lengths (Å) |
|-------------------|------------------|---------------------|------------------|
| Co(1)-N(5) | 1.924(4) | Co(2)-N(11) | 1.930(4) |
| Co(1)-N(3) | 1.924(4) | N(8)-B(2) | 1.538(7) |
| Co(1)-N(1) | 1.936(4) | N(10)-B(2) | 1.548(7) |
| N(2)-B(1) | 1.531(7) | N(12)-B(2) | 1.535(7) |
| N(4)-B(1) | 1.525(7) | Br(1)-Co(3) | 2.3728(9) |
| N(6)-B(1) | 1.531(8) | Br(2)-Co(3) | 2.3610(10) |
| Co(2)-N(7) | 1.919(4) | Br(3)-Co(3) | 2.4670(8) |
| Co(2)-N(9) | 1.923(4) | Br(3)-Co(3)#3 | 2.4820(8) |
| Bond angles (deg) | | Bond angles (deg) | |
| N(5)#1-Co(1)-N(5) | 180.00(15) | N(7)-Co(2)-N(11)#2 | 90.90(16) |
| N(5)#1-Co(1)-N(3) | 90.52(17) | N(9)-Co(2)-N(11)#2 | 90.14(16) |
| N(5)-Co(1)-N(3) | 89.48(17) | N(7)-Co(2)-N(11) | 89.10(16) |
| N(3)-Co(1)-N(3)#1 | 180.0(3) | N(9)-Co(2)-N(11) | 89.86(16) |
| N(5)#1-Co(1)-N(1) | 91.03(17) | N(11)#2-Co(2)-N(11) | 180.000(1) |
| N(5)-Co(1)-N(1) | 88.97(17) | N(12)-B(2)-N(8) | 105.6(4) |
| N(3)-Co(1)-N(1) | 89.09(16) | N(12)-B(2)-N(10) | 106.5(4) |
| N(3)#1-Co(1)-N(1) | 90.91(16) | N(8)-B(2)-N(10) | 106.1(4) |
| N(1)-Co(1)-N(1)#1 | 180.000(1) | Co(3)-Br(3)-Co(3)#3 | 85.97(3) |
| N(4)-B(1)-N(2) | 107.4(4) | Br(2)-Co(3)-Br(1) | 117.35(4) |
| N(4)-B(1)-N(6) | 107.0(4) | Br(2)-Co(3)-Br(3) | 110.06(4) |
| N(2)-B(1)-N(6) | 105.7(4) | Br(1)-Co(3)-Br(3) | 113.03(3) |
| N(7)-Co(2)-N(7)#2 | 180.00(18) | Br(2)-Co(3)-Br(3)#3 | 110.98(3) |
| N(7)-Co(2)-N(9) | 89.50(16) | Br(1)-Co(3)-Br(3)#3 | 108.96(3) |
| N(7)-Co(2)-N(9)#2 | 90.50(16) | Br(3)-Co(3)-Br(3)#3 | 94.03(3) |
| N(9)-Co(2)-N(9)#2 | 180.000(1) | | |

Table 4.8.: Selected bond lengths (Å) and angles (deg) for complex (2).

Structure of HB(pz)₂(Hpz)CoBr₂ (3)

Figure 4.8 shows the ORTEP drawing of complex (3) with atomic labels. The blue crystal is monoclinic, in the space group $P 21/c$ with unit cell dimensions $a = 9.2706(6)$ Å, $b = 15.254(1)$ Å, $c = 10.6149(8)$ Å. Both Co and B atoms are coordinated tetrahedrally, and their distance amounts to 3.249 Å. This value is apparently larger than those observed in complex (1) (3.159 Å), complex (2) (av. 3.067 Å), and Tp_2Co (av. 3.195(4)) Å [19], corresponding to the fact that the Tp only coordinates as dipodand, losing some of its chelate power. However, the average $N - Co$ bond length does not differ significantly from that in complex (1). It shows an average $N - Co$ distance of 2.011(3) Å slightly shorter than 2.084(8) Å for complex (1), even shorter than that for Tp_2Co (2.129(7) Å). It can be explained by less steric hindrance around the tetrahedral Co in complex (3). The average $Co - Br$ length of 2.3761(8) Å is in good agreement with values for the $Co - Br$ single bond in other coordination compounds, such as complex (2) (av. 2.3669(9) Å), and complex (1) (2.3945(17) Å for $Br - Co(2)$). As expected, the tetrahedral coordination geometry of Co is distorted because of the steric restriction of the chelating ligand, giving $N(3)Co(1)N(1) = 93.15(14)^\circ$ as opposed to $N(4)B(1)N(2) = 112.0(4)^\circ$ on the opposite position of the six-membered chelate ring. The boron bears a neutral pyrazole substituent. The pyrazole ring is positioned perpendicular to the $Co(1) - B(1) - N(6)$ plane leaving the amine nitrogen atom far away from the metal center. The boron atom is not coplanar with this pyrazolyl ring owing to the torsion angle of $C(8) - C(9) - N(6) - B(1)$ of $165.8(4)^\circ$, showing that the ring is bent away from Br(2). No apparent hydrogen bond is found between H and Br since the closest $H \cdots Br$ distance is 3.889 Å, which is far beyond 1.41 Å for $H - Br$ bond. Some important crystallographic data and bond lengths and angles of complex (3) are listed in Table 4.10 and Table 4.12.

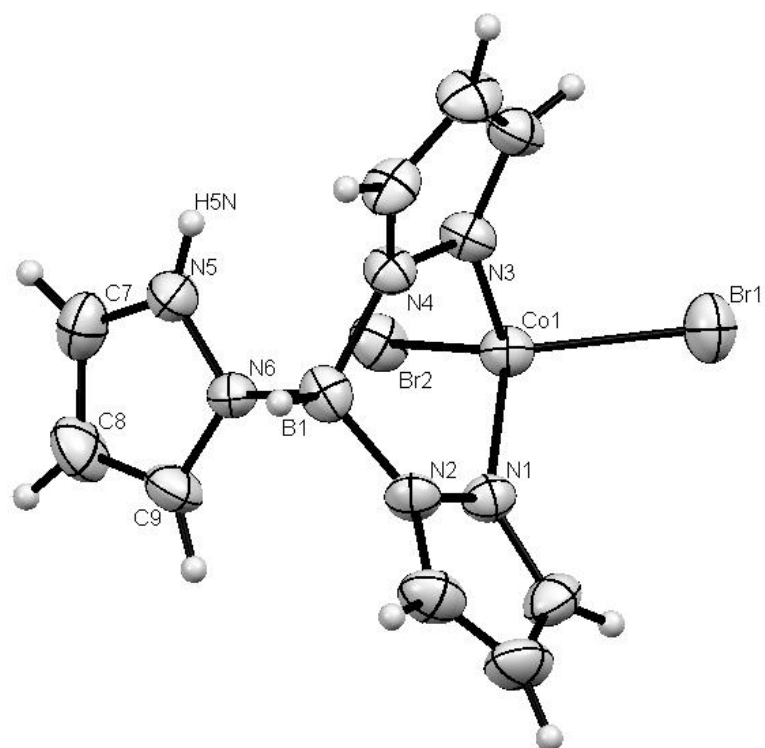


Figure 4.8.: ORTEP drawing of the crystal structure of complex (**3**) with selected atoms labeled. The thermal ellipsoids represent the probability level of 50 %.

| | |
|-----------------------------|---|
| Empirical formula | C ₉ H ₁₁ B Br ₂ Co N ₆ |
| Formula weight | 432.8 |
| Temperature | 293(2) K |
| Wavelength | 0.71073 Å |
| Crystal system, space group | Monoclinic, P 2 ₁ /c |
| Unit cell dimensions | a = 9.2706(6) Å alpha = 90 deg. b = 15.254(1) Å beta = 102.708(7) deg. c = 10.6149(8) Å gamma = 90 deg. |
| Volume | 1464.32(17) Å ³ |
| Final R indices [I > 2σ(I)] | R ₁ = 0.0415, wR ₂ = 0.0537 |
| R indices (all data) | R ₁ = 0.0793, wR ₂ = 0.0610 |

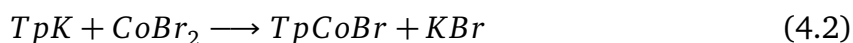
Table 4.10.: Selected crystallographic data for complex (**3**).

| Bonds | Bond lengths (Å) | Bonds | Bond angles (deg) |
|-------------|------------------|-------------------|-------------------|
| N(1)-Co(1) | 2.011(3) | N(2)-B(1)-N(4) | 112.0(4) |
| N(2)-B(1) | 1.519(6) | N(2)-B(1)-N(6) | 106.1(4) |
| N(3)-Co(1) | 2.012(3) | N(4)-B(1)-N(6) | 107.6(4) |
| N(4)-B(1) | 1.539(6) | N(1)-Co(1)-N(3) | 93.15(14) |
| N(5)-N(6) | 1.354(5) | N(1)-Co(1)-Br(1) | 110.97(11) |
| N(6)-B(1) | 1.576(6) | N(3)-Co(1)-Br(1) | 111.14(11) |
| Co(1)-Br(1) | 2.3706(8) | N(1)-Co(1)-Br(2) | 115.93(10) |
| Co(1)-Br(2) | 2.3816(8) | N(3)-Co(1)-Br(2) | 116.45(11) |
| | | Br(1)-Co(1)-Br(2) | 108.54(3) |

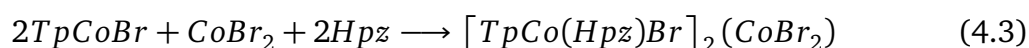
Table 4.12.: Selected bond lengths (Å) and angles (deg) for complex (3).

4.1.2.3 Discussion

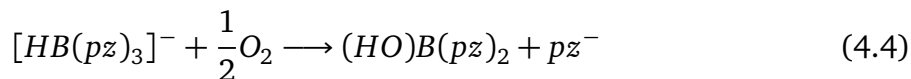
Since the tetrahedral half-sandwich $TpCoCl$ was reported to be thermodynamically unstable with respect to the more favored octahedral Tp_2Co , I attempted to prepare its bromide analogue. The reaction proves that rather than the expected tetrahedral geometry, Co(II) would prefer a coordination number of six to satisfy the octahedral geometry. Thus, $TpCoBr$ can only be an intermediate product of the metathesis reaction



and will be further transformed to other more stable compounds quickly. The most thermodynamically stable product will be Tp_2Co , in which the Co(II) ion is octahedrally coordinated by two Tp ligands resulting in the most symmetrical full sandwich structure. If the reaction 4.2 is carried out at high temperature, Tp_2Co would be the only product. However, at room temperature, a competitive reaction takes place simultaneously to give the complex (1):

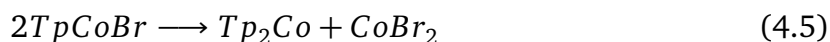


in which the free pyrazole Hpz assumedly comes from the reaction of Tp^- with a very small amount of oxygen dissolved in the solvent THF accompanied with $(HO)B(pz)_2$ as additional product:

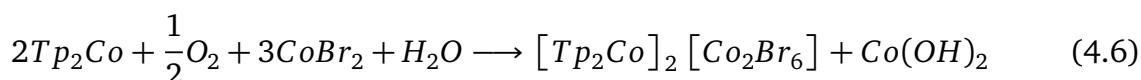


In acidic environment, pz^- will be protonated to become Hpz molecule. Nevertheless, the Equation 4.4 is only a conjectured reaction to account for the source of free pyrazole. No $(HO)B(pz)_2$ was isolated from the reaction mixture. Infrared spectroscopy and an X-ray single crystal diffraction confirmed the trinuclear structure of complex (1), of which two terminal Co(II) centers are octahedrally coordinated. The molecule can be considered as two Co ions with supporting ligands of a Tp scorpionate and a bromide respectively, which are linked by a tetrahedrally surrounded Co unit, while two pyrazoles are coordinated to complete an octahedral geometry. Comparing to the distorted square pyramidal geometry around Cu in $[TpCuCl]_2$ [90], the Tp ligand in complex (1) probably has less structural strain as it binds to Co in a more symmetric fashion.

In solution a ligand disproportionation reaction for $TpCoBr$



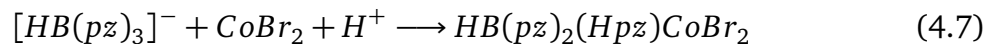
could happen; and in presence of oxygen dissolved in the solvent, Tp_2Co is oxidized to $[Tp_2Co]^+$:



giving complex (2). Although the chemistry of Tp has been already extensively investigated, reports about the $[Tp_2Co]^+$ cation are surprisingly rare [108]. Though Tp_2Co is a very chemically stable compound, only few papers related to $[Tp_2Co]^+$ are available. [23, 48, 39, 24] The ionic compound (2) has two discrete $[Tp_2Co]^+$ cations with quite similar structure, and a dinuclear Co(II) dianion rather than $[CoBr_4]^{2-}$, in agreement with the observation of Gentile and Shankoff [43], who reported the only example of $[Co_2Br_6]^{2-}$ dianion before, but didn't analyze it structurally. Hence in this work, the detailed structure of this anion is reported for the first time.

Compound (3) represents a complex, in which TpH acts as a neutral ligand donating two pairs of electrons to the metal center. It is regarded as a side-product from the preparation of the cobalt complex containing Tp ligands, having an unusual coordina-

tion mode of protonated Tp ligand. The source of the proton on Tp is unknown yet. It might come from impurities in the starting material or the solvent. So the generation of complex (3) can be expressed as



Although all of the solvents have been properly pretreated to eliminate residual amounts of water and oxygen, the oxidation of cobalt and protonation of Tp indicate that even trace amount of water and oxygen could participate in the reaction. Thus the metathesis of TpK and $CoBr_2$ is very air-sensitive. Probably it was the reason why the ligand disproportionation reaction did not happen dominantly, because partial amount of TpK was transformed to the protonated species.

4.2 Synthesis of cobalt tris(3,5-dimethyl-pyrazolyl)borate complexes

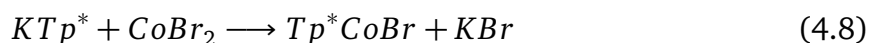
Since the attempt to prepare half-sandwich complexes from TpK and $CoBr_2$ afforded a variety of products, attention was directed towards the analogous reaction of potassium hydrotris(3,5-dimethyl-pyrazolyl)borate (Tp^*K). Unlike the unsubstituted Tp ligand, the methyl groups on the pyrazolyl 3- and 5-position of Tp^* could exert both steric and electronic influence on its reactivity, thereby leading to different products. Although the cone angle for Tp^* is relatively larger than that for Tp , the formation of stable Tp^*_2Co is still an inevitable trend during most reactions related. Thus preparation of half-sandwich $Tp^*Co - L$ complexes gained limited success because the ligand disproportionation to the full-sandwich structure dominated the reaction in most cases.

So far complexes concerning the half-sandwich $Tp^*Co - L$ structure are scarce. Marks and Ibers, et al. prepared Tp^*CoSR type of complex through addition of $NaSR$ into a mixture of Tp^*K and CoX_2 ($X = Cl, Br$) without isolation of the intermediate Tp^*CoX . [103] Another tetrahedral Co(II) Tp^* complex $Tp^*Co(NO)$ was synthesized through the reaction of $[(TMEDA)Co(NO)_2]$ $[BPh_4]$ with Tp^*K in THF at -78° by Wieghardt, et al.. [106] Besides these tetrahedral cobalt complexes, examples of five- and six-coordinated systems were also reported, [66, 100] in which the bis(μ -hydroxo)cobalt complex $(Tp^*Co)_2(\mu - OH)_2$ is of particular interest as it can be further oxidized to $(Tp^*Co)_2(\mu - O)_2$ with Co(III) centers by H_2O_2 at low temperature. [50] In most cases, the tetrahedral half-sandwich Tp^* cobalt complex with halogen as supporting ligand is of great importance for preparation of other more complicated structures, because the anionic halogen could be easily substituted by a variety of electron donors.

Thus the investigation of preparing $Tp^*Co - X$ type complexes seem to be a valuable goal.

4.2.1 Synthesis of bromo[hydrotris(3,5-dimethyl-pyrazolyl)borato]cobalt

Bromo[hydrotris(3,5-dimethyl-pyrazolyl)borato]cobalt (Tp^*CoBr) was synthesized via the metathesis reaction of KTp^* and $CoBr_2$:



When 1 equiv. KTp^* was added into a solution of 1 equiv. $CoBr_2$ in THF at room temperature, the ligand interchange happened quickly with concomitant precipitation of KBr . Removal of the solvent gave a product of blue color in 46% yield, which is stable in air and well soluble in dichloromethane and THF. Single crystals suitable for X-ray diffraction were grown from a CH_2Cl_2 solution, into which petroleum ether was diffused. HTp^*CoBr_2 (5), an analogue of complex (3), was isolated as a coproduct in addition to Tp^*CoBr (4). Tp^*CoBr shows limited stability in solution and can be oxidized to an ionic compound (6) with $[Tp_2^*Co]^+$ cation. (Figure 4.9)

4.2.1.1 Spectroscopic characterization

Characterization of complex (4)

The IR spectrum of Tp^*CoBr (4) is shown in Figure 3. The $C - H$ bond stretching from the ring is assigned at 3121 cm^{-1} while the methyl ν_{C-H} is at 2962 and 2927 cm^{-1} . The vibration at 2542 cm^{-1} arises from the $B - H$ bond stretching indicating the presence of Tp^* . The $C = C$ pyrazolyl bond stretch is seen at $\nu_{C=C} = 1540\text{ cm}^{-1}$; and the bands at 1447 , 1418 , 1388 , and 1347 cm^{-1} are due to the pyrazolyl ring stretch and CH_3 “rocking” deformation. The $C - H$ in-plane bending is observed at 1173 cm^{-1} close to the $B - N$ bond stretching of 1064 cm^{-1} . At 982 cm^{-1} one can see the pyrazolyl ring breathing, and the $C - H$ out-of-plane deformation is located at $\gamma_{C-H} = 800\text{ cm}^{-1}$. The vibration at 464 cm^{-1} is attributed to ν_{N-Co} of the complex.

The EI-MS spectrum (Figure 4.11) reveals the molecular ion peak at $m/z = 435$, whereas peaks at 356 and 340 denote the fragment ions $[M - Br]^+$ and $[M - pz^*]^+$, respectively. The isotope pattern for the molecular ion is in full agreement with the theoretical calculated value.

Since in complex (4) Co is in d^7 electronic configuration, all the $^1\text{H-NMR}$ signals are shifted towards the paramagnetic region. In the proton NMR spectrum (Figure 4.12),

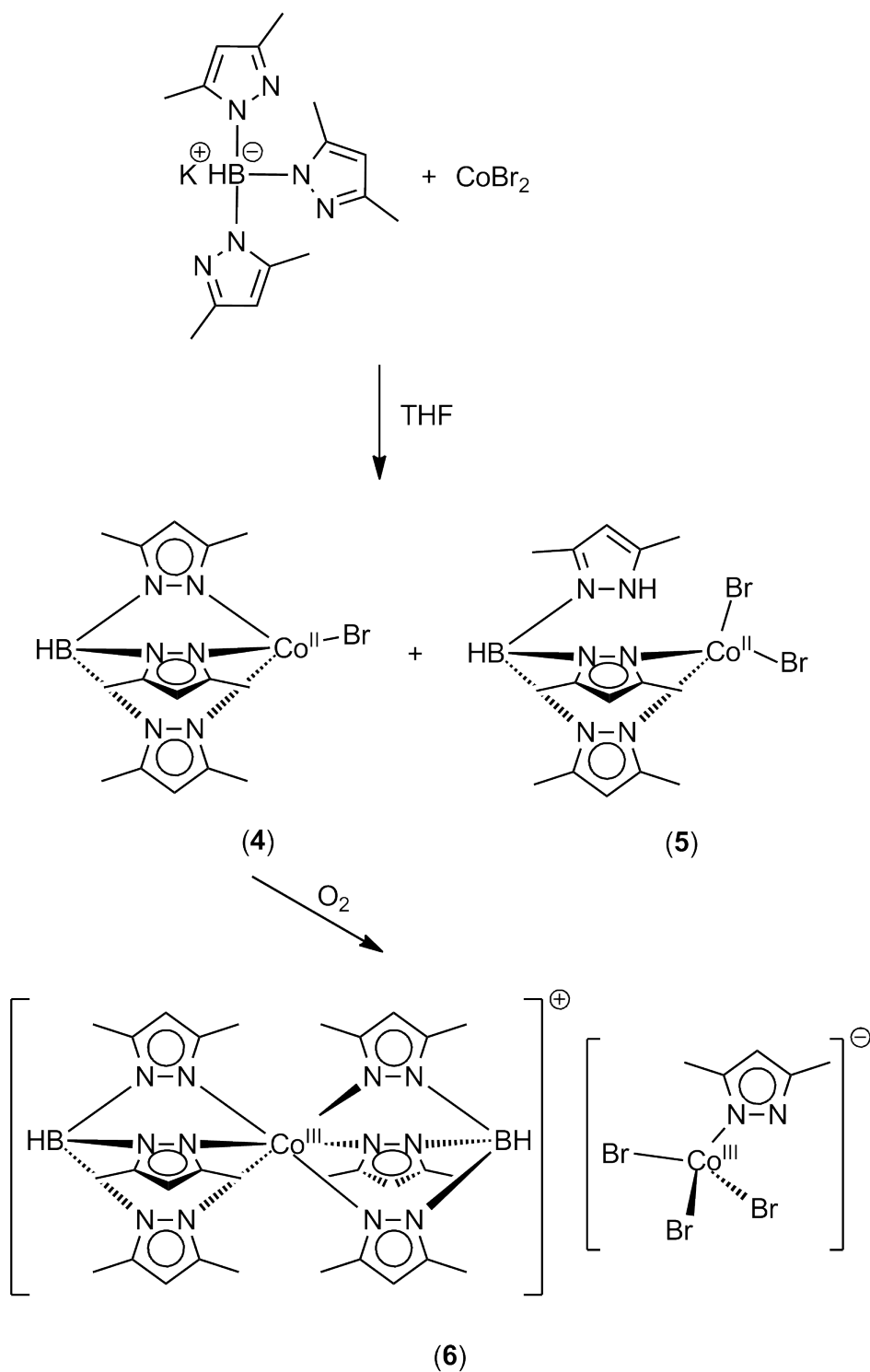


Figure 4.9.: Reaction of Tp^*K with $CoBr_2$.

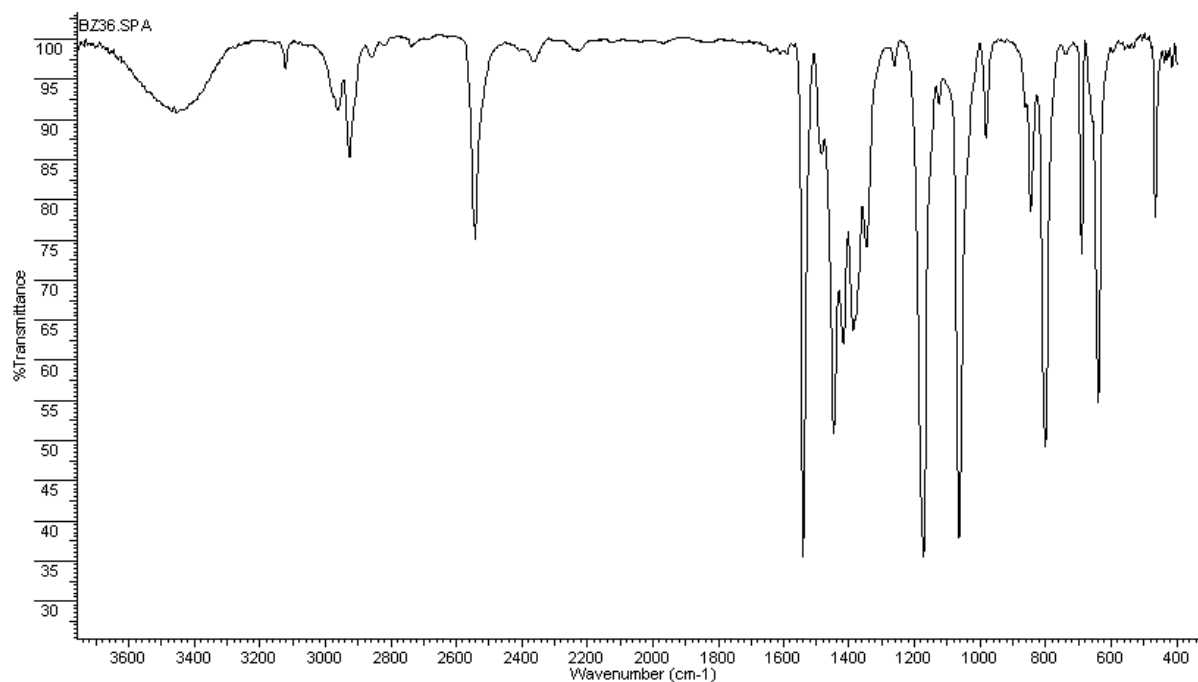


Figure 4.10.: IR spectrum of complex (4).

the methyl protons are thus found at 13.06 and 13.60 ppm, whereas the proton on the pyrazolyl ring appears at 80.30 ppm with an integral ratio of 1:6, corresponding to the proposed chemical formulation of (4). The peak at -39.74 ppm is assigned to the proton on the boron atom.

Characterization of complex (5)

The coproduct (5) was also isolated and characterized by its IR spectrum (Figure 4.13). The presence of a $N-H$ function is clearly recognized by the strong band of 3349 cm^{-1} , coming from one of the pyrazolyl rings of Tp^* being protonated. $\nu_{B-H} = 2507\text{ cm}^{-1}$ is shifted to smaller wavenumbers than that for (4) in accordance with the weaker ligand field about the cobalt center arising from the dipodal coordination. Higher frequencies are found for the $C=C$ valence stretch of the unbonded pyrazolyl ring at $\nu_{C=C} = 1630$ and 1568 cm^{-1} in addition to the pyrazolyl ring stretches at 1542, 1470, 1444, and 1415 cm^{-1} , compared to those of (4). All the other bands in the fingerprint region are consistent with those for complex (4) except the new $N-Co$ vibration bands at 566, 465, and 428 cm^{-1} .

Characterization of complex (6)

Compound (6) represents an oxidized product of (4) with two Co(III) centers. In its IR spectrum (Figure 4.14), one can observe that the ν_{B-H} stretch appears at a higher frequency (2551 cm^{-1}) than that for complex (4), indicating a strengthening of the

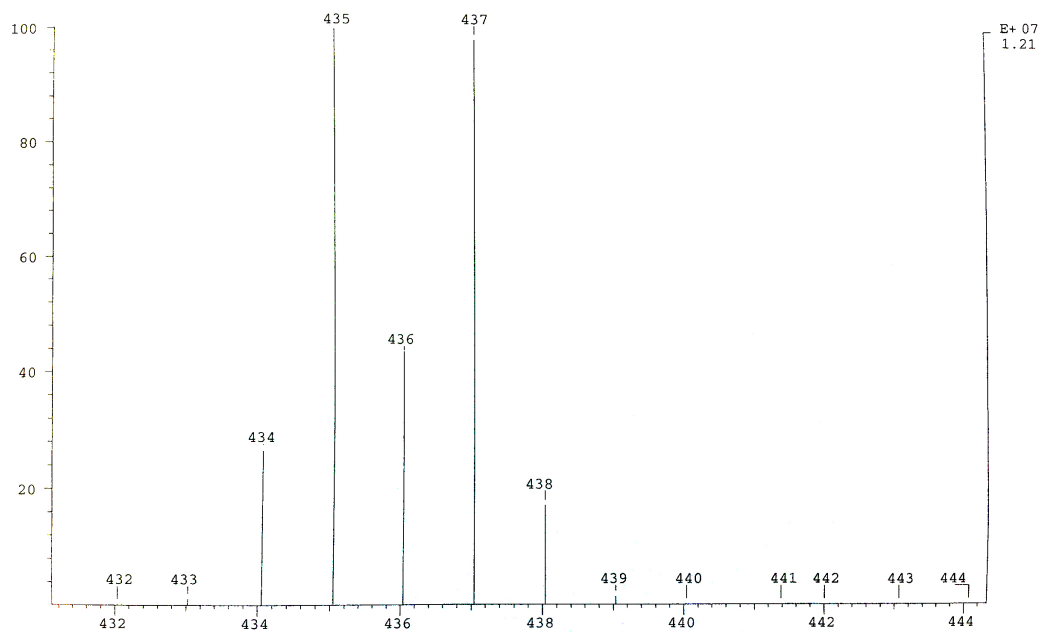
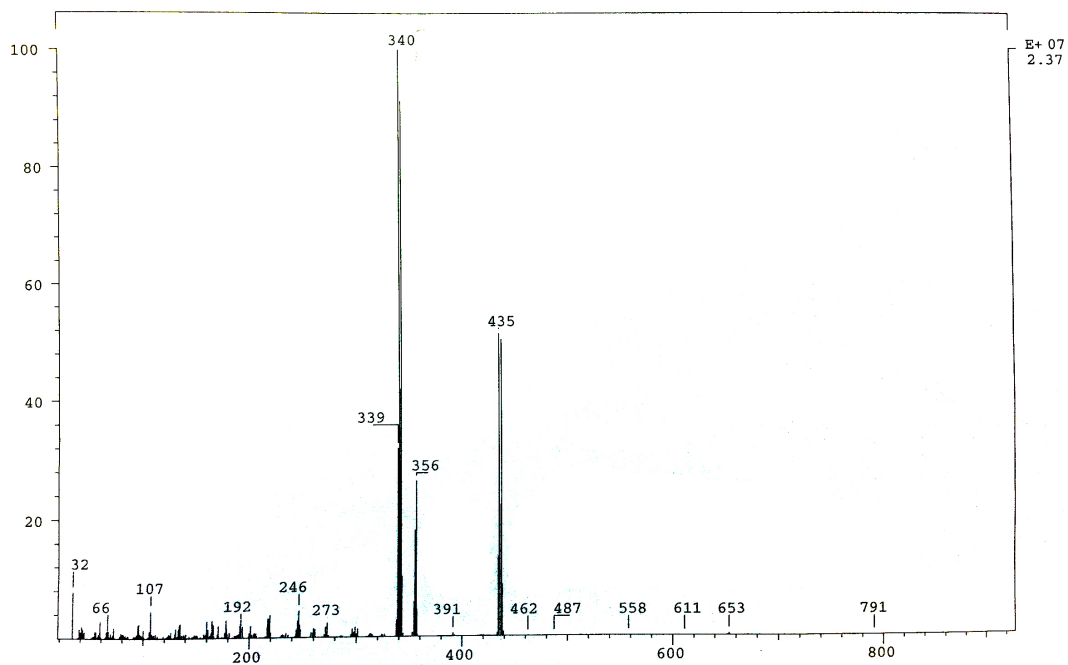


Figure 4.11.: Mass spectrum (above) and isotope pattern (bottom) of complex (4).

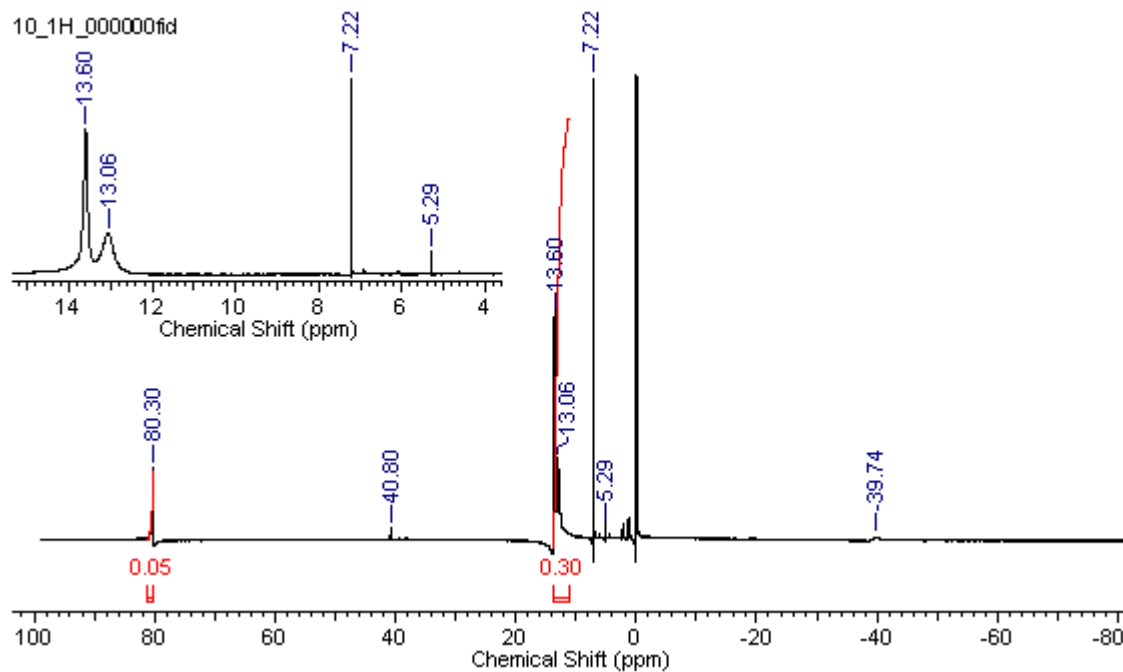


Figure 4.12.: Proton NMR spectrum of complex (4).

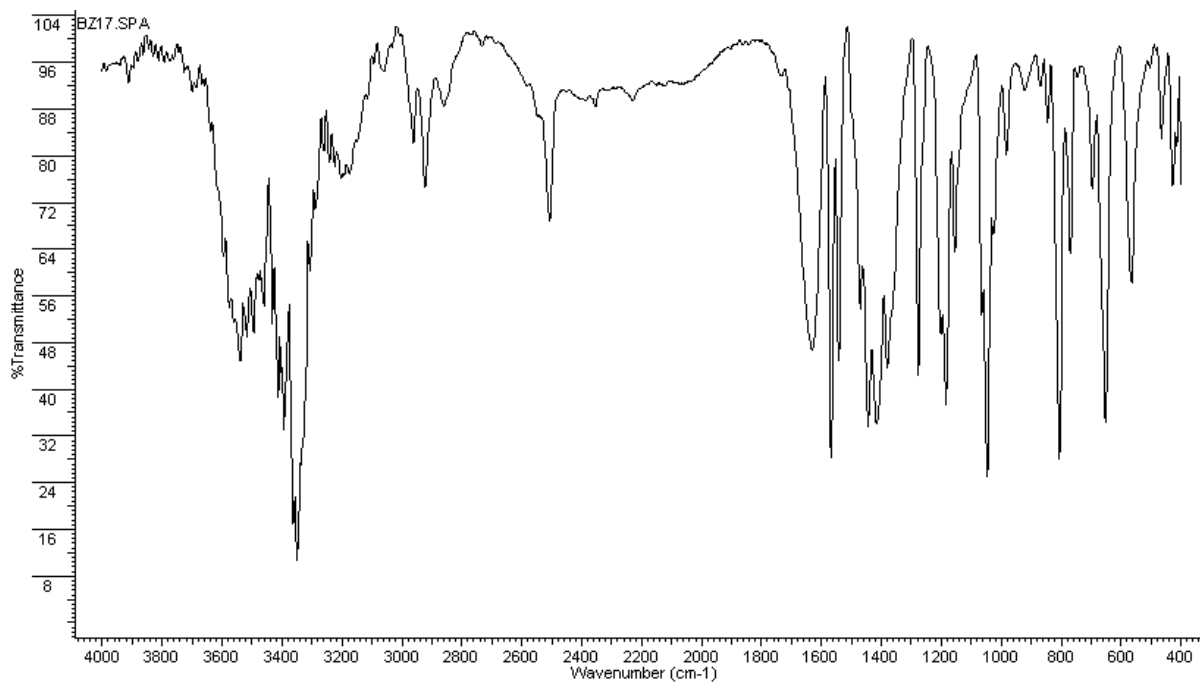


Figure 4.13.: IR spectrum of complex (5).

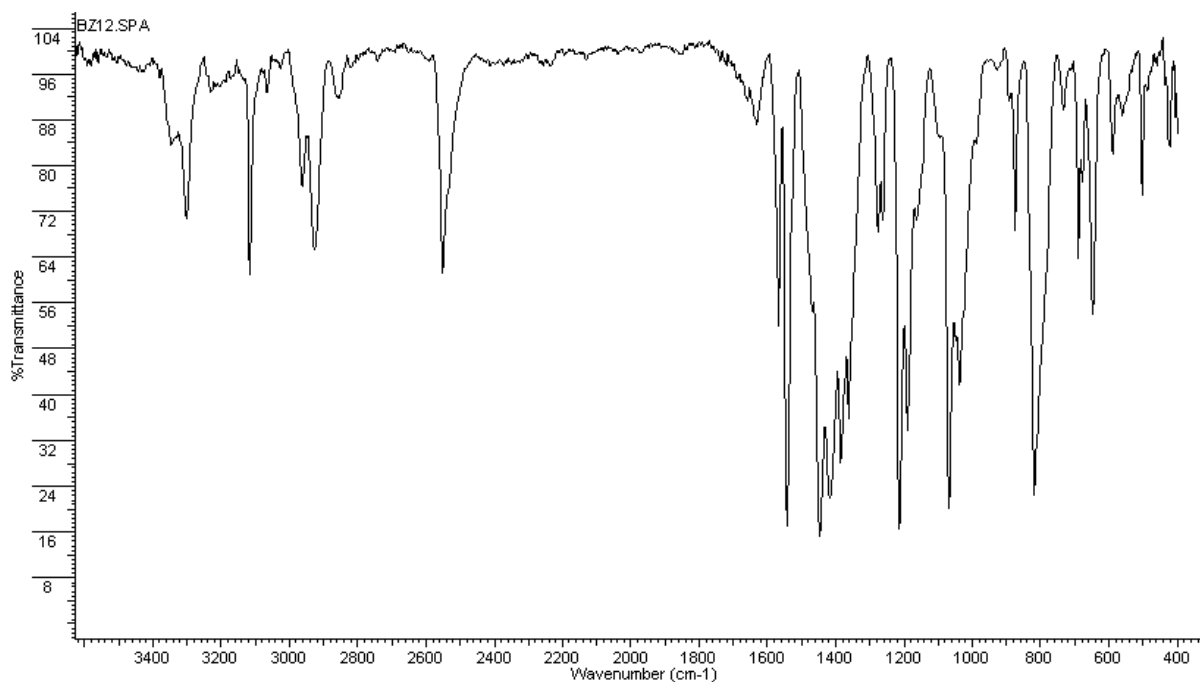


Figure 4.14.: IR spectrum of complex (6).

$B-H$ bond due to the change from Co(II) to Co(III). The methyl and pyrazolyl ν_{C-H} vibrations are found at 2926 and 3116 cm^{-1} , respectively. The pyrazolyl ring stretch locates at similar positions as for complex (4). The $\nu_{B-N} = 1069 \text{ cm}^{-1}$ is shifted 5 cm^{-1} to higher frequency compared to (4), which is another indication of the stronger coordination bond in (6). Below the $C-H$ out-of-plane bending at 819 cm^{-1} , several new $N-Co$ stretching vibrations at 588, 559, 504, 421 cm^{-1} are found.

The proton NMR spectrum of (6) was recorded in a solution of $CDCl_3$ and is presented in Figure 4.15. Two methyl proton signals are detected, in which the protons on the pyrazolyl 3-position of Tp^* are deshielded by the nitrogen coordinating the Co(III) ion and appear downfield shifted at 2.372 ppm, whereas the 5-positional protons are shown at 0.492 ppm. One can see the chemical shift for the pyrazolyl 4-positional protons at 5.61 ppm, whose peak integral gives a ratio to those for the two types of methyl protons of 1:3:3, consistent with its molecular structure. In its ^{13}C NMR spectrum (Figure 4.16), five different types of carbon atoms are present. The two kinds of methyl carbon signals at 12.18 and 13.78 ppm, are assigned to the Tp^* 5-substituted and 3-substituted methyl, respectively. The signal of the pyrazolyl 4-positional carbon of the Tp^* ligand is located at 96.19 ppm, while the carbons in the 3- and 5-position of pyrazole are observed at 110.67 and 154.97 ppm, respectively. Signals from the pyrazolyl ring of $[CoBr_3pz^*]^-$ are not distinguishable in these spectra probably because the chemical shifts of the cation and the anion are too similar to be distinguishable.

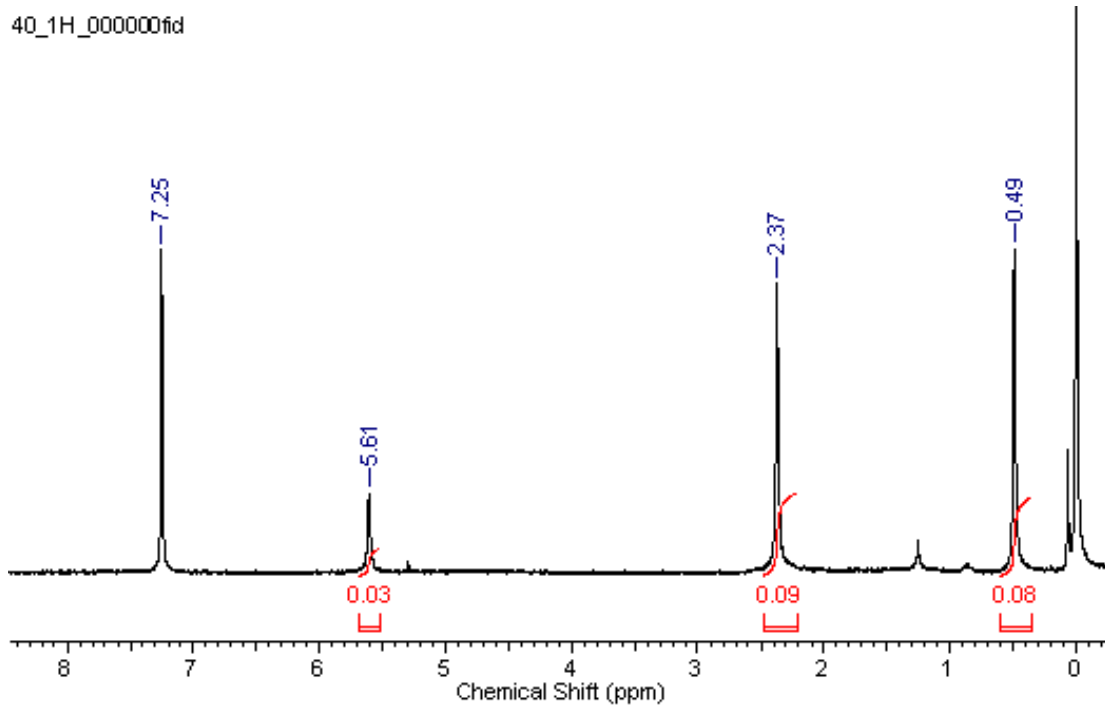


Figure 4.15.: Proton NMR spectrum of complex (6).

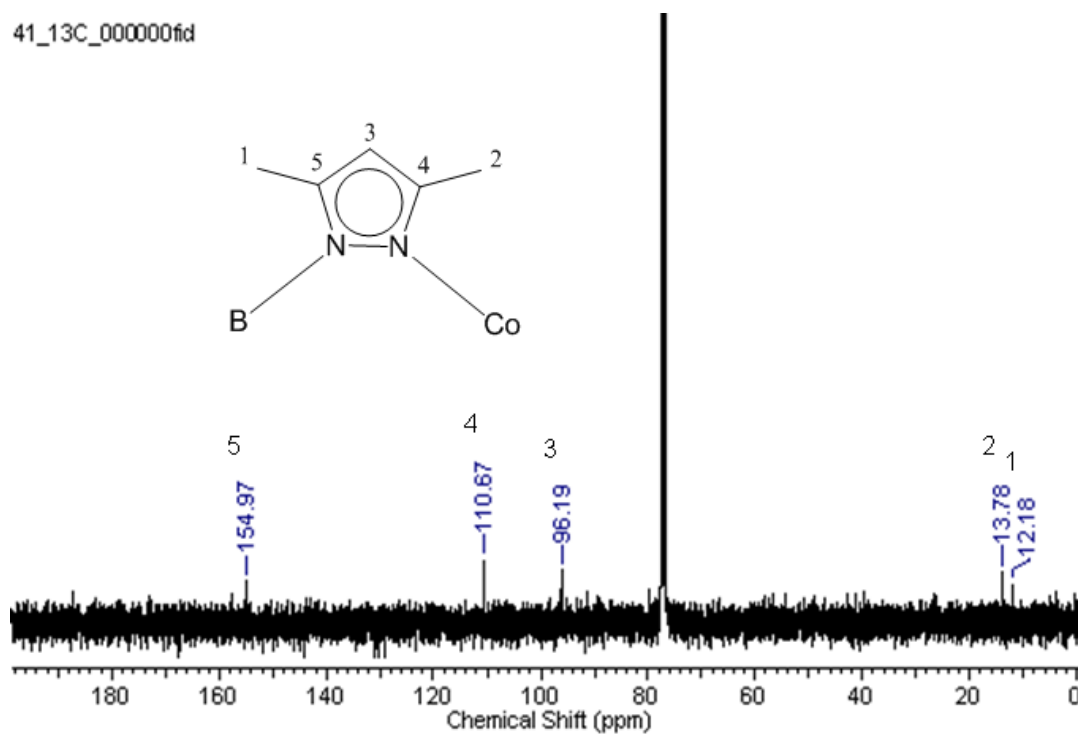


Figure 4.16.: Proton decoupled ^{13}C NMR spectrum of complex (6).

4.2.1.2 X-ray crystal structure determination

Structure of HB(3,5-Me₂ pz)₃CoBr (**4**)

A blue single crystal of (**4**) was obtained by the gas-phase diffusion of petroleum ether into a saturated solution of (**4**) in dichloromethane. The crystal was determined to belong to the orthorhombic crystal system in the space group $Pmc2_1$ with unit cell dimensions of $a = 13.2210(7)$ Å, $b = 8.1477(3)$ Å, $c = 17.679(1)$ Å. Two independent molecules coexist in an asymmetric unit. Figure 4.17 shows an ORTEP drawing of the structure. Both independent molecules display a distorted tetrahedral cobalt center and C_3 symmetry along the $B - Co$ axis. The mean $Co - N$ length is 2.001 Å, which is quite close to the values previously reported for $Tp^*Co(SC_6F_5)$ (1.99 Å) [103] and $Tp^*Co(NO)$ (2.007 Å) [106], and shorter than those for (**1**) (2.084(8) Å) and (**3**) (2.011(3) Å). The shortened bond length relates to a corresponding stronger coordinating bond between Tp^* and Co, arising from the electron releasing effect of the methyl groups. Meanwhile, from the structure scheme shown in Figure 4.17, the cobalt center is sterically shielded by the methyl groups in the 3-positions, which is presumably responsible for the retarded tendency to dimerize. [103] The average $Co - Br$ distance is 2.3324(15) Å, slightly shorter than 2.3945(17) Å for (**1**) and 2.3761(8) for (**3**), consisting with the stronger ligand field about Co. The mean $B - N$ distance of 1.557 Å is comparable to the common value of Tp^* . [103, 102] Due to the tridentate chelation, the tetrahedral coordination geometry is compressed along the $B - Co$ vector leaving a mean $NCoN = 94.2^\circ$. This value exceeds that for $Tp^*Co(SC_6F_5)$ (92.2°) moderately, probably because of greater steric repulsion between Tp^* and $-SC_6F_5$. This lateral compression of structure is also seen from the expansion of av. NBN from 102° for $Tp^*Co(SC_6F_5)$ to $108.7(5)^\circ$ for (**4**). The B, Co, and Br are almost in a line with av. $BCoBr = 178.43^\circ$, indicating that the tetrahedral geometry is merely umbrella distorted. Table 4.16 and Table 4.14 show the basic crystallographic parameters and some important bond lengths and angles of complex (**4**).

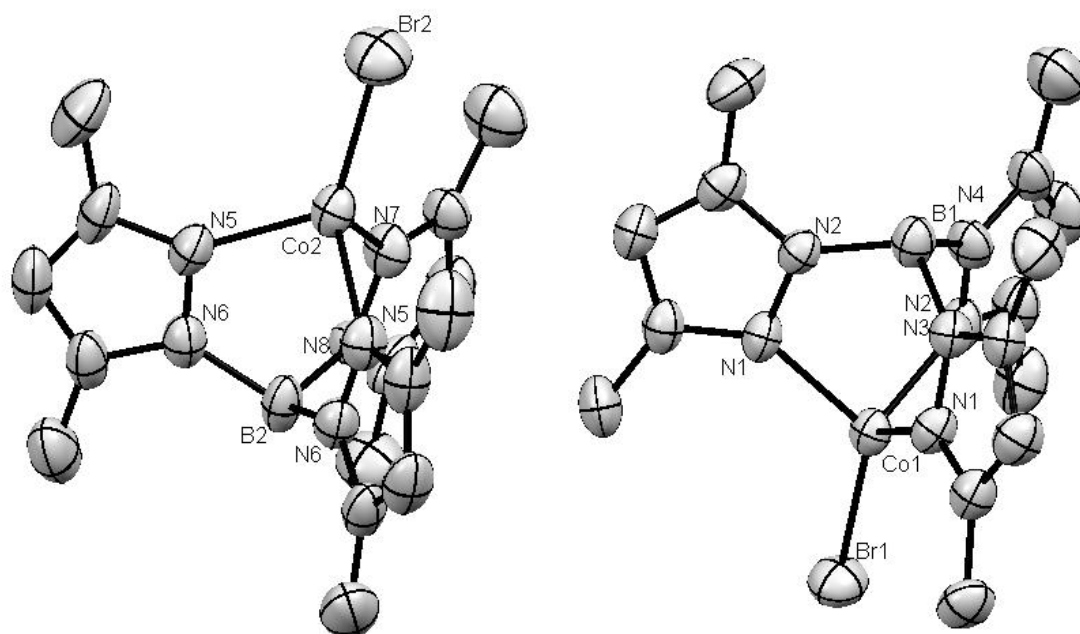


Figure 4.17.: ORTEP drawing of the crystal structure of complex (**4**) with selected atoms labeled. The thermal ellipsoids represent the probability level of 50 %. All hydrogen atoms are omitted for clarity.

| | |
|-----------------------------|---|
| Empirical formula | C ₁₅ H ₂₂ B Br Co N ₆ |
| Formula weight | 436.04 |
| Temperature | 293(2) K |
| Wavelength | 0.71073 Å |
| Crystal system, space group | Orthorhombic, P m c 21 |
| Unit cell dimensions | a = 13.2210(7) Å alpha = 90 deg. b = 8.1477(3) Å beta = 90 deg. c = 17.679(1) Å gamma = 90 deg. |
| Volume | 1904.40(16) Å ³ |
| Final R indices [I > 2σ(I)] | R1 = 0.0457, wR2 = 0.0879 |
| R indices (all data) | R1 = 0.0703, wR2 = 0.0972 |

Table 4.14.: Selected crystallographic data for complex (**4**).

| Bonds | Bond lengths (Å) | Bonds | Bond angles (deg) |
|-------------|------------------|-------------------|-------------------|
| B(1)-N(2) | 1.551(7) | N(2)#1-B(1)-N(2) | 110.2(6) |
| B(1)-N(4) | 1.574(11) | N(2)-B(1)-N(4) | 107.3(4) |
| Br(1)-Co(1) | 2.3377(14) | N(1)#1-Co(1)-N(1) | 92.6(2) |
| Co(1)-N(1) | 1.996(4) | N(1)-Co(1)-N(3) | 94.72(17) |
| Co(1)-N(3) | 2.008(6) | N(1)-Co(1)-Br(1) | 122.69(12) |
| B(2)-N(8) | 1.546(11) | N(3)-Co(1)-Br(1) | 121.72(19) |
| B(2)-N(6) | 1.561(7) | N(8)-B(2)-N(6) | 108.9(5) |
| Br(2)-Co(2) | 2.3270(16) | N(6)-B(2)-N(6)#2 | 109.5(6) |
| Co(2)-N(5) | 1.998(4) | N(5)#2-Co(2)-N(5) | 92.9(2) |
| Co(2)-N(7) | 2.012(5) | N(5)-Co(2)-N(7) | 95.12(18) |
| | | N(5)-Co(2)-Br(2) | 123.24(13) |
| | | N(7)-Co(2)-Br(2) | 119.8(2) |

Table 4.16.: Selected bond lengths (Å) and angles (deg) for complex (4).

Structure of HB(3,5-Me₂pz)₂(3,5-Me₂pzH)CoBr₂ (5)

In the molecular unit of complex (5) (Figure 4.18), only two of the pyrazolyl rings of *Tp*^{*} donate electrons to Co center, leaving the last ring protonated with the proton pointing at a coordinating bromide. The molecule crystallized in the monoclinic system, space group *P21/n*. The average *N – Co* bond length in (5) of 2.002 Å is almost the same as that for (4); and the mean *Br – Co* distance is 2.362 Å, close to values observed commonly. Just like complex (4), the tetrahedral coordination geometry about Co is laterally compressed along the *Co(1) – Br(2)* vector resulting in a similar reduced *N(1) – Co(1) – N(6)* angle of 95.37°. As is shown in Figure 4.18, the *Co(1) – Br(1)* bond points to the same side of the six-membered chelate ring as the unbonded pyrazolyl ring; and the Br(1) atom locates in the vicinity of the pyrazolyl proton with *Br(1)···H(4A)* distance of 2.494 Å. Although the *Br(1)···H(4A)* distance is too large to satisfy a hydrogen bond, the attraction between both atoms makes the Br(1) bent more towards the *Tp*^{*} ligand resulting in an average *BrCoN* = 108.22° comparing to that for Br(2) of 114.34°. If a detailed comparison of the *B – N* bond lengths of (4) and (5) is made, one could notice that the *B(1) – N(3)* distance for the unbonded ring in (5) (1.587 Å) is longer than the mean *B – N* bond length of (4) (1.557 Å), whereas those for the other bonded rings have an relatively shorter average value of 1.532 Å, representing the structural feature of this unusual dipodal *HTp*^{*} chelate compound as a side-product from the preparation of (4). *N(2)B(1)N(5)* equals to 114.01°, which is larger than the average *N – B – N* angle of (4), mainly because of the less steric strain

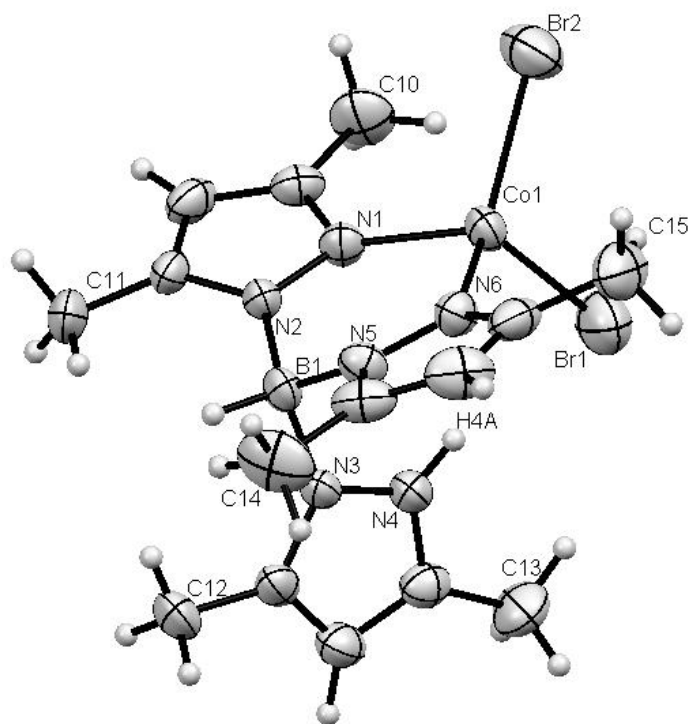


Figure 4.18.: ORTEP drawing of the crystal structure of complex (5) with selected atoms labeled. The thermal ellipsoids represent the probability level of 50 %.

in the molecule. Some important bond lengths and angles of complex (5) are listed in Table 4.20; and the basic crystallographic data are summarized in Table 4.18.

| | |
|-----------------------------|---|
| Empirical formula | C ₁₅ H ₂₃ B Br ₂ Co N ₆ |
| Formula weight | 516.95 |
| Temperature | 293(2) K |
| Wavelength | 0.71073 Å |
| Crystal system, space group | Monoclinic, P2 ₁ /n |
| Unit cell dimensions | a = 10.9103(4) Å alpha = 90 deg. b = 14.3221(6) Å beta = 102.246(4) deg. c = 13.6442(6) Å gamma = 90 deg. |
| Volume | 2083.51(15) Å ³ |
| Final R indices [I > 2σ(I)] | R1 = 0.0652, wR2 = 0.1759 |
| R indices (all data) | R1 = 0.0975, wR2 = 0.1997 |

Table 4.18.: Selected crystallographic data for complex (5).

| Bonds | Bond lengths (Å) | Bonds | Bond angles (deg) |
|-------------|------------------|-------------------|-------------------|
| N(1)-Co(1) | 2.000(5) | N(1)-Co(1)-N(6) | 95.4(2) |
| N(2)-B(1) | 1.532(9) | N(1)-Co(1)-Br(2) | 112.49(15) |
| N(3)-B(1) | 1.587(9) | N(6)-Co(1)-Br(2) | 116.17(17) |
| N(5)-B(1) | 1.531(9) | N(1)-Co(1)-Br(1) | 107.90(17) |
| N(6)-Co(1) | 2.004(5) | N(6)-Co(1)-Br(1) | 108.57(16) |
| Co(1)-Br(2) | 2.3595(12) | Br(2)-Co(1)-Br(1) | 114.53(5) |
| Co(1)-Br(1) | 2.3649(13) | N(5)-B(1)-N(2) | 114.0(5) |
| | | N(5)-B(1)-N(3) | 109.0(5) |
| | | N(2)-B(1)-N(3) | 109.4(5) |

Table 4.20.: Selected bond lengths (Å) and angles (deg) for complex (5).

Structure of $[[\text{HB}(\text{3,5-Me}_2\text{pz})_3]_2\text{Co}][\text{CoBr}_3(\text{3,5-Me}_2\text{pz})]$ (6)

Complex (6) is an ionic compound and crystallizes in the monoclinic system and space group $P2_1/m$. An ORTEP scheme is shown in Figure 4.19. From its crystal structure, the compound consists of a cation and an anion; both ions contain cobalt coordination centers, one of which is octahedrally coordinated, whereas the other one has a distorted tetrahedral geometry. The Co(1)-centered cation has a C_3 axis along the $B \cdots \text{Co} \cdots B$ axis. The mean $N - \text{Co}(1)$ distance is 1.940 Å, which is significantly shorter than the respective distance in (4) (2.001 Å) and (5) (2.002 Å). It may be attributed to the smaller ionic radius of Co^{3+} than that of Co^{2+} . Additionally, the one more positive charge on Co brings about a stable 18- e^- configuration about Co. In consequence, the average $N - \text{Co} - N$ angle is increased from 86.8° for Tp_2^*Co to 91.1° for (6), and $\text{Co} \cdots B$ distance is reduced from 4.29 Å to 3.01 Å, [80] manifesting a more regular and compact octahedral coordination geometry about Co^{3+} in (6). In parallel, the mean $N - B$ bond length, which is exactly consistent with that of (2), is concomitantly shortened from 1.557 Å for (4) to 1.535(7) Å for (6). Another interesting observation arises from the arrangement of methyl groups on the pyrazolyl 3-position. The six groups locate around the coordination center in a circle, thereby providing a good shielding of the central cobalt from contacts to other ligands. Notice that the average $Br - \text{Co}(2)$ bond distance of 2.398 Å of the anion is even longer than those of (2) (2.367 Å), (3) (2.376 Å), (4) (2.332 Å), and (5) (2.362 Å), although the cobalt atom has one more positive charge. This observation could be a consequence of both steric and electrostatic repulsions between the binding Br^- -ions. By this means the three negative-charged soft bromide ligands around the Co(2) can maintain a stable structural configuration. Considering the ligands binding to these tetrahedral cobalt centers together with their mean $Br - \text{Co}$ distances, one can also deduce that the $Br - \text{Co}$ bond strength is to some extent dependent on the strength of ligand field exerted by the chelate σ -type pyrazolyl donors. A stronger ligand field stabilized by the chelate pyrazolyl ligand could bring about a shorter $Br - \text{Co}$ bond distance. For there is only one pyrazolyl ring coordinating to the cobalt ion in the anion of (6), the lack of chelate effect results in a relatively long $Br - \text{Co}$ bond, representing a weak ligand field. This conjecture is also supported by the longer $N(7) - \text{Co}(2)$ bond of (6) (2.036(7) Å) than the average values of (3) (2.011(3) Å), (4) (2.001 Å), and (5) (2.002 Å). The tetrahedral geometry suffers an off-axis distortion approaching a trigonal pyramid with three bromides as base and the apex of nitrogen bent toward the Br(2) in an angle $N(7)\text{Co}(2)\text{Br}(2)$ of 98.2(2)°. Both the pyrazolyl ring and the $\text{Co}(2) - \text{Br}(2)$ bond locate in the mirror plane of the anion. Some important bond lengths and angles of complex (6) are listed in Table 4.24, and Table 4.22 shows its basic crystallographic data.

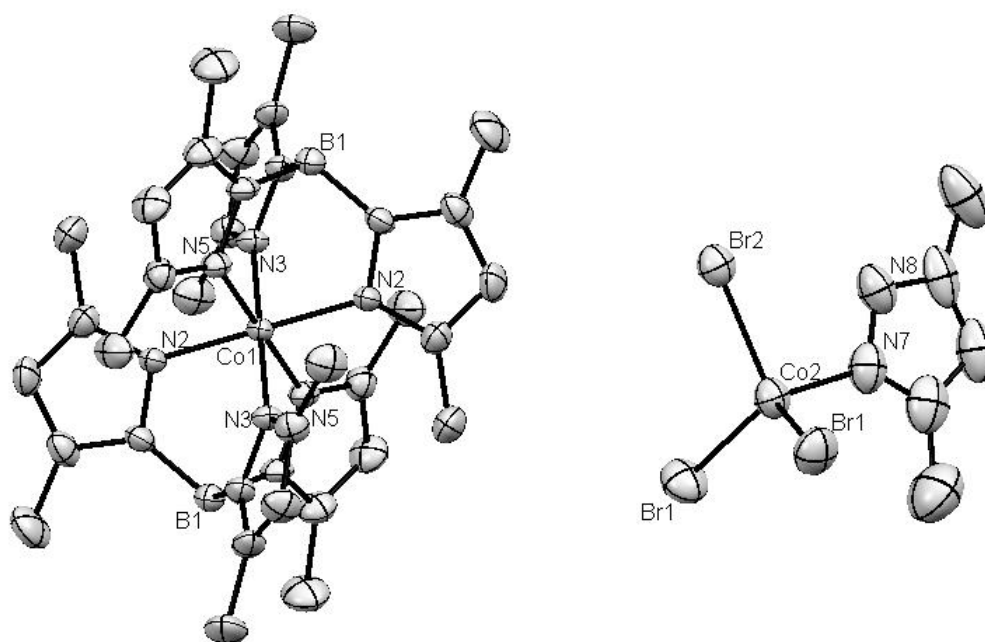


Figure 4.19.: ORTEP drawing of the crystal structure of complex (6) with selected atoms labeled. The thermal ellipsoid represent the probability level of 50 %. All hydrogen atoms are omitted for clarity.

| | |
|-----------------------------|---|
| Empirical formula | C ₃₀ H ₄₄ B ₂ Co N ₁₂ , C ₅ H ₇ Br ₃ Co N ₂ |
| Formula weight | 1047.11 |
| Temperature | 294(2) K |
| Wavelength | 0.71073 Å |
| Crystal system, space group | Monoclinic, P2 ₁ /m |
| Unit cell dimensions | a = 8.8856(4) Å alpha = 90 deg. b = 23.8580(10) Å beta = 92.329(4) deg. c = 10.5237(5) Å gamma = 90 deg. |
| Volume | 2229.10(17) Å ³ |
| Final R indices [I > 2σ(I)] | R1 = 0.0623, wR2 = 0.1064 |
| R indices (all data) | R1 = 0.1116, wR2 = 0.1232 |

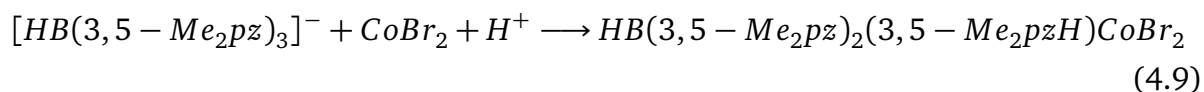
Table 4.22.: Selected crystallographic data for complex (6).

| Bonds | Bond lengths (Å) | Bonds | Bond lengths (Å) |
|-------------------|-------------------|---------------------|-------------------|
| B(1)-N(4) | 1.527(7) | Co(1)-N(5) | 1.939(4) |
| B(1)-N(6) | 1.538(7) | Co(1)-N(2) | 1.941(4) |
| B(1)-N(1) | 1.540(7) | Co(1)-N(3) | 1.941(4) |
| Br(1)-Co(2) | 2.3809(9) | Co(2)-N(7) | 2.036(7) |
| Br(2)-Co(2) | 2.4331(15) | | |
| Bonds | Bond angles (deg) | Bonds | Bond angles (deg) |
| N(4)-B(1)-N(6) | 106.9(4) | N(2)-Co(1)-N(3)#1 | 88.96(16) |
| N(4)-B(1)-N(1) | 108.0(4) | N(5)#1-Co(1)-N(3) | 88.83(16) |
| N(6)-B(1)-N(1) | 107.6(4) | N(5)-Co(1)-N(3) | 91.17(16) |
| N(5)#1-Co(1)-N(5) | 180.0(2) | N(2)-Co(1)-N(3) | 91.04(16) |
| N(5)#1-Co(1)-N(2) | 89.01(16) | N(3)#1-Co(1)-N(3) | 180.0(2) |
| N(5)-Co(1)-N(2) | 90.99(16) | N(7)-Co(2)-Br(1) | 110.03(11) |
| N(5)-Co(1)-N(2)#1 | 89.01(16) | Br(1)-Co(2)-Br(1)#2 | 115.26(6) |
| N(2)-Co(1)-N(2)#1 | 180.0(3) | N(7)-Co(2)-Br(2) | 98.2(2) |
| N(5)-Co(1)-N(3)#1 | 88.83(16) | Br(1)-Co(2)-Br(2) | 111.02(4) |

Table 4.24.: Selected bond lengths (Å) and angles (deg) for complex (6).

4.2.1.3 Discussion

Methyl groups on the 3- and 5-position of the pyrazolyl ring in *Tp* can exert inductive effects through hyperconjugation to the ring to make the N-donor more electron rich. Meanwhile, comparing to the unsubstituted *Tp*, the *Tp*^{*} ligand is more sterically demanding leading to larger steric hindrance than *Tp* for building a molecule. The reaction between *Tp*^{*}*K* and *CoBr*₂ illustrated these influences of the methyl groups, in a way that the electron richer nitrogen facilitates a stronger tetrahedral ligand field making the tetrahedral *Tp*^{*}*CoBr* (4) stable and separable; in the mean time formation of a dimeric structure like [*TpCuCl*]₂ [90] was precluded due to the shielding effect of the 3-methyl groups. [103] As is in the case of reaction 4.7, a side-product to the tripodal (4), *HB*(3,5-*Me*₂*pz*)₂(3,5-*Me*₂*pzH*)*CoBr*₂ (5), was isolated as well, which resulted from the reaction:



Nevertheless, compared to the crystal structure of (3), the unbonded pyrazolyl ring of (5) is rotated by ca. 90° along its *B* – *N* axis with the protonated nitrogen pointing

to one of the bromides, which is much closer to the structural feature of Tp^* in the tridentate coordination geometry; the distance between this free nitrogen and the cobalt center is reduced from 3.858 Å for (3) to 3.556 Å for (5). This new configuration is most probably due to the steric influence from the methyl substituents on the pyrazolyl ring. Repulsion between the methyl groups is thereby minimized by the almost parallel arranged $C - CH_3$ bonds, which facilitates a potential formation of $H \cdots Br$ hydrogen bonds.

A comparison of infrared $B - H$ stretching frequencies of the scorpionate complexes (1) to (6) so far prepared and their corresponding mean $Co - N$ bond lengths as well as the mean N-B-N angles are listed in Table 4.25. For hydrotris(pyrazolyl)borate complexes, the ν_{B-H} stretching frequencies in the IR spectrum are very sensitive to changes in coordination mode as well as the underlying alterations of the electronic distribution and configuration within the whole molecule [28]. Upon coordination to metal centers, a gradual change in the orbital hybridization of the boron atom of Tp^x from sp^3 to sp^2 can be observed, considering that the frequency of $B - H$ bond stretch is only related to the content of the s -component of the hybridized orbital of boron. Increasing ν_{B-H} frequencies indicate the hybridized orbital containing more s -component resulting in a stronger $B - H$ bond, which is due to molecular steric requirements and the overall electronic charge distribution due to the coordination to a metal ion. Therefore the three $B - N$ bonds would manifest two different classes of bond lengths, because one of them must have more p -orbital contributions compared to the other two bonds containing more hybridized orbital. Also the value of angle NBN would tend to be more close to 90° . These trends one can observe from the structure parameters of complex (4) and (5), in which the $B(1) - N(4)$ bond length of (4) (both are 1.574(11) Å) is substantially different from another two B-N bonds (1.551(7) Å) of the same boron, so is for (5) (1.587(9) Å for $B(1) - N(3)$ vs. 1.531(9) Å for $B(1) - N(5)$ and 1.532(9) Å for $B(1) - N(2)$). The ν_{B-H} of (4) at 2542 cm^{-1} is 35 cm^{-1} larger than that of (5), in agreement with its smaller av. NBN of 108.7° in comparison to 110.8° in (5), which most probably arises from the stronger tripodal coordination bond in (4) compared with the dipodal coordination in (5). The observation that the $B - H$ stretching absorption of Tp^x compound is correlated with its structural feature determined by the coordinating behavior and the substituents of Tp^x ligand is also supported by a 13 cm^{-1} higher frequency shift of ν_{B-H} of (1), with respect to the $B - H$ stretching frequency of Tp_2Co . This discrepancy is also in accordance with the differences in their av. $N - B - N$ angles of 1.2° (Table 4.25), accompanied by 0.04 Å shorter in bond length for (1), demonstrating that the orbital sp^3 - sp^2 transition of the boron atom of Tp is more severe in (1) than in Tp_2Co , which is attributed to the tighter coordination of Tp to Co in (1) than in Tp_2Co ; and by the same comparison between (4), (5) and (6), respectively. If one

| complex | ν_{B-H} (cm ⁻¹) | \bar{d}_{Co-N} (Å) | $N\bar{B}N$ (°) |
|-------------------------------|---------------------------------|----------------------|-----------------|
| Tp_2Co | 2464 [28] | 2.124 [80] | 108.9 [19] |
| $[TpCo(Hpz)]_2CoBr_4$ (1) | 2477 | 2.084 | 107.7 |
| $[Tp_2Co]_2[Co_2Br_6]$ (2) | 2532 | 1.926 | 106.4 |
| $[Tp_2Co]Cl$ | 2549 [28] | - | - |
| $[Tp_2Co][PF_6]$ | 2518, 2530 [48] | 1.925 [48] | - |
| Tp_2^*Co | 2506 [28] | 2.138 [80] | - |
| Tp^*CoBr (4) | 2542 | 2.001 | 108.7 |
| $HB(pz^*)_2(Hpz^*)CoBr_2$ (5) | 2507 | 2.002 | 110.8 |
| $[Tp_2^*Co][CoBr_3pz^*]$ (6) | 2551 | 1.940 | 107.5 |

Table 4.25.: Comparison of infrared $B - H$ stretches, average $Co - N$ distances, and average values of NBN of some Tp and Tp^* complexes.

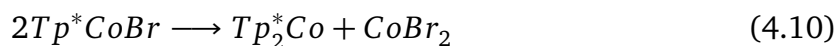
compares the data for a pair of analogues differing from the scorpionate ligands, for instance $[Tp_2Co]^+$ and $[Tp_2^*Co]^+$, a contradiction that the latter has higher frequency of ν_{B-H} but larger av. NBN is found, whose av. $Co - N$ distance is also longer. A competition between the steric and electronic influences of substituted methyl group is referred to explanations for such complexity, that the inductive effect favors electron donation of the nitrogen while the bulky substituents also give steric hindrance to prevent a ligand from approaching metal center too closely. These two contrary influences exert a net effect on the stability of the individual complex. Apparently, in the case of Tp_2Co and Tp_2^*Co , the steric influence dominates the formation of the molecule that Tp_2Co has a stronger ligand field strength, which has been confirmed by De Alwis and Schultz with electronic spectroscopy. [28] The larger ν_{B-H} of Tp_2^*Co therefore arises from the inductive effect of the methyl groups on the 5-position of the pyrazolyl rings. Table 4.26 shows an extended comparison of their structural parameters. Corresponding to the elongated $Co - N$ distance of Tp_2^*Co , its average intraligand $N \cdots N$ distance and $N - Co - N$ bite angle are both increased, representing a lateral expansion for Tp^* to create space for the methyl substituents; nevertheless, two Tp^* ligands get closer to each other than two Tp ligands, which is represented by the decreased $Co \cdots B$ and interligand $N \cdots N$ distance of Tp_2^*Co with respect to Tp_2Co , probably for a relatively stable structural conformation minimizing the methyl-methyl steric repulsion.

The $Co(II)$ of Tp^*CoBr (4) with seven electrons in its valence orbital was oxidized to d^6 $Co(III)$ when a solution of (4) in dichloromethane got in contact with air. The structure changed from tetrahedral coordination geometry to a more symmetric octahedral geometry with two identical Tp^* ligands. The resulting compound (6) consists of $[Tp_2^*Co]^+$ cation and $[CoBr_3pz^*]^-$ anion, in which both cobalt atoms are in +3 oxidation state. This transformation shows that even at room temperature, (4) is reactive in solution.

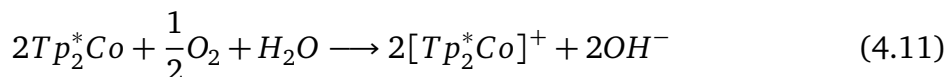
| complex | Co – N (Å) | Co···B (Å) | r _{N...N} (intra) (Å) | r _{N...N} (inter) (Å) | NCoN (°) |
|--|------------|------------|--------------------------------|--------------------------------|----------|
| <i>Tp</i> ₂ Co | 2.124 | 4.35 | 2.89 | 3.13 | 85.5 |
| [<i>Tp</i> ₂ Co] ⁺ | 1.926 | 3.07 | 2.71 | 2.74 | 89.3 |
| <i>Tp</i> ₂ *Co | 2.138 | 4.29 | 2.93 | 3.11 | 86.8 |
| [<i>Tp</i> ₂ *Co] ⁺ | 1.940 | 3.01 | 2.77 | 2.72 | 91.1 |

Table 4.26.: Comparison of selected structural parameters for *Tp*₂Co, [*Tp*₂Co]⁺ (**2**), *Tp*₂*Co, and [*Tp*₂*Co]⁺ (**6**). Data for *Tp*₂Co and *Tp*₂*Co are from [80].

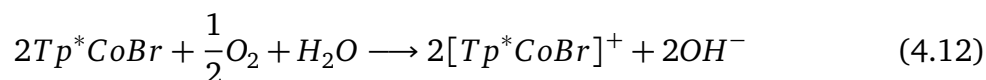
In dichloromethane, the half-sandwich complex can disproportionate (Reaction 4.10) if ample reaction time is provided.



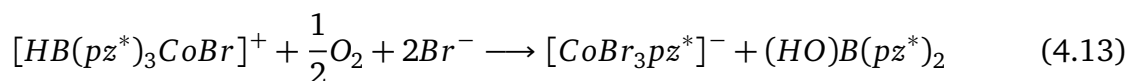
And the neutral octahedral product was finally oxidized to [*Tp*₂*Co]⁺ in solution:



In addition, the Co(II) ion in (**4**) is also prone to be oxidized under conditions of oxygen- and moisture-enriched environment in solution as described in Equation 4.14:



In presence of oxygen and water, the cation [*Tp**CoBr]⁺ is unstable. Providing that the anion [*CoBr*₃*pz**][−] of (**6**) has a separated pyrazolyl group, a *B* – *N* splitting reaction induced by *Co*³⁺ could happen, during which the *Tp*[−] unit was oxidized. A supposed reaction mechanism is schemed in Figure 4.20 (Equation 4.13)



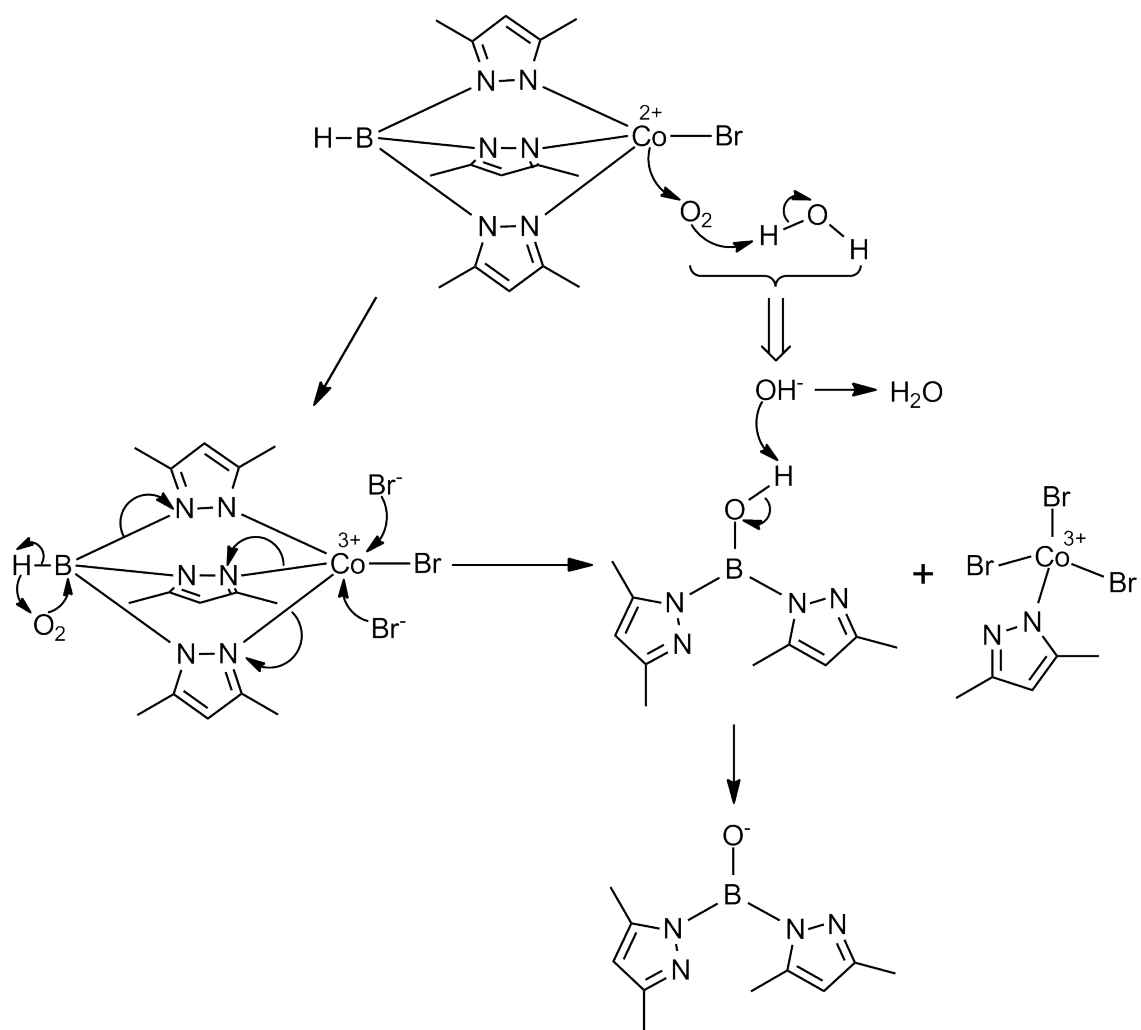
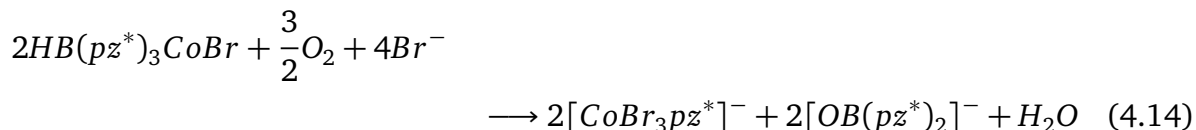
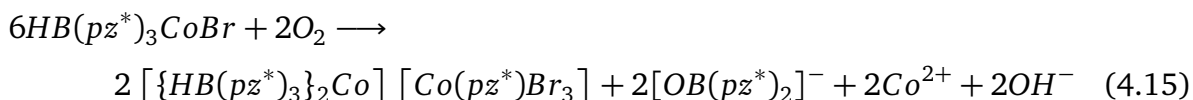


Figure 4.20.: Co^{3+} induced B-N splitting.

where the acid $(HO)B(pz^*)_2$ could undergo neutralization reaction with the hydroxyl anion released from Equation 4.12. Therefore the oxidation of Tp^*CoBr can be written as



In consideration of the ligand disproportionation reaction and the following oxidation of (4) (Equation 4.10, 4.11), one can observe a net consequence composed of two different oxidative pathways of Tp^*CoBr , which respectively afforded the cation and anion of (6). The whole oxidation along with the $B - N$ splitting inside Tp^* can be written as



where the dication Co^{2+} might exist in $Co(OH)_2$ form because bluish-green powders were found surrounding the crystals of (6), consisting with one of the appearances of cobalt(II) hydroxide. [84, 67]

In contrast to extensively explored and reported reactions of Tp^* scorpionates with Co^{2+} , properties and structures of complexes containing the $[Tp_2^*Co]^+$ cation are not reported. It has stronger $Co - N$ bonds and ligand field strength about the cobalt center, as Co^{3+} is more electrophilic and has smaller ionic radius so that enhanced electron donation can be expected. Table 4.25 shows that the $B - H$ bond stretch of (6) is much higher than those of (4) and (5) as a consequence of the smaller NBN angle of (6) initiated by the shorter $Co - N$ distance which in turn arises from stronger ligand field strength. Similar observations are also found for its Tp analogues. Including complex (2), all three so far prepared complexes containing $[Tp_2Co]^+$ have higher ν_{B-H} and shorter \bar{d}_{Co-N} than Tp_2Co . However, the reason for various ν_{B-H} values of $[Tp_2^*Co]^+$ complexes with different counterions is unclear yet. Detailed comparisons in a structural aspect between Tp_2^*Co and $[Tp_2^*Co]^+$ in Table 4.26 show unambiguously a more stable octahedral coordination structure of the latter. Comparing to Tp_2^*Co , the cation of (6) has a regular octahedral geometry around cobalt with $NCoN$ closer to 90° , to which two chelating ligands cling more firmly resulting in a more compact CoN_6 moiety than Tp_2^*Co ; and the almost undistorted coordination geometry gives indication of larger ligand field splitting $|\Delta_o|$ resulting in low-spin electron configuration. Yet if steric

factors are considered, the repulsion among the methyl groups on pyrazolyl 3-position of Tp^* counteracts their inductive effect. The $[Tp_2^*Co]^+$ cation in (6) has longer $Co-N$ bonds than the cation $[Tp_2Co]^+$ in (2) just like their d^7 neutral analogues, as the steric restriction caused by the methyl substituents prevents two Tp^* ligands from approaching very close to the cobalt ion. The ligands must only enlarge the bite angle and get closer to each other to create more space for the methyl groups to achieve a stable steric configuration in spite of the extended $Co-N$ bond length. For both Tp_2^*Co and $[Tp_2^*Co]^+$ situations, the $B \cdots Co$ distance is decreased to reduce the interligand repulsion caused by the 3-positional substituents; and it seems that the ligand disproportionation from Tp^*CoBr to Tp_2^*Co can be more easily retarded than its Tp analogue because a half-sandwich $TpCoBr$ cannot even be isolated, which makes (4) more versatile molecule for synthesis of other half-sandwich scorpionate complexes. Furthermore, both the average $B \cdots Co$ distance (2.955 Å) and $N-Co$ bond length of (4) are substantially shorter than those of octahedral Tp_2^*Co due to less interligand steric repulsion of the molecule, which means Co is bonded more tightly, and shielded more effectively by the Tp^* scorpionate in (4), if shielding effect of the 3-methyl groups is taken account of. All of these features mentioned above would offer a future opportunity to synthesize half-sandwich Tp^*ML complexes starting from Tp^*CoBr .

4.2.2 Reaction of bromo[tris(3,5-dimethyl-pyrazolyl)borato]cobalt with thiophenolate

Donors such as thiolate anion which can offer more than one electron lone pairs are usually applied as potential bridging ligands for transition metal complex. In order to examine their coordinating properties with Tp^*Co unit, the bromide of Tp^*CoBr (4) was substituted by a thiolate donor, and the ligand exchange could occur in a one-pot reaction by addition of the thiolate directly after preparation of Tp^*CoBr without separation of the precursor. For preparing a thiophenolate derivative of (4), thiophenol ($PhSH$) was treated with nBuLi at $-78^\circ C$, and the deprotonated species was added into the mixture of $CoBr_2$ and Tp^*K in THF. The blue solution of Tp^*CoBr turned gradually into a green solution of Tp^*CoSPh (7). The crude product was extracted with dichloromethane after removal of the solvent from the reaction mixture; and crystalline material was obtained by storing of saturated solution of (7) in dichloromethane at $-30^\circ C$. Green needle-like crystals which are very air-sensitive were confirmed to be the tetrahedrally coordinated cobalt complex with Tp^* and SPh ligands by single crystal X-ray structure determination and IR spectroscopy. (Figure 4.21)

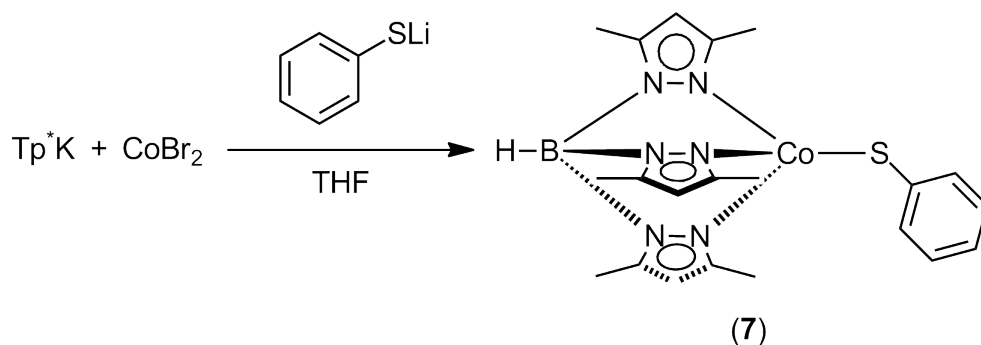


Figure 4.21.: Synthetic route for Tp^*CoSPh (7).

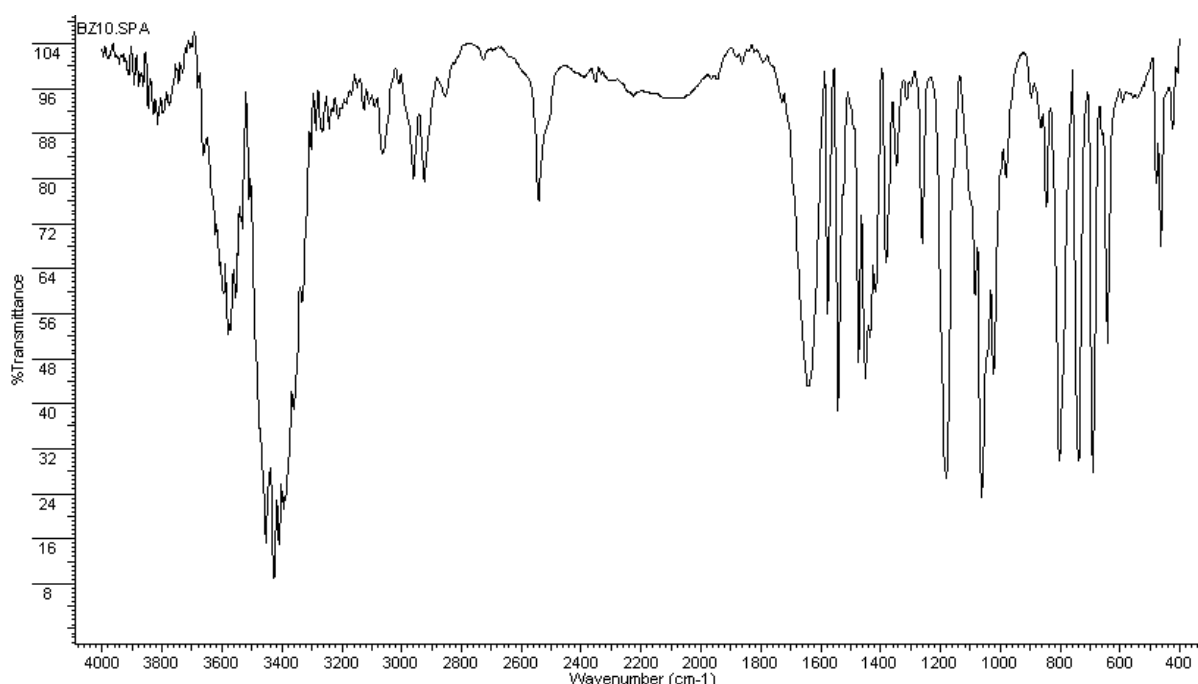


Figure 4.22.: IR spectrum of complex (7).

4.2.2.1 IR spectroscopic investigation

The sample for IR spectroscopy contained residue of thiophenol, which is illustrated by strong $S-H$ vibration bands around 3420 cm^{-1} in the IR spectrum of (7) (Figure 4.22). In the $C-H$ bond stretch region, aromatic ν_{C-H} bands are assigned at 3127 cm^{-1} for the pyrazolyl ring and 3064 cm^{-1} for the phenyl ring, respectively; whereas methyl $C-H$ stretching vibrations are seen at 2960 and 2924 cm^{-1} . Its $B-H$ stretching frequency at 2542 cm^{-1} indicates the tripodal coordinating mode to cobalt, which is in the same region as for (4). Peaks at 1642 and 1576 cm^{-1} are due to the $C=C$ aromatic ring stretch of the phenyl group; and the absorptions of the pyrazolyl ring stretch along with the rocking deformation δ of the methyl substituents are located between 1542 and 1347 cm^{-1} . Two strong vibrations at 1180 and 1062 cm^{-1} are due to the in-plane $C-H$

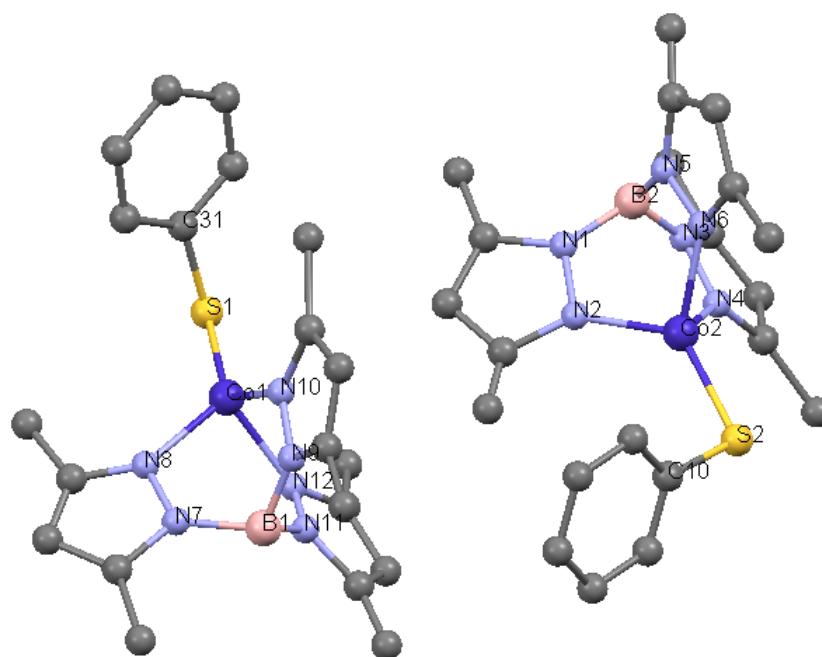


Figure 4.23.: Ball and stick model of the molecular structure of (7). All hydrogen atoms are omitted for clarity.

bend and $B - N$ stretch, respectively. A $S - C$ stretching band at 738 cm^{-1} proves the presence of thiophenolate group in the molecule. The $N - Co$ coordinating bond stretch is found at 479 and 464 cm^{-1} .

4.2.2.2 X-ray crystal structure determination of (7)

Complex (7) crystallizes in the orthorhombic space group $Pca2_1$ with two independent molecules in an asymmetric unit. The compound is very air-sensitive and the sample decomposed quickly during the crystallographic measurement. Therefore the R-factor is so large that a precise ORTEP diagram cannot be drawn due to inadequate quality of the single crystal. Figure 4.23 shows a ball and stick model of the molecular structure of (7), in which the $Co(II)$ ion is pseudotetrahedrally coordinated by three N atoms of a Tp^* and a S atom of a benzenethiolate group, and the coordination geometry about cobalt is subjected to large trigonal off-axis distortion. Further discussions about the crystallographic parameters of (7) are impossible, because the experimental data available are insufficient. Some important crystallographic data for complex (7) are shown in Table 4.28.

| | |
|-----------------------------|--|
| Empirical formula | C ₂₁ H ₂₇ B Co N ₆ S |
| Formula weight | 465.29 |
| Temperature | 293(2) K |
| Wavelength | 0.71073 Å |
| Crystal system, space group | Orthorhombic, P c a 21 |
| Unit cell dimensions | a = 27.934(5) Å alpha = 90 deg. b = 7.9067(7) Å beta = 90 deg. c = 20.966(3) Å gamma = 90 deg. |
| Volume | 4630.7(11) Å ³ |
| Final R indices [I > 2σ(I)] | R1 = 0.2135, wR2 = 0.4195 |
| R indices (all data) | R1 = 0.3301, wR2 = 0.4824 |

Table 4.28.: Selected important crystallographic data for complex (7).

4.2.2.3 Discussion

The bromide of (4) could be replaced by a bulky Lewis-basic *SPh*⁻ group retaining the pseudotetrahedral geometry about Co to form *Tp*^{*}*CoSPh* (7) (Reaction 4.16).



Although cobalt atom in both the educt and product remained tetra-coordinated, some evidences, for instance that the color of compound has turned from blue to green after the substitution; and the different extent of coordination geometry distortions for the two cobalt complexes, show that their d-orbital splitting patterns no longer keep unchanged. Ligand-field theory states that the original d-orbitals of transition metal is split into two sets of energy levels after a tetrahedral coordination, of which are three *t*₂^{*} orbitals of higher energy and two *e* orbitals of lower energy; distortion of geometry arises from changes in either shape and assembling of molecular orbitals or electron configuration about the central metal atom, which is usually affected by the nature of ligand approaching to it. Interaction of atomic orbitals of a tridentate facially coordinating chelate ligand and the metal center often reduces the energy level of a molecular orbital of *a*₁ symmetry within the *t*₂^{*} set, causing the orbital located above the degenerate *e* orbitals providing a 1*a*₁ + 2*e* set of lower energy (Figure 4.24), which is similar to the orbital arrangement of sandwich *Cp*₂^R*M* complexes. This interconversion relevant to a molecular distortion is called the “new case”. [56] Tetrahedral complex with this type of orbital splitting will demonstrate the umbrella distortion (Figure 4.25), in

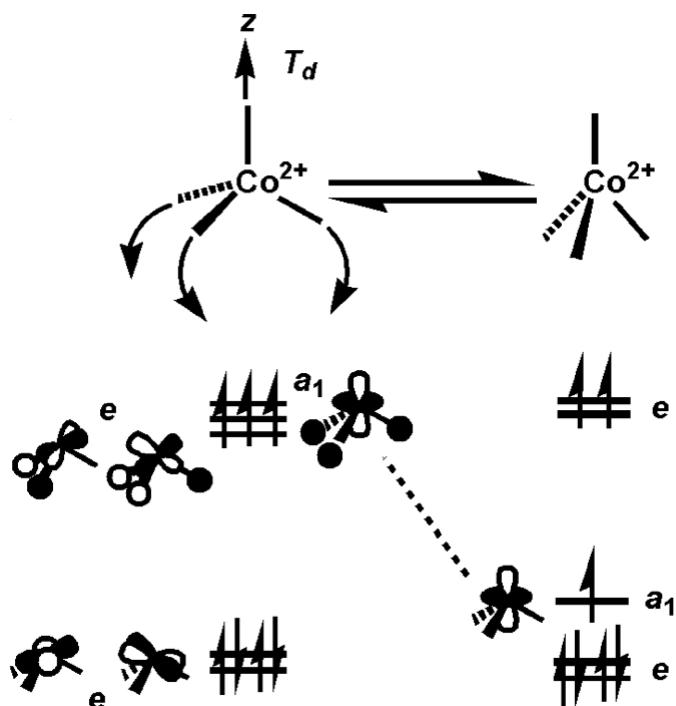


Figure 4.24.: d-orbital splitting diagrams stemming from coordination of chelate L_3 ligand. [56]

which three coordination bonds of chelating ligand collapse along their trisecting axis. For pseudotetrahedral complexes containing Tp^x ligand, this axis is along the $B - M$ vector. Structures of Tp^*CoBr and Tp^*CoSPh both displaying umbrella distortion support the fact that half-sandwich complex with tripodal Tp^* ligand owns an approximate two-over-three d-orbital splitting diagram, revealing a degree of resemblance in coordinating behavior to transition metal ion between Tp^x and Cp^R ligands.

Other than umbrella distortion, the off-axis distortion, in which the $M - X$ bond of Tp^xMX is not coincident with the $B - M$ vector, is also of great interest to give insights into further metal-ligand bonding features. The thiolate donor usually ex-

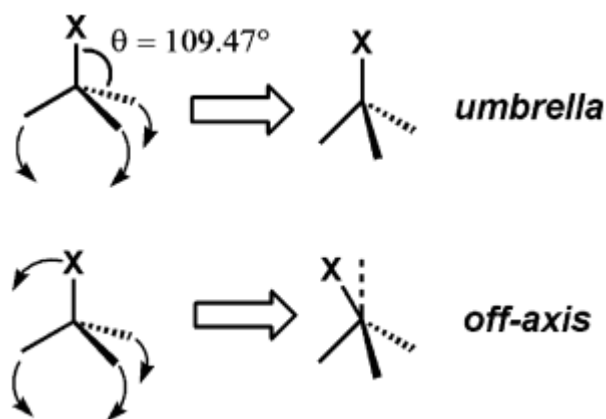


Figure 4.25.: Umbrella and off-axis distortions. [56]

| complex ^a | $B \cdots Co \cdots X$ | $Co - N(1)$ | $Co - N(2)$ | $Co - N(3)$ | av. $NCoN$ |
|-------------------------|------------------------|-------------|-------------|-------------|------------|
| $Tp^*Co(NO)$ [106] | 173.44 | 2.010(4) | 2.009(3) | 2.009(3) | - |
| $Tp^*Co(SC_6F_5)$ [103] | - | 1.97(2) | 2.01(2) | 1.98(2) | 92.2 |
| Tp^*CoBr (4) | 179.33 | 2.009 | 1.997 | 1.997 | 94.01 |

^a data taken from one molecule of two symmetrical molecules in the unit cell.

Table 4.29.: Comparison of key bond lengths (Å) and angles (°) of pseudotetrahedral Tp^*CoX complexes (**4**), $Tp^*Co(NO)$ and $Tp^*Co(SC_6F_5)$.

hibits a great tendency to form cobalt complex with off-axis distorted tetrahedral geometry [56]. Theoretical DFT studies performed by Jenkins and Peters [56] on $[PhBP_3]CoS(2,6 - Me_2 - Ph)$ exhibit a large off-axis distortion as well, revealing that the π^* orbital of S donor also took part in coordination bonding leading to a d-orbital splitting of Co more comparable with the octahedral two-over-three pattern, which explained the octahedrally oriented distortion of tetrahedral geometry. A similar explanation could also be used to describe the bonding nature of half-sandwich Tp^* complex. Among the three Tp^*CoX compounds of (**4**), (**7**) and $Tp^*Co(NO)$ [106] (Table 4.29), π^* orbitals of SPh interact with Co orbitals most dramatically providing the largest distortion toward octahedral coordination geometry about Co. This preference for the d-orbital arrangement resembling the pattern of $Cp_2^R M$ is due to the electronic and steric close relationship between compounds with Tp^x and Cp^R ligands.

4.2.3 Reaction of bromo[tris(3,5-dimethyl-pyrazolyl)borato]cobalt with pyrazole

The preservation of the half-sandwich tetrahedral structure of Tp^*CoBr after Br being substituted by SPh stimulated me to expand the reaction scope by attempting to introduce other substituting ligands to the Co center, aiming at to find a proper bridging ligand for a multinuclear scorpionate complex with mixed valency. Both bromide and thiolate donors studied so far are soft ligands which have been already proven to maintain mono-nuclear tetrahedral Tp^*CoX constitution. What would happen if that's a hard donor being introduced into the coordination sphere of the metal ion? Will the Co center retain the mononuclear half-sandwich structure or be part of a new complex in which the Tp-metal centers are linked by the hard coordinating ligand, if the intramolecular steric repulsion is restrained? Encouraged by these questions, 3,5-dimethyl-pyrazolate anion (pz^{*-}) was selected to react with Tp^*CoBr , because it has a structure imitating the hard electron donating unit of Tp^* , whose two pyrazolyl nitrogen donors might coordinate to different Co centers respectively providing room between the Tp^*Co units. This would reduce the steric repulsion, if a bridged complex would

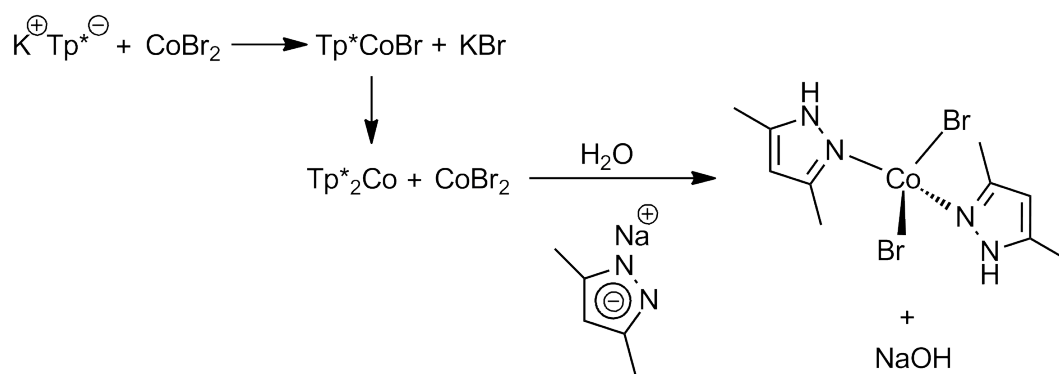


Figure 4.26.: Reaction of $\text{Tp}^* \text{CoBr}$ with Napz^* .

be built up. The pyrazolyl ring also features large π -conjugation that could facilitate possible electronic communications.

The reaction was performed in a one-pot manner similar to Reaction 4.16. CoBr_2 and KTp^* were mixed together in THF and a $\text{Na}(\text{pz}^*)$ solution was added. Stirring at room temperature overnight left a violet reaction mixture, which was subsequently filtered and concentrated. Unfortunately, in presence of sodium pyrazolate the reaction was so sensitive to water and a strong tendency to ligand disproportionation was observed. The colorless $\text{Tp}^*_2 \text{Co}$ as well as tetrahedral di(3,5-dimethyl-pyrazolyl)cobalt(II) bromide were the only products obtained in this reaction. (Figure 4.26).

The less steric requiring analogue pz^- was then chosen as next candidate as substituting reagent to $\text{Tp}^* \text{CoBr}$. To prevent the product from proceeding to further ligand disproportionation, an excess of CoBr_2 must be maintained during the substitution. Hence the former reaction manipulation was abandoned and the experiment was carried out through addition of a mixture of all the electron donors to a CoBr_2 solution in THF. A solution of pyrazole in THF was deprotonated with $^n\text{BuLi}$, and to the resulting species was added an equivalent amount of $\text{K}^+ \text{Tp}^{*\ominus}$. This freshly formed white suspension was dropped into a THF solution containing 1 equiv. CoBr_2 . The mixture was stirred for 12 hours resulting in a violet solution. Removal of the solvent followed by extraction of product with toluene afforded a brown powder, which was recrystallized in dichloromethane at -30°C . The brown product was moderately air-stable in the solid state and was soluble in toluene and dichloromethane but not in acetonitrile. An X-ray single crystal structure determination showed that this product was a dinuclear bridged structure, $\text{Tp}^* \text{Co}(\mu - \text{pz})_2(\mu - \text{O}_2) \text{CoTp}^*$ (**8**) (Figure 4.27).

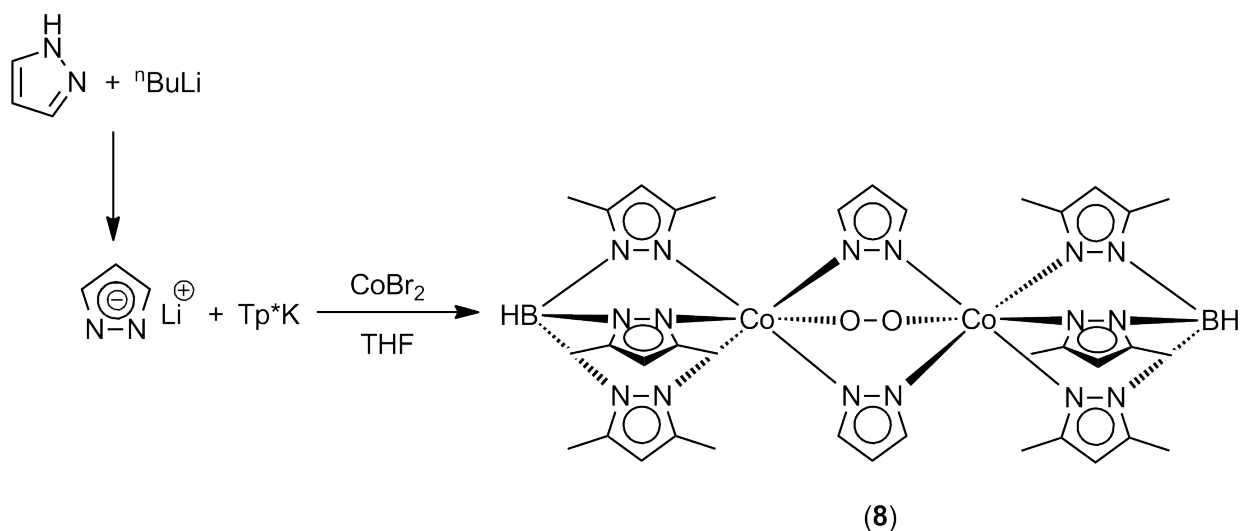


Figure 4.27.: Preparation of complex **(8)**.

4.2.3.1 X-ray crystal structure determination

X-ray single crystal diffraction revealed the brown crystal of complex **(8)** to be in the triclinic $P-1$ space group. The molecule contains two sets of Tp^*Co units bridged by two uni-charged pyrazolyl linkers and a peroxo group, with both Co centers satisfy octahedral coordination geometry. (Figure 4.28) The $Co \cdots Co$ distance is 3.591 Å, excluding the possibility of direct metal-metal bond. Both terminal Tp^* ligands coordinate to a Co ion in a tridentate fashion, giving an average $Co-N$ bond length of 2.056 Å. This value is not only much larger than that for the similar Co(III)-centered $[Tp_2^*Co]^+$ (1.940 Å) **(6)**, but even larger than those for **(4)**, **(7)** and $Tp^*Co(NO)$ [106], which contain Co(II) centers with tetrahedral coordination geometry. The bridging pyrazolyl rings bind to the Co ions in an average $Co-N$ distance of 1.938(11) Å that is larger than the mean $N-Co$ bond length of $[Tp_2Co]^+$ (1.926 Å) **(2)** as well. This observation illustrates that the octahedral ligand field about the two Co centers in **(8)** is weakened in comparison to its symmetrically coordinated Tp_2^*Co analogues. Each of the Co ions obtains an electron pair in the π^* orbital of the peroxo anion O_2^{2-} , which couldn't realize an orbital overlap as large as for pyrazolyl nitrogen with the Co d orbitals due to steric constraints. Thus the $Co-N$ bond strength for terminal Tp^* lessens consequently. Comparable $Co-N$ bond parameters are found in $(Tp^*Co^{III})_2(\mu-O)_2$ (2.059 Å) and $(Tp^{Me_3}Co^{III})_2(\mu-O)_2$ (2.031 Å) [50], which are rare examples containing dinuclear bridged structures similar to **(8)**, having average $Co-N$ distances close to that of **(8)** as well. Noteworthy observations come from the comparison of $N-Co$ bond lengths for Tp^* : the $N(5)-Co(1)$ (2.112(12) Å) and $N(13)-Co(2)$ (2.117(12) Å) bonds opposite to the O-donor are distinctly longer than other $N-Co$

| | |
|-------------------------------|---|
| Empirical formula | C36 H50 B2 Co2 N16 O2 |
| Formula weight | 878.4 |
| Temperature | 293(2) K |
| Wavelength | 0.71073 Å |
| Crystal system, space group | Triclinic, P -1 |
| Unit cell dimensions | a = 10.967(1) Å alpha = 67.71(1) deg. b = 12.815(1) Å beta = 83.76(1) deg. c = 16.425(2) Å gamma = 74.378(1) deg. |
| Volume | 2057.0(4) Å ³ |
| Final R indices [I>2sigma(I)] | R1 = 0.1808, wR2 = 0.4024 |
| R indices (all data) | R1 = 0.2783, wR2 = 0.4563 |

Table 4.31.: Selected important crystallographic parameters for complex **(8)**.

bonds in the same octahedron, respectively. It is most likely ascribed to the trans effect [17, 59, 20] exerted by the O_2^{2-} ligand, which labilizes the $N - Co$ coordination bond trans to it, illustrating an unusual extended bond length. The av. $O - Co$ bond length of **(8)** (1.919 Å) is longer than those of resembling dioxo bridged complexes $[\{(NH_3)_5Co\}_2(\mu - O_2)](SO_4)_2 \cdot 4H_2O$ (1.88 Å) and $[\{(NH_3)_5Co\}_2(\mu - O_2)](NO_3)_5$ (1.89 Å) [96, 71, 6]; However, in contrast, the $O - O$ distance of **(8)** (1.239(14) Å) is remarkably short with respect of peroxide anion, whose usual scale is around 1.4 Å. [6, 53, 57] The bite angle (av. $NCoN$) of 87.6° for Tp^* settles itself between the values for Tp_2^*Co and $[Tp_2^*Co]^+$, whereas the $B \cdots Co$ distance (3.137 Å) as well is observed between those for the two reference complexes correspondingly. Unlike most of mono-bridged dioxo compounds owning a $trans-\mu - 1, 2 - O_2$ bridging group, the two Tp^*Co units of **(8)** are *cis*-linked by the $O - O$ bridge due to conformational restrictions from the other two pyrazolyl bridges. However, the two Co ions and $O - O$ bridge are not coplanar but twisted with a $Co(1) - O(1) - O(2) - Co(2)$ torsion angle of $13(2)^\circ$. The central unit of **(8)**, which is much like a “basket with a handle” composed of two oxygens, bears an average $Co - O - O$ angle of 127.5° that is larger than those for mono-bridged peroxide and superoxide complexes [6, 53] probably due to steric elongation from the pyrazolyl skeleton. The important crystallographic data for **(8)** is listed in Table 4.31, and its selected bond lengths and angles are shown in Table 4.33.

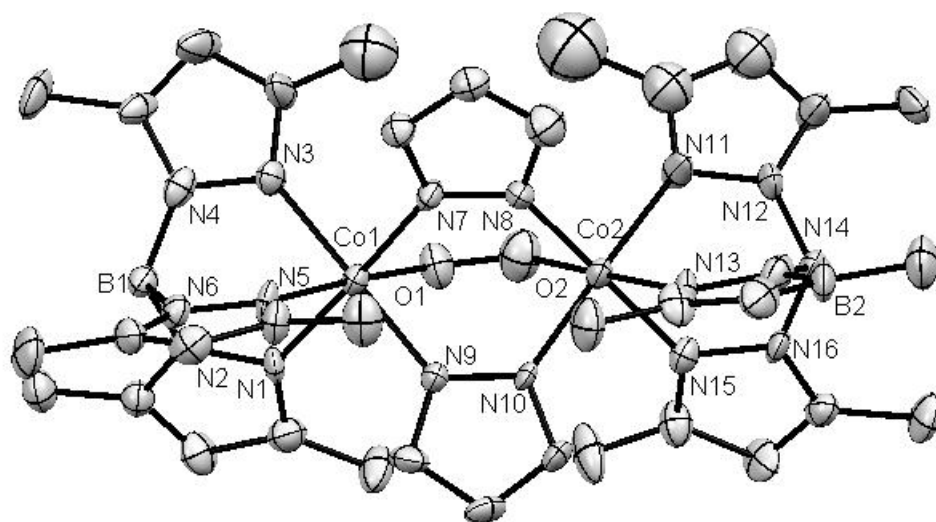


Figure 4.28.: ORTEP drawing of the crystal structure of complex (8) with selected atoms labeled. The thermal ellipsoids represent the probability level of 30 %. All hydrogen atoms are omitted for clarity.

| Bonds | Bond lengths (Å) | Bonds | Bond lengths (Å) |
|------------------|-------------------|-------------------|-------------------|
| Co(1)-N(9) | 1.940(11) | Co(2)-N(15) | 2.034(12) |
| Co(1)-N(7) | 1.942(11) | Co(2)-N(13) | 2.117(12) |
| Co(1)-O(1) | 1.946(12) | N(2)-B(1) | 1.53(2) |
| Co(1)-N(3) | 2.035(12) | N(4)-B(1) | 1.51(2) |
| Co(1)-N(1) | 2.042(12) | N(6)-B(1) | 1.53(2) |
| Co(1)-N(5) | 2.112(12) | O(1)-O(2) | 1.239(14) |
| Co(2)-O(2) | 1.891(14) | N(12)-B(2) | 1.52(2) |
| Co(2)-N(10) | 1.929(11) | N(14)-B(2) | 1.56(2) |
| Co(2)-N(8) | 1.939(12) | N(16)-B(2) | 1.49(2) |
| Co(2)-N(11) | 1.996(13) | | |
| Bonds | Bond angles (deg) | Bonds | Bond angles (deg) |
| N(9)-Co(1)-N(7) | 89.1(5) | N(10)-Co(2)-N(11) | 177.6(6) |
| N(9)-Co(1)-O(1) | 86.2(5) | N(8)-Co(2)-N(11) | 93.1(6) |
| N(7)-Co(1)-O(1) | 89.2(5) | O(2)-Co(2)-N(15) | 93.4(5) |
| N(9)-Co(1)-N(3) | 179.4(5) | N(10)-Co(2)-N(15) | 91.3(5) |
| N(7)-Co(1)-N(3) | 91.5(5) | N(8)-Co(2)-N(15) | 178.5(5) |
| O(1)-Co(1)-N(3) | 93.9(5) | N(11)-Co(2)-N(15) | 86.4(6) |
| N(9)-Co(1)-N(1) | 92.9(5) | O(2)-Co(2)-N(13) | 178.5(5) |
| N(7)-Co(1)-N(1) | 178.0(5) | N(10)-Co(2)-N(13) | 91.4(5) |
| O(1)-Co(1)-N(1) | 90.7(5) | N(8)-Co(2)-N(13) | 90.5(5) |
| N(3)-Co(1)-N(1) | 86.5(5) | N(11)-Co(2)-N(13) | 89.0(6) |
| N(9)-Co(1)-N(5) | 91.8(5) | N(15)-Co(2)-N(13) | 88.0(5) |
| N(7)-Co(1)-N(5) | 92.7(5) | O(2)-O(1)-Co(1) | 126.6(10) |
| O(1)-Co(1)-N(5) | 177.2(5) | O(1)-O(2)-Co(2) | 128.4(11) |
| N(3)-Co(1)-N(5) | 88.1(5) | N(4)-B(1)-N(2) | 107.7(13) |
| N(1)-Co(1)-N(5) | 87.4(5) | N(4)-B(1)-N(6) | 109.6(12) |
| O(2)-Co(2)-N(10) | 88.8(5) | N(2)-B(1)-N(6) | 107.6(12) |
| O(2)-Co(2)-N(8) | 88.0(6) | N(16)-B(2)-N(12) | 107.7(14) |
| N(10)-Co(2)-N(8) | 89.2(5) | N(16)-B(2)-N(14) | 109.1(13) |
| O(2)-Co(2)-N(11) | 90.9(7) | N(12)-B(2)-N(14) | 106.5(13) |

Table 4.33.: Selected bond lengths (Å) and angles (deg) of complex (**8**).

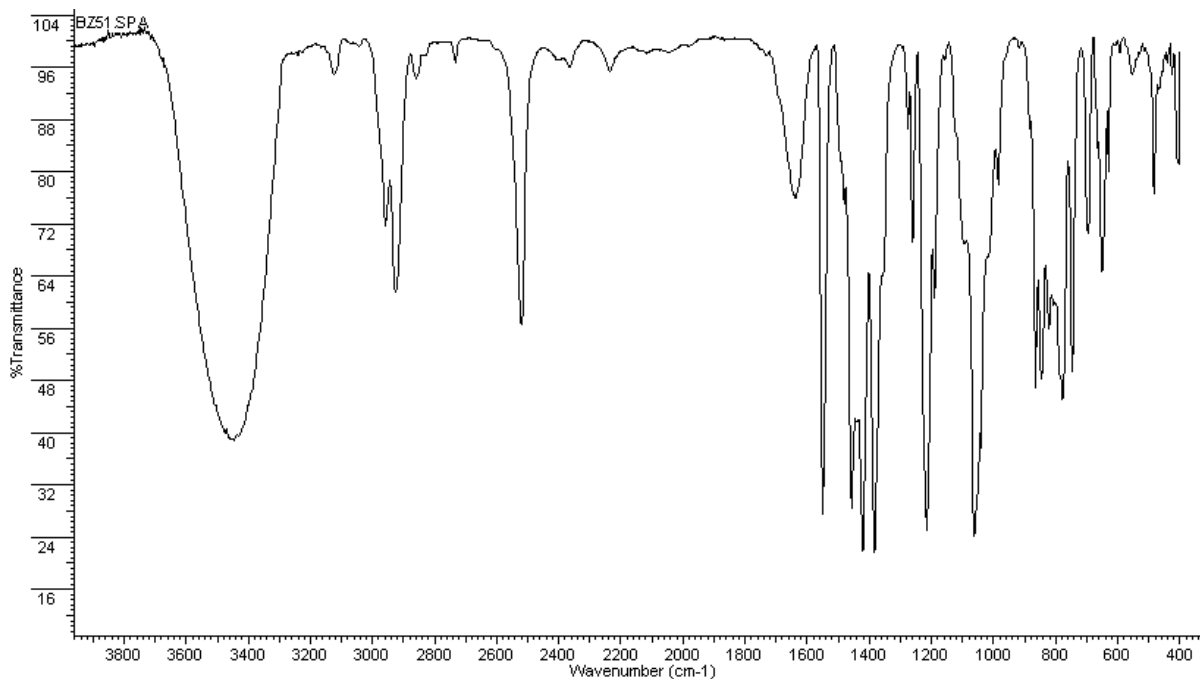


Figure 4.29.: IR spectrum of complex (**8**).

4.2.3.2 Spectroscopic characterization of complex (**8**)

The IR spectrum of complex (**8**) is shown in Figure 4.29. Obviously the single vibration present at 2521 cm^{-1} can be assigned to ν_{B-H} , in agreement with the tripodal coordination mode for the terminal Tp^* ligands. It was observed that the compound is slightly hygroscopic; and the broad $O-H$ stretching band at 3448 cm^{-1} gives clear evidence for the presence of absorbed water probably by both KBr and (**8**). The ν_{C-H} for methyl group is at 2958 and 2927 cm^{-1} as well as a weak band at 3123 cm^{-1} that is assigned to the phenyl $C-H$ stretching mode. Resembling other Tp^*Co analogues previously described, the pyrazolyl ring stretching mode along with the CH_3 rocking deformation are represented by bands at 1637 , 1550 , 1457 , 1421 , and 1384 cm^{-1} . In the fingerprint region, two strong vibrations at 1215 and 1062 cm^{-1} are assigned to the $C-H$ in-plane deformation and $B-H$ bond stretching mode, respectively. Two bands at 866 and 845 cm^{-1} may be ascribed to the peroxide $O-O$ stretching vibration; and those at 776 and 747 cm^{-1} correspond to the $C-H$ out-of-plane deformation of the pyrazolyl rings. The $Co-N$ bond stretch gives two bands at 484 and 406 cm^{-1} .

The 1H NMR spectrum of (**8**) (Figure 4.30) shows signals in the expected region. The unsymmetrical bridge, consisting of two pyrazolyl rings and a peroxide group, results in four different types of methyl protons which are divided into two sets: The pyrazolyl 3-methyl protons appear at low field because of the deshielding effect of the nitrogen bonded to Co, of which those from the pyrazolyl rings facially coordinating to Co to-

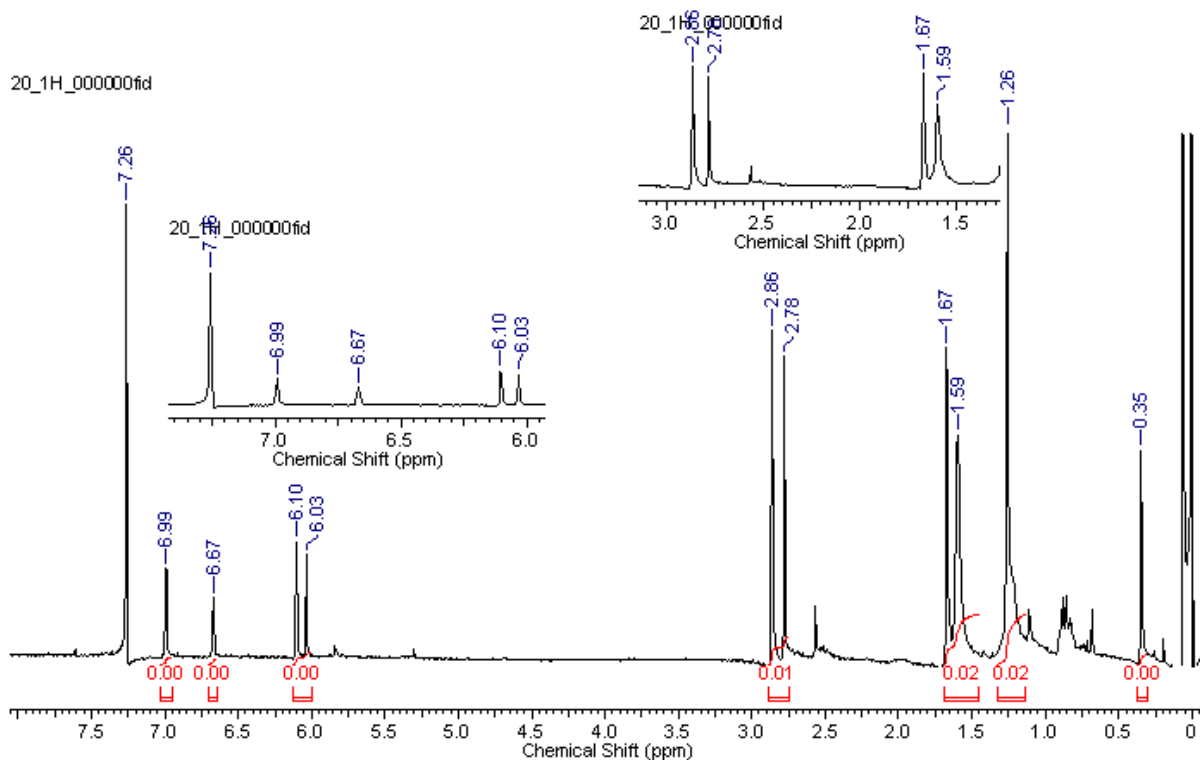
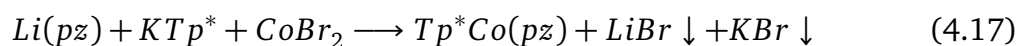


Figure 4.30.: ^1H NMR spectrum of complex (**8**) in CDCl_3 .

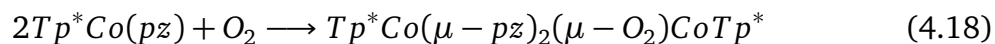
gether with the peroxide group resonate at 2.86 ppm, and those from the meridionally coordinating pyrazole with respect to the oxygen donor are found at 2.78 ppm. Their integrals give a ratio of 2:1 as expected. For the methyl protons on the boron, chemical shifts of 1.59 and 1.67 represent for those on the same facial and meridional pyrazolyl rings respectively, with an integral ratio of 2:1 as well. The same interpretation can be also applied to the pyrazolyl 4-position protons: those on the meridional pyrazolyl rings of Tp^* in the coordination sphere opposite to O are assigned at 6.03 ppm, and on the other rings of Tp^* at 6.10 ppm. Regarding the two bridging pyrazolyl groups, protons on the 4- and 3-position are assigned at 6.67 and 6.99 ppm, respectively, both are shifted downfield due to deshielding arising from coordination to two Co centers. There are other signals in the high-field that are believed not belonged to the complex, of which 1.26 ppm comes from the residue of water in the solvent and another peak at 0.35 ppm is probably due to methyl groups on some unknown impurities.

4.2.3.3 Discussion

Reaction of CoBr_2 with KTp^* and $\text{Li}(\text{pz})$ leads to the precipitation of KBr and LiBr from the organic solvent which is the driving force of the reaction:



Under exposure to air, oxygen molecule would coordinate to Co, resulting in a bridged complex with two octahedral Co centers:



Its NMR spectrum proves the final product to be diamagnetic. According to previous reported $O - O$ distances of peroxide group linking two metal centers, the $O - O$ bond length of **(8)** is neither in accordance to that for the anterior coordination complex [96, 71, 6, 53] nor ionic compound [38, 57], disclosing a much shorter value close to the magnitude of a neutral dioxygen ligand; and its $Co - O$ distance is not as short as for analogous dioxo cobalt complexes [96, 71, 6] reported earlier, neither. This controversy may be explained in terms of the nature of bonding between O and Co in **(8)**. Since the coordination of Co(II) with Tp^* and pz^- was carried out under oxygen-free conditions, it is reasonable to speculate that the molecule of **(8)** was accomplished in two steps: Firstly, the tetra-coordinate $Tp^*Co(pz)$ would dimerize to yield a bridged complex $Tp^*Co^{II}(\mu - pz_2)Co^{II}Tp^*$; and secondly, an dioxygen molecule could insert into the Co centers becoming a third bridge. Due to the molecular orbital combination of the dioxygen single occupied degenerate π^* orbitals and the Co d orbitals, the former unpaired d-electron in Co resides now in a new forming bonding orbital of more oxygen properties, meaning that the Co(II) is oxidized by oxygen to Co(III). This bonding orbital might possess more covalent nature with lower energy, which accounts for the shorter $O - O$ bond length comparing with that for O_2^{2-} anion. And the long $Co - O$ bond length relative to those of more ionic nature is hence comprehensible, as ionic bond is normally much stronger than covalent bond.

5 Linked multinuclear copper complexes

5.1 Synthesis of chloranilate bridged dinuclear copper complex

For linked copper complexes, a variety of mono and dinuclear Cu(II) complexes with tetraoxolene ligands have been reported with respect to intramolecular electronic and magnetic interactions. [86, 37, 104, 36, 16, 40, 41, 119] However, there is still no example of a tetraoxolene Cu(I) complex reported, to the best of my knowledge. One reason might be that a Cu(I) cation has a fully occupied d^{10} electronic configuration without an unpaired spin which exhibits poor magnetic properties related to the metal center; and another one might be the usual instability of Cu(I) ion in air, prohibiting the formation of such a kind of complex. Nevertheless, since in the tetraoxolene copper complexes, besides the double negative charged bridging ligand, the terminal supporting ligands usually applied are neutral, therefore most of the dinuclear tetraoxolene Cu(II) complexes are charge bearing that demand appropriate counter ions. In contrast, the dinuclear chloranilate Cu(I) complex would be a neutral molecule without a counter ion; furthermore, its redox behavior could be rich as it would call for a relative low oxidation potential to generate a mixed-valence compound. Due to intramolecular electron transfer, the ambiguous oxidation states of the electron-rich Cu(I) center and the redox non-innocent chloranilate acceptor attract great research interest.

It is well known that the bidentate ligand 1,1'-bis-(diphenylphosphino)ferrocene (dppf) is widely used in coordination compounds due to its versatile coordination ability adapting its bite angle to various coordination geometries. It has become an indispensable important ligand to stabilize the Cu(I) moiety for studying of the valence interaction of Cu(I) ion and redox non-innocent ligands. Diez et al. found that dppf could indeed stabilize the Cu(I) ion within a coordination framework. [33] The $Cu(dppf)^+$ moiety has recently proven to be an excellent metal-ligand fragment for investigation of the redox behavior of multinuclear Cu(I) complex because of its chemical stability as well as an additional redox-active site ("ferrocene" center); and a number of new complexes of Cu(I) have been reported, containing $Cu(dppf)^+$ building blocks. [91, 93, 92, 83]

All of these discoveries described previously prompted me to pay closer attention to the redox properties and connected with it the electronic communication in the chloranilate (CA^{2-}) bridged Cu(I) complex. A tetranuclear $[(dppf)Cu]_2(CA)$ complex (**9**) was thus successfully prepared and is the first tetraoxolene linked dinuclear Cu(I) complex isolated so far (Figure 5.1).

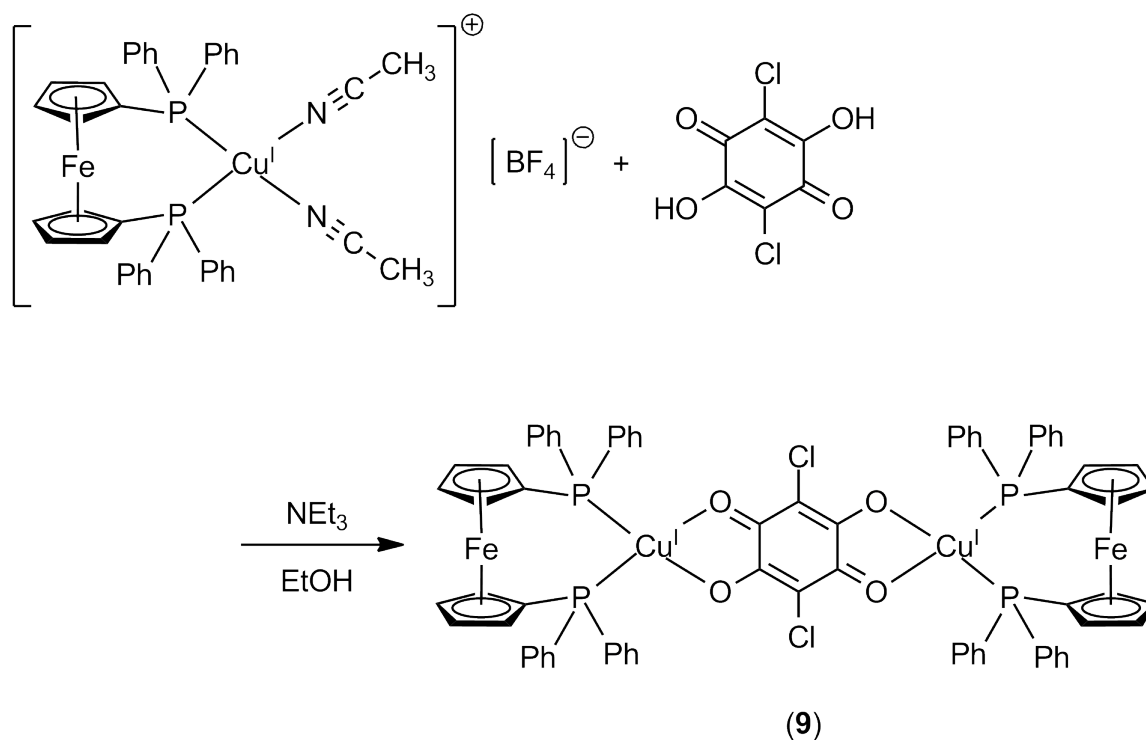


Figure 5.1.: Preparation of $[(dppf)Cu]_2(CA)$.

5.1.1 Preparation of $[(dppf)Cu]_2(CA)$

Chloranilic acid (H_2CA) was dissolved in oxygen free ethanol and completely deprotonated with triethyl amine (NEt_3). Two equivalents of $[Cu(\kappa^2 - P,P - dppf)(CH_3CN)_2](BF_4)$ were added into the solution of the deprotonated species, and the mixture was stirred at room temperature for 12 hours. (Figure 5.1) A red brown powder precipitated from the solution and was collected by filtration, washed, and recrystallized from a solvent mixture of dichloromethane and petroleum ether. The product obtained is stable in the air, and well soluble in common organic solvents.

5.1.2 X-ray crystallographic determination of $[(dppf)Cu]_2(CA)$

A single crystal of (9) suitable for X-ray crystallographic determination was grown at room temperature from a saturated solution in dichloromethane layered with petroleum ether. The molecule has a bridged structure, in which two $(dppf)Cu$ moieties are linked by a bis-bidentate chelating chloranilate ligand resulting in a neutral tetranuclear Fe_2Cu_2 metal core. (Triclinic $P\bar{1}$ space group with unit cell dimensions $a = 11.1228(19)$ Å, $b = 11.569(2)$ Å, $c = 13.270(2)$ Å, $\alpha = 83.280(3)^\circ$, $\beta = 71.412(3)^\circ$, $\gamma = 71.086(3)^\circ$, some important crystallographic data are listed in Table 5.2) Each Cu center is coordinated by two O as well as two P donors in a pseudotetrahedral geometry, and the whole

molecule has a center of symmetry in the middle of the chloranilate ring (Figure 5.2). The two $C - O$ bonds of the chloranilate ligand have very similar bond lengths with $C1 - O1 = 1.259(3) \text{ \AA}$ and $C2 - O2 = 1.254(3) \text{ \AA}$ in comparison to a number of chloranilate molecular linkers in similar dinuclear complexes. [78, 77, 14, 86, 60, 37, 41] The $C - C$ lengths in the bridging ring are unequal, of which $C1 - C2$ holds the longest bond length of $1.532(4) \text{ \AA}$ whereas the other two bonds of the central symmetrical six-membered carbon skeleton have $C - C$ distances of $1.392(4) \text{ \AA}$ and $1.406(3) \text{ \AA}$, respectively. The $C - Cl$ distance ($1.735(3) \text{ \AA}$) is comparable with that for other CA^{2-} dianions. [78, 77, 3, 40, 86, 37, 41] Because of the lack of a positive charge on the Cu(I) ion, the $Cu - O$ bond length for (9) is slightly longer than that for Cu(II) chloranilate bridged complexes [40, 13, 86, 60, 37, 104, 41], most of which are coordinated in pseudo trigonal-bipyramidal or square pyramidal geometry. However, unlike these Cu(II) compounds mostly presenting two different $Cu - O$ bond lengths, (9) possesses more symmetrical bridging bonds with similar $Cu - O$ bond lengths ($Cu - O1 = 2.084(2) \text{ \AA}$ and $Cu - O2 = 2.0943(19) \text{ \AA}$). This is presumably referable to specific coordination geometries: when the $Cu - O$ bond locates towards the apical direction in a pseudo square pyramidal or trigonal-bipyramidal coordination moiety, its bond length is often prolonged comparing to another $Cu - O$ bond in the same molecule, as reported for $[Cu_2(bpy)_2(CH_3OH)_2(CA)]^{2+}$ [40], $[Cu_2(Me_5dien)_2(CA)]^{2+}$ [86], and $[Cu_2(terpy)_2(CA)]^{2+}$ [37]; while if both $Cu - O$ bonds are in symmetrical positions, e.g. in the base plane of a square pyramidal or a trigonal-bipyramidal, they tend to display similar bond lengths [13, 104, 41]. From the two almost equivalent $Cu - O$ bonds of (9), one could confirm that in this pseudotetrahedral moiety about Cu, the metal ions are symmetrically bridged by the oxygens. The distorted tetrahedral geometry about Cu is ascribed to the chelation by both of the bidentate ligands. The bite angle $O1Cu1O2$ for the CA^{2-} is $78.41(7)^\circ$ whereas that for the *dppf* is $112.07(3)^\circ$, where the phosphorus donors bind to the Cu ion with $d_{p1-Cu1} = 2.2251(8) \text{ \AA}$ and $d_{p2-Cu1} = 2.2424(8) \text{ \AA}$, whose average value is consistent with that for other complexes having a fragment of $(dppf)Cu(I)$. [91, 93, 92, 83] A staggered conformation with a pseudo local D_{5d} symmetry is adopted by the ferrocenyl moiety. The $Fe \cdots Cu$ distance is 4.010 \AA comparable to 4.025 \AA for $[(dppf)CuL](BF)_4$ (L = N-(2-methyl-5,8-di-oxo-5,8-dihydroquinolin-7-yl)acetamide) prepared by Paretzki et al. [83] The two Cu(I) centers are almost coplanar with the chloranilate bridge, each deviating from the CA^{2-} plane by a torsion of 2.72° ; and the separation between the two Cu centers is 7.940 \AA . The table below shows the selected bond lengths and angles.

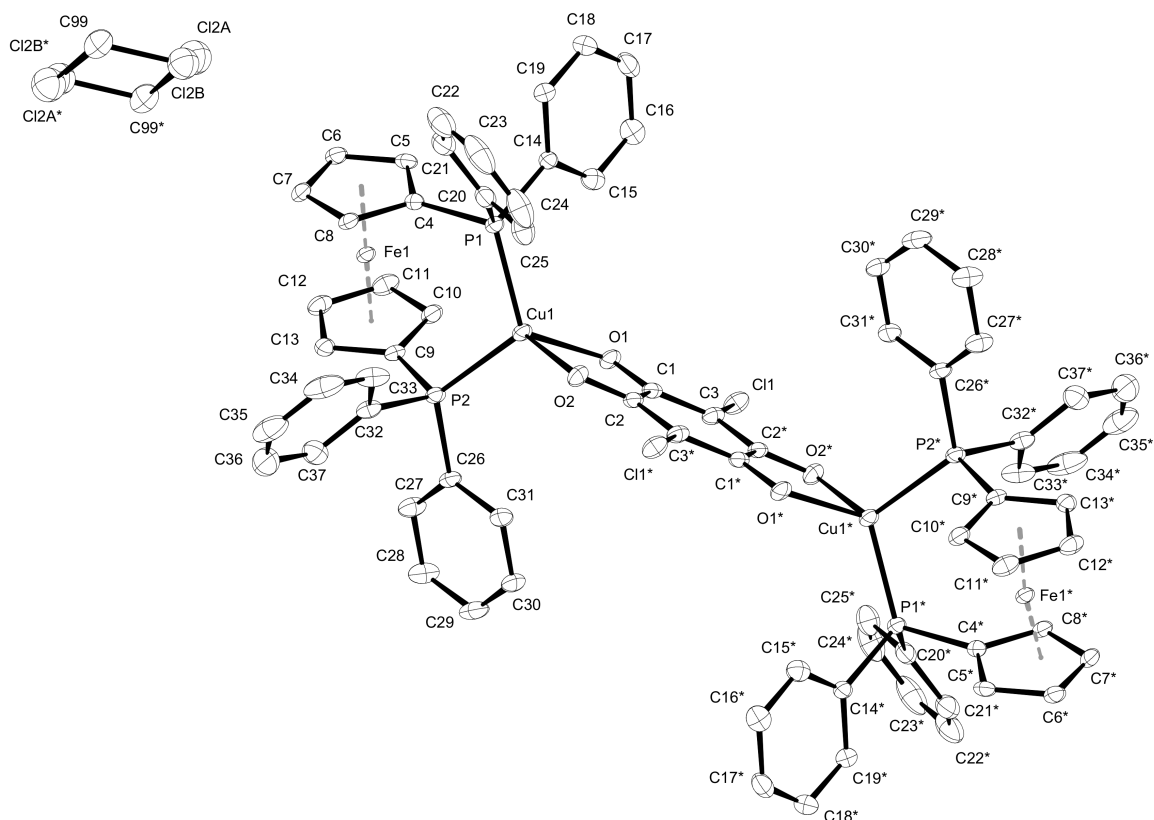


Figure 5.2.: ORTEP drawing of the crystal structure of complex (**9**). The thermal ellipsoids represent the probability level of 50 %. All hydrogen atoms are omitted for clarity.

| | |
|-----------------------------|---|
| Empirical formula | C ₇₅ H ₅₈ Cl ₄ Cu ₂ Fe ₂ O ₄ P ₄ |
| Color | orange |
| Formula weight | 1527.67 g · mol ⁻¹ |
| Temperature | 100 K |
| Wavelength | 0.71073 Å |
| Crystal system, space group | Triclinic, P -1 |
| Unit cell dimensions | a = 11.1228(19) Å alpha = 83.280(3) deg. b = 11.569(2) Å beta = 71.412(3) deg. c = 14.270(2) Å gamma = 71.086(3) deg. |
| Volume | 1646.3(5) Å ³ |
| Final R indices [I > 2σ(I)] | R1 = 0.0465 wR2 = 0.1084 |
| R indices (all data) | R1 = 0.0731 wR2 = 0.1207 |

Table 5.2.: Selected important crystallographic data for complex (**9**).

| Bonds | Bond lengths (Å) | Bonds | Bond lengths (Å) |
|------------------|-------------------|------------------|-------------------|
| Cu(1)-P(1) | 2.2251(8) | Cu(1)-P(2) | 2.2424(8) |
| Cu(1)-O(1) | 2.084(2) | Cu(1)-O(2) | 2.0943(19) |
| Cl(1)-C(3) | 1.735(3) | P(1)-C(4) | 1.817(3) |
| P(1)-C(14) | 1.830(3) | P(1)-C(20) | 1.824(3) |
| P(2)-C(9) | 1.808(3) | P(2)-C(26) | 1.824(3) |
| P(2)-C(32) | 1.829(3) | O(1)-C(1) | 1.259(3) |
| O(2)-C(2) | 1.254(3) | C(1)-C(2) | 1.532(4) |
| C(1)-C(3) | 1.392(4) | C(2)-C(3)* | 1.406(3) |
| Bonds | Bond angles (deg) | Bonds | Bond angles (deg) |
| P(1)-Cu(1)-P(2) | 112.07(3) | O(1)-Cu(1)-P(1) | 119.97(6) |
| O(1)-Cu(1)-P(2) | 111.03(6) | O(1)-Cu(1)-O(2) | 78.41(7) |
| O(2)-Cu(1)-P(1) | 117.70(6) | O(2)-Cu(1)-P(2) | 113.77(6) |
| C(4)-P(1)-Cu(1) | 115.11(8) | C(4)-P(1)-C(14) | 99.94(12) |
| C(4)-P(1)-C(20) | 102.93(13) | C(14)-P(1)-Cu(1) | 119.58(9) |
| C(29)-P(1)-Cu(1) | 113.54(10) | C(20)-P(1)-C(14) | 103.52(13) |
| C(9)-P(2)-Cu(1) | 108.52(9) | C(9)-P(2)-C(26) | 103.16(12) |
| C(9)-P(2)-C(32) | 105.14(12) | C(26)-P(2)-Cu(1) | 119.84(9) |
| C(26)-P(2)-C(32) | 102.64(13) | C(32)-P(2)-Cu(1) | 115.95(10) |
| C(1)-O(1)-Cu(1) | 114.77(18) | C(2)-O(1)-Cu(1) | 114.28(18) |
| O(1)-C(1)-C(2) | 115.9(2) | O(1)-C(1)-C(3) | 125.3(3) |
| C(3)-C(1)-C(2) | 118.9(2) | O(2)-C(2)-C(1) | 116.5(2) |
| O(2)-C(2)-C(3)* | 124.6(3) | C(1)-C(3)-Cl(1) | 119.2(2) |
| C(1)-C(3)-C(2)* | 122.2(3) | C(2)*-C(3)-Cl(1) | 118.6(2) |

Table 5.4.: Selected bond lengths (Å) and angles (deg) of complex (9).

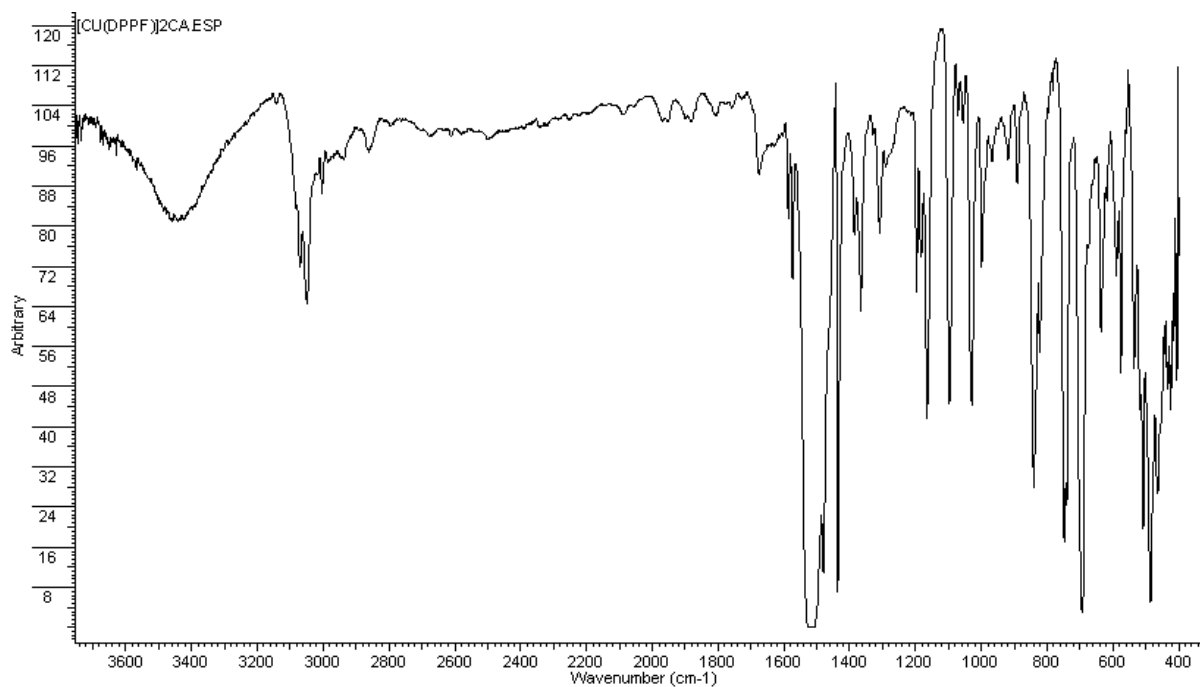


Figure 5.3.: IR spectrum of complex (9).

5.1.3 IR spectroscopy of [(dppf)Cu]₂(CA)

The IR spectrum of the product was recorded with a KBr sample at room temperature (Figure 5.3). The spectrum exhibits only one strong $C - O$ absorption at 1508 cm^{-1} , showing that there is only one kind of $C - O$ bond in the complex despite of the single and double $C - O$ bonds coexisting in the free chloranilic acid, demonstrating an electronic conjugation within the bridging ligand due to coordination with the Cu center. The chloranilate $C - Cl$ valence stretch is found at 840 cm^{-1} , together with the $C = C$ and $C - C$ bond stretching at 1573 cm^{-1} and 1365 cm^{-1} respectively, providing evidence of the presence of chloranilate ligand. A strong signal at 486 cm^{-1} arises from the $C - P$ valence stretch of the dppf ligand. Vibrations at $3070, 3048\text{ cm}^{-1}$ are ascribed to the $C - H$ bond stretching of the phenyl and cyclopentadiene rings, whose $C - H$ out-of-plane deformations are located at 747 and 693 cm^{-1} . The $C = C$ ring stretching of the phenyl group are shown unambiguously at 1480 and 1435 cm^{-1} , whereas the $C - H$ in-plane bend deformations result in bands at $1165, 1096,$ and 1029 cm^{-1} .

5.1.4 NMR spectroscopy of [(dppf)Cu]₂(CA)

As is shown in Figure 5.4, protons on the cyclopentadienyl ring resonate at 4.22 and 4.24 ppm, whereas a multiplet in the region 7.19 to 7.52 ppm represents the phenyl protons of the diphenylphosphinyl group. The solvent molecule of dichloromethane in-

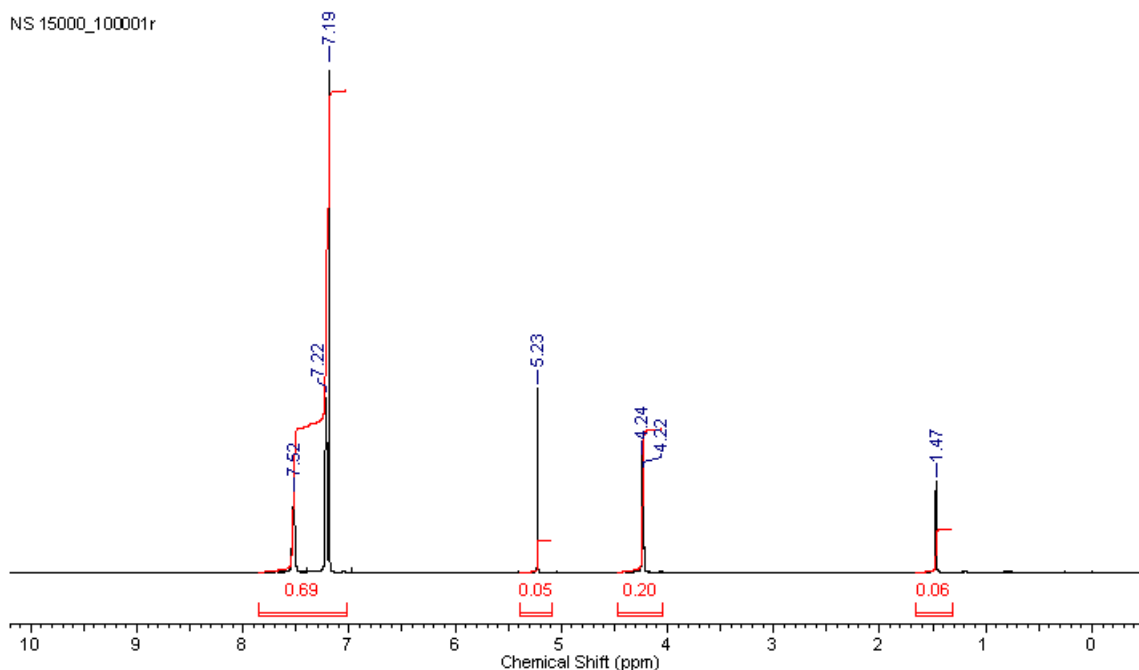


Figure 5.4.: ^1H NMR spectrum of complex (9).

incorporated in the crystal lattice of the complex (see Figure 5.2) displays a proton signal at 5.23 ppm. The integrals of the respective protons at the phenyl and cyclopentadienyl positions display a ratio of 5:2 which is consistent with the formulation of dppf. The presence of chloranilate ligand can be proven by the ^{13}C NMR spectrum of the complex (Figure 5.5), in which the chlorine-bearing carbon (C3) is present at 106.97 ppm while carbons attached with the oxygen donor (C1 and C2) provide only one signal at 175.17 ppm. Chemical shifts at 73.98 and 76.35 ppm stem from carbons on the C_p ring of dppf, of which the latter representing the C_p 2-carbons (C5, C8, C10, and C13) is shifted downfield due to the deshielding effect of the substitution of phosphorus; and the ipso, ortho, meta, and para carbons of the phenyl group are displayed at 136.14, 136.38, 132.20, and 130.88 ppm, respectively. The combined information from the NMR spectra supports the composition of the product that is in good agreement with a chloranilate bridged $dppf(\text{Cu})^+$ dimeric structure.

5.1.5 UV-vis spectroscopy of $[(dppf)\text{Cu}]_2(\text{CA})$

The UV-vis spectrum of (9) performed in dichloromethane at room temperature is shown in Figure 5.6. A strong absorption at 297.1 nm and a broad band with low absorbance at 480.4 nm are observed. Previous investigation of the UV-vis absorption of p-benzoquinone proved that the molecule had a high-intensity band at 245 nm, a medium-intensity band at 285 nm, and a band with low-intensity at 435 nm, of which the first two bands are due to the aromatic $\pi - \pi^*$ transitions whereas the last one was

NS 15000_101001r

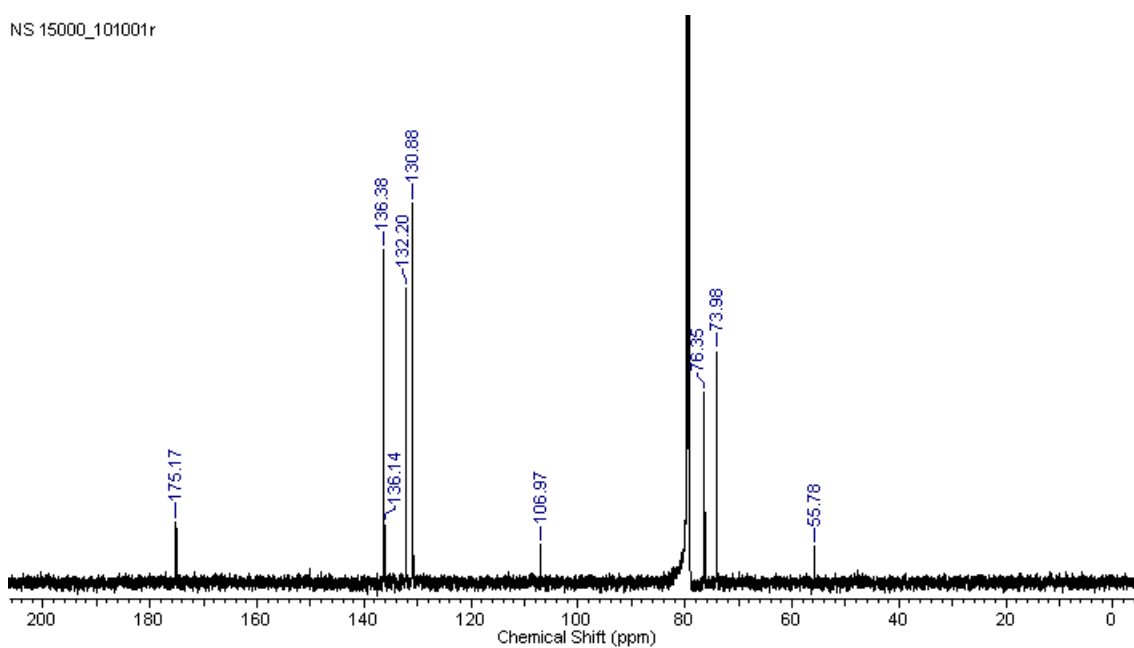


Figure 5.5.: ^{13}C NMR spectrum of complex (9).

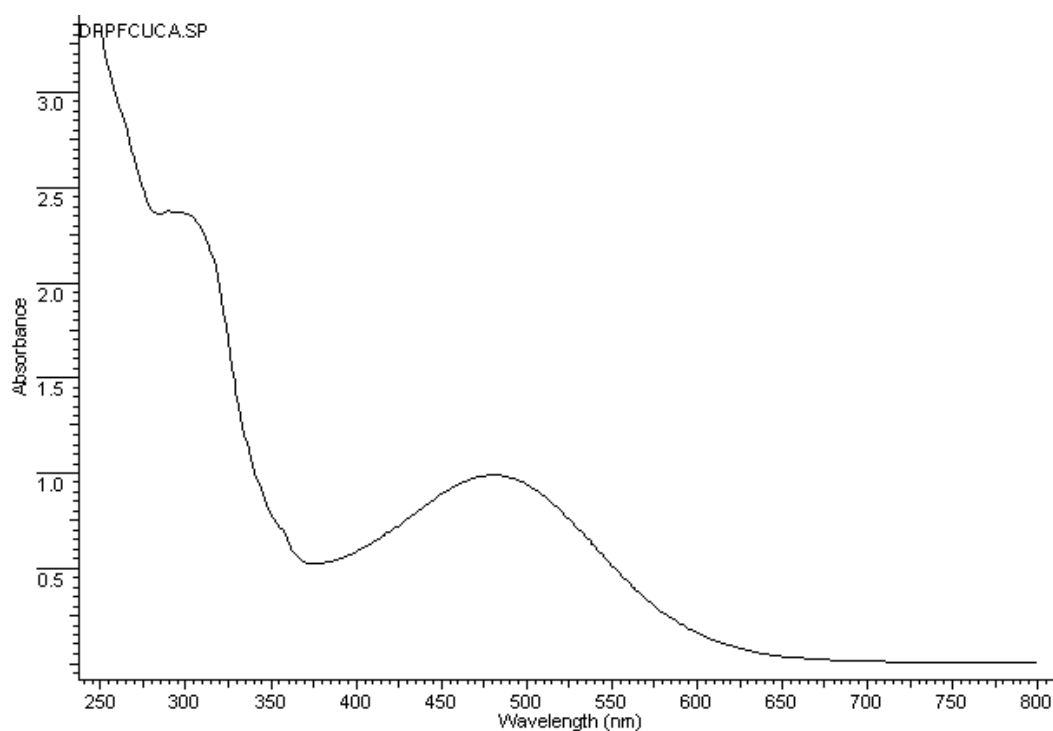


Figure 5.6.: UV-vis spectrum of complex (9). (in dichloromethane)

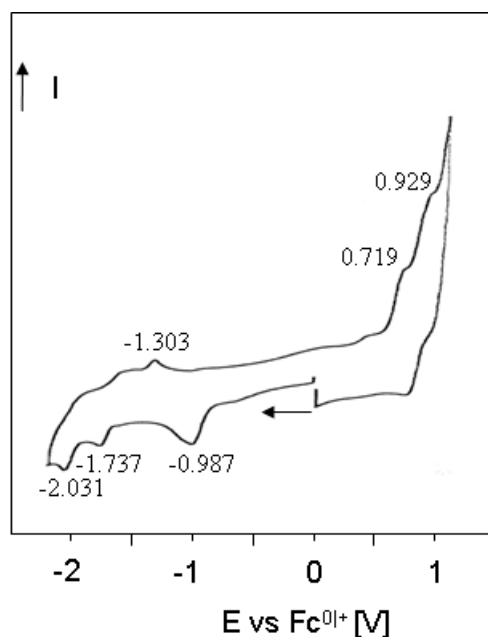


Figure 5.7.: Cyclic voltammogram (-2.20 - 1.10 V) of complex (**9**).

assigned to the $n - \pi^*$ transition corresponding essentially to the excitation from non-bonding molecular orbitals having mainly oxygen character. [10, 111] In comparison, chloranilic acid presented only two absorptions in the UV-vis region at 330 and 530 nm, respectively, the intensity of the former band being 20 times higher than that for the latter. [7] Comparing the positions of the band at 297.1 nm in Figure 5.6 as well as the $\pi - \pi^*$ transition bands for p-benzoquinone, this absorption (297.1 nm) can be ascribed to one of the $\pi - \pi^*$ transitions of the bridging ligand. In contrast with the UV spectrum of chloranilic acid, whose $\pi - \pi^*$ absorptions are so adjacent to each other that they are hardly distinguishable and eventually merge into one band, the difference in energy of the two $\pi - \pi^*$ transitions is clearly detectable due to the coordination to copper; meanwhile, the $n - \pi^*$ transition of the CA^{2-} ligand is unambiguously present in the vis-region at 480.4 nm.

5.1.6 Cyclic Voltammetry of $[(dppf)Cu]_2(CA)$

The redox behavior of complex (**9**) was studied by cyclic voltammetry in dimethoxyethane (DME). 0.1 M of $[Bu_4N][PF_6]$ was added as auxiliary electrolyte and ferrocene as internal reference. The voltage scan started from 0 to -2.20 V, then turned back and continued increasing to 1.10 V with scan rate of 100 mV/s. Figure 5.7 shows the cyclic voltammogram of (**9**) at 298 K, in which a reduction at -0.987 V corresponding to a two-electron transition as well as two one-electron reduction waves at -1.737 and -2.031 V are present. All the three peaks are irreversible and no corresponding oxidation wave

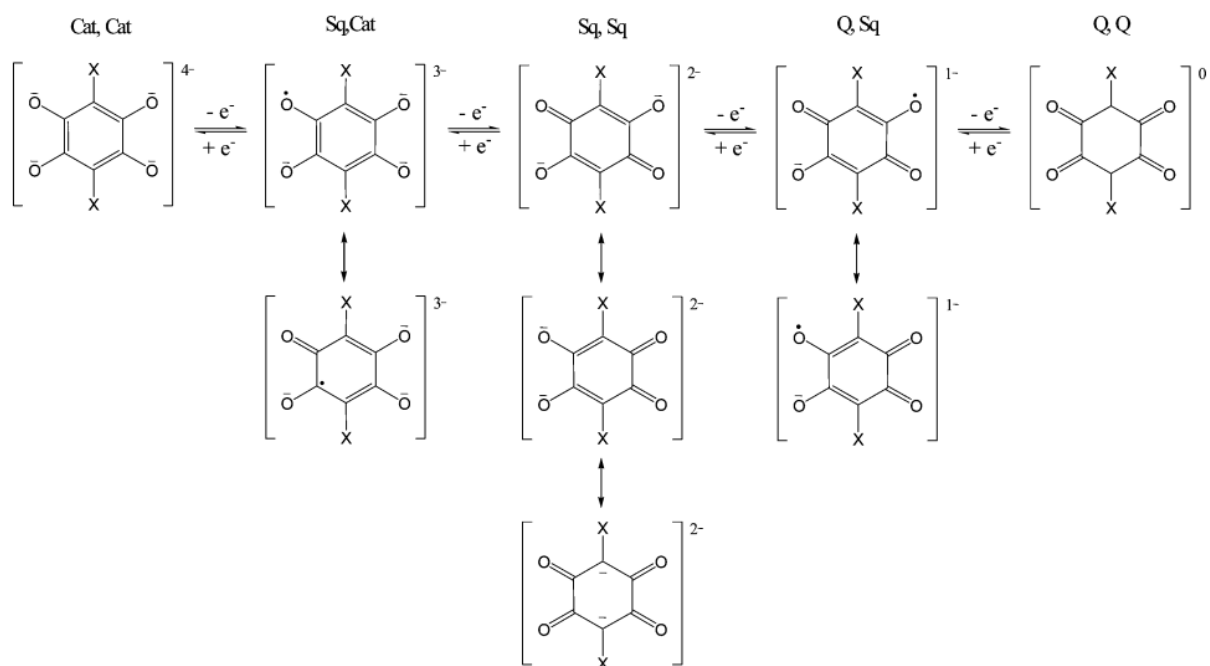


Figure 5.8.: Various states of the tetraoxolene ligand. "Cat", "Sq", and "Q" denote catechol, semiquinone, and quinone, respectively. [45]

for the first two-electron reduction is observed. In the reverse scan after reaching the negative maximum at -2.2 V, two indistinct shoulder-like oxidation waves relevant to the one-electron reductions arise whereas a new oxidation peak at -1.303 V is found. Another two irreversible oxidation waves appear when the voltage is scanned into the positive potential region. Those are at 0.719 and 0.929 V respectively, which likewise do not have explicit reductive responses, neither.

5.1.7 Discussion

The most prominent property of chloranilate moiety is that in the structure it behaves not only as coordinating ligand donating electron lone pairs into metal orbitals, but can participate in the intramolecular electronic communication through an interaction with a metal center of so called "valence-tautomerism", hence it is announced as "non-innocent". Therefore, the assignment of the oxidation state of this kind of ligand and each metal center incorporated is difficult because of the charge transfer taking place between the metal ion and the non-innocent ligand. With the help of X-ray crystal structure determination, the elucidation of the exact redox state of chloranilate ligand in (9) is possible because the various states of chloranilate ligand have their distinctive molecular structures (as are shown in Figure 5.8), which could be distinguished through their bonding parameters. The important bond lengths for the "core linker moiety" (Figure 5.11) of some tetraoxolene bridged metal complexes so far prepared are

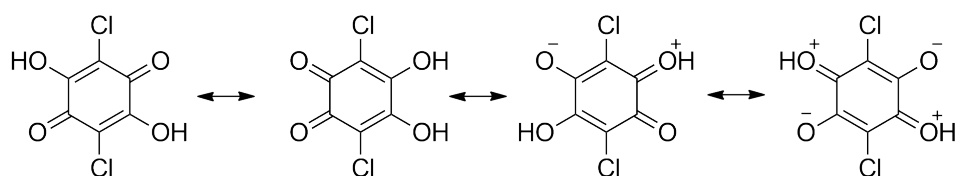


Figure 5.9.: Resonance structures of chloranilic acid.

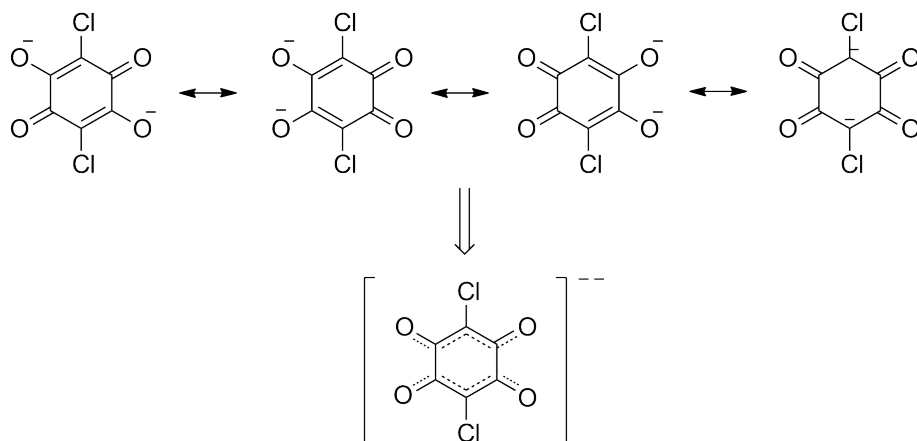


Figure 5.10.: Resonance structures (above) and the combined formula (below) of chloranilate dianion.

summarized in Table 5.5, from which a correlation between the possible valence charge distribution and the molecular structure of the bridging ligand can be undertaken.

In the crystal structure of free chloranilic acid (H_2CA), it was found that the $C - OH$ bond (1.317 \AA) is shorter than its usual value of 1.34 \AA , and the $C - C$ bonds parallel to the $C - Cl$ bonds are significantly longer than those parallel to the $C - O$ bonds. These observations account for the resonance structures of H_2CA (Figure 5.9), indicating the single and double bonds within the molecule are smoothed by electronic delocalization. [3] More pronounced conjugation was found for the crystal structure

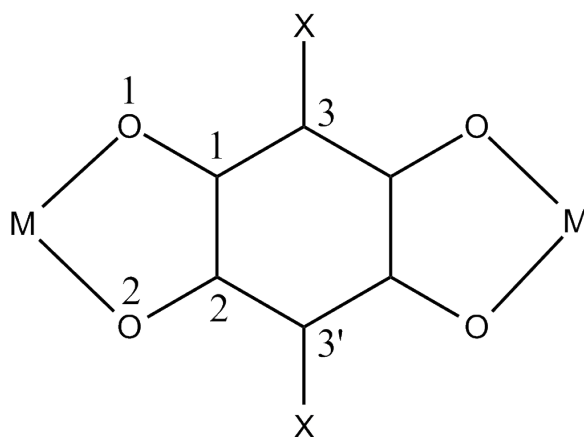


Figure 5.11.: Bridging tetraoxolene ligand moiety. ($X = H$ or Cl)

| Complexes | C1-C3 | C1-C2 | C2-C3' | C1-O1 | C2-O2 |
|---|-------------|-----------|-----------|------------|-----------|
| [{(TPA)Co} ₂ CA] ²⁺ [78] | 1.372(5) | 1.527(5) | 1.409(5) | 1.266(4) | 1.246(4) |
| [{(TPA)Co} ₂ CA] ⁺ [78] | 1.386(3) | 1.473(3) | 1.400(3) | 1.304(3) | 1.282(2) |
| [{(TPyA)Fe} ₂ DBQ] ²⁺ [76] | 1.399 (av.) | 1.524(2) | - | 1.269(5) | 1.275(5) |
| [{(TPyA)Co} ₂ CA] ²⁺ [77] | 1.372(5) | 1.527(5) | 1.409(5) | 1.266(4) | 1.246(4) |
| [{(TPyA)Co} ₂ CA] ⁺ [77] | 1.386(3) | 1.473(3) | 1.400(3) | 1.304(3) | 1.282(2) |
| [{(TPyA)Fe} ₂ CA] ²⁺ [77] | 1.382(3) | 1.528(3) | 1.405(3) | 1.270(3) | 1.251(3) |
| [{(tripod)Co ^{III}] ₂ (dhbq)] ²⁺ [49] | 1.392(9) | 1.45(1) | 1.39(1) | 1.313(8) | 1.311(8) |
| [{(tripod)Co ^{III}] ₂ (CA)] ²⁺ [49] | 1.390(5) | 1.442(6) | 1.385(7) | 1.311(5) | 1.321(5) |
| CA ²⁻ [3] | 1.407(9) | 1.535(8) | 1.401(6) | 1.243(6) | 1.253(8) |
| [Mo ₂ (DAniF) ₃] ₂ CA [21] | 1.380(6) | 1.475(7) | 1.390(6) | 1.285(6) | 1.292(6) |
| [{Os(PPh ₃) ₂ (pap)} ₂ CA] ²⁺ [46] | 1.393(7) | 1.502(7) | 1.401(7) | 1.281(6) | 1.276(6) |
| [Os(PPh ₃) ₂ (CO) ₂] ₂ CA [46] | 1.399(10) | 1.447(11) | 1.394(10) | 1.302(8) | 1.310(9) |
| [Rh(cod)] ₂ CA [14] | 1.381(15) | 1.520(14) | 1.396(17) | 1.257(15) | 1.283(15) |
| [{Cu(bpy)} ₂ CA] ²⁺ [40] | 1.390(3) | 1.520(4) | 1.383(4) | 1.262(4) | 1.262(4) |
| [CuCl(HL1)] ₂ CA [13] | 1.393(2) | 1.530(2) | 1.398(2) | 1.2627(19) | 1.259(2) |
| [{Cu(Me ₅ dien)} ₂ CA] ²⁺ [86] | 1.382(8) | 1.542(8) | 1.380(8) | 1.245(7) | 1.257(7) |
| [{Cu(terpy)} ₂ CA] ²⁺ [60] | 1.417(10) | 1.550(10) | 1.390(10) | 1.216(8) | 1.273(9) |
| [{Cu(terpy)(DMSO)} ₂ CA] ²⁺ [60] | 1.421(5) | 1.530(5) | 1.370(4) | 1.236(4) | 1.276(4) |
| [{Cu(terpy)} ₂ CA] ²⁺ [37] | 1.381(7) | 1.536(7) | 1.411(6) | 1.266(5) | 1.245(6) |
| [{Cu(tmen)} ₂ CA] ²⁺ [104] | 1.396(10) | 1.516(11) | 1.368(9) | 1.263(9) | 1.268(8) |
| [{Cu(L2)} ₂ CA] ²⁺ [41] | 1.385(5) | 1.530(5) | - | 1.268(5) | 1.252(5) |
| H ₂ CA [4] | 1.345 | 1.512 | 1.446 | 1.317 | 1.229 |

Table 5.5.: Comparison of crucial bonding parameters (in Å) of the tetraoxolene bridging ligand for some metal complexes. The labels of the carbon atoms are corresponding to those shown in Figure 5.11. (TPA = tris(2-pyridylmethyl)amine, TPyA = tris(2-pyridylmethyl)amine, DBQ = 2,5-di-tert-butyl-3,6-dihydroxy-1,4-benzoquinone, DAniF = N,N'-di-p-anisylformamidinate, cod = cycloocta-1,5-diene, bpy = 2,2'-dipyridyl, L1 = 3,3-bis(1-methylimidazol-2-yl)propionate, Me₅dien = 1,1,4,7,7-pentamethyldiethylenetriamine, terpy = 2,2':6,2''-terpyridine, tmen = N,N,N',N'-tetramethylethylenediamine, L2 = 1,4,7-trimethyl-1,4,7-triazacyclononane)

of chloranilate dianion; the negative charge can move more freely above and below the molecular plane without the constraint of hydrogen to make the $C - O$ lengths almost equal to each other as well as the bond lengths of the $C - C$ bonds parallel to the $C - O$ direction. [4] A combined description of the charge distribution and bond order of CA^{2-} is illustrated in Figure 5.10. From the structural data listed in Table 5.5, it seems like the extent of conjugation is largely dependent on the metal coordinated and its supporting ligand, which determine the energy level and spatial orientation of the overlapping valence orbital. Some dinuclear Cu(II) complexes with chloranilate dianion, for example $[Cu(Me_5dien)_2CA]^{2+}$, $[Cu(tmen)_2CA]^{2+}$, $[Cu(bpy)_2CA]^{2+}$, and $[CuCl(HL1)]_2CA$, have proven to share a great charge delocalization which gives rise to almost equidistant $C - O$ bonds as well as their parallel aligned $C - C$ bonds with a bond order of 1.5, where the $C - C$ bonds in the $C - Cl$ direction remain a bond order of 1 from their bond lengths. [86, 104, 40, 13] They have different coordination geometries but all their $Cu - O$ bonds are in the equatorial plane of no matter the octahedral, the square pyramidal, or the trigonal bipyramidal coordination structure, which allows satisfying orbital overlap facilitating free movement of electrons. In contrast, similar chloranilate bridged Cu(II) complexes with insufficient orbital overlap due to steric restriction arising from the terminal ligand, e.g. $[Cu(terpy)_2CA]^{2+}$, $[Cu(L2)_2CA]^{2+}$, and $[Cu(terpy)(DMSO)_2CA]^{2+}$, usually have $C - O$ bonds with different lengths. [37, 41, 60] The coordinated metal ions are also essential to the valence delocalization. Comparing to copper, the structural information of tetraoxolene bridged complexes with less electron-rich metal centers, such as Co(II) and Fe(II), for instance $[Rh(cod)]_2CA$, $[(TPA)Co]_2CA^{2+}$, $[(TPyA)Fe]_2DBQ^{2+}$, $[(TPyA)Co]_2CA^{2+}$, and $[(TPyA)Fe]_2CA^{2+}$, usually doesn't show bonds conjugations as great as those in the copper complexes. [14, 78, 76, 77] Nevertheless in the linked osmium compound prepared by Gupta et al., $[Os(PPh_3)_2(pap)]_2CA^{2+}$ (Figure 5.12), which is stabilized with triphenylphosphine and 2-(phenylazo)pyridine as supporting ligands, large charge delocalization in CA^{2-} was observed and proven by its structural parameters. [46] The different degree in electronic mobility among various chloranilate complexes is therefore a demonstration of different energy levels of their overall molecular orbitals, which are determined by the valence overlap between CA^{2-} and M^{n+} , in which the valence electrons of each $L - M$ moiety bridged by the tetraoxolene ligand reside; i.e. greater orbital overlap stemming from either steric preference (ligand originated) or large valence extension (metal originated) would favor the electronic delocalization within the bridging ligand, thus electronic and magnetic communication between the metal centers, or the metal center and the bridging ligand is more likely to take place. For example in the crystal structure of the chloranilate linked tetranuclear Mo complex prepared by Cotton et al., $[Mo_2(DAniF)_3]_2CA$ (Figure 5.13), the $C - O$ bonds (1.285(6) Å and 1.292(6)

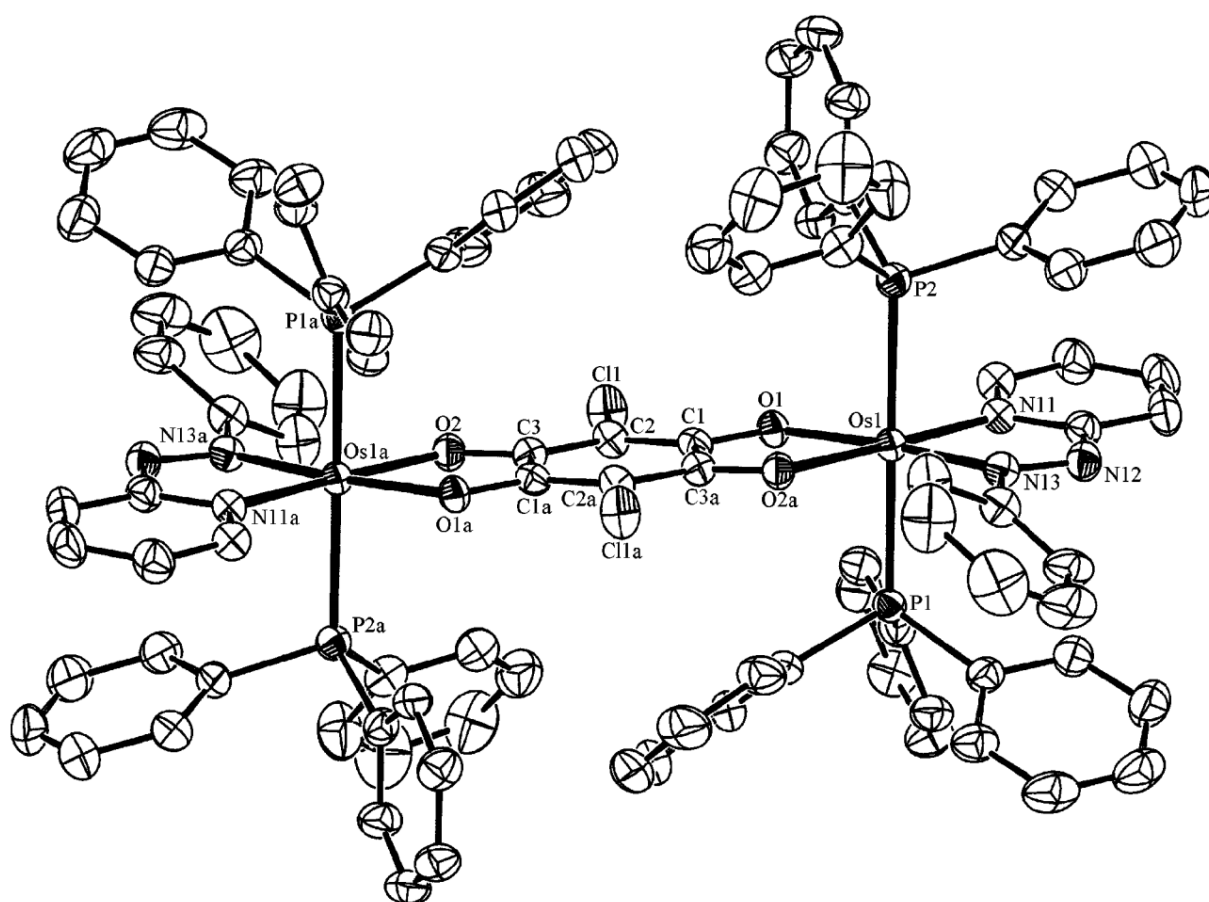


Figure 5.12.: Molecular structure of $[\{\text{Os}(\text{PPh}_3)_2(\text{pap})\}_2\text{CA}]^{2+}$ (pap = 2-(phenylazo)pyridine) prepared by Gupta et al.. [46]

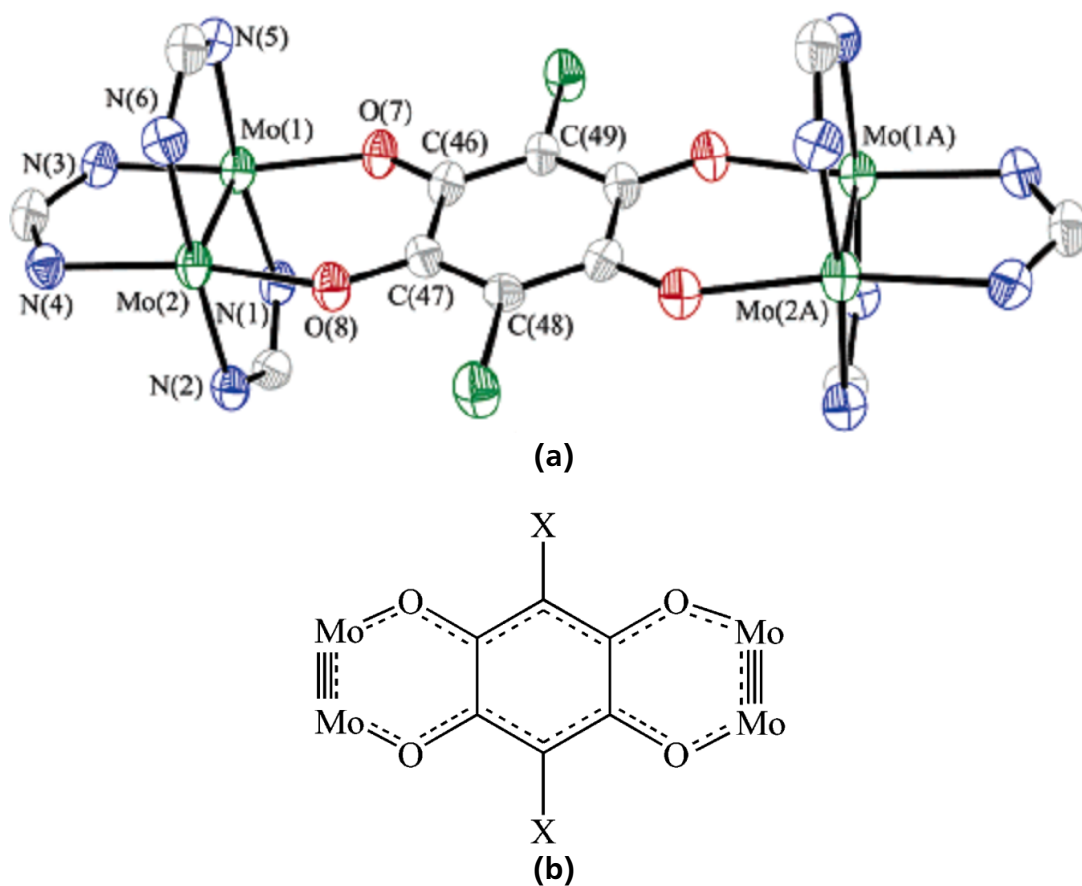


Figure 5.13.: Structure (Fig. 5.13a) and scheme of the core moiety (Fig. 5.13b) of $[Mo_2(DAniF)_3]_2CA$ prepared by Cotton et al., $DAniF = N,N'$ -di-*p*-anisylformamidinate, $X = Cl, Br$. [21]

Å) [21] are markedly longer than those for CA^{2-} dianion (1.243(6) Å and 1.253(8) Å) [3] while the $C - C$ bonds parallel to the $C - Cl$ are shorter comparing to those in CA^{2-} , indicating that the bridging ligand has already been partially reduced to CA^{3-} through valence tautomerization with one of the $[Mo_2]$ units due to significant large orbital overlap between CA^{2-} and the metal ions. [21] For the first chloranilate bridged Cu(I) compound ever prepared, the charge distribution within the redox active bridging ligand as well as the metal centers is an issue of prime importance. Either its nearly equidistant $C - O$ bonds or the $C - C$ lengths along the chain $O1 - C1 - C3 - C2^* - O2^*$ is in good agreement with those for the isolated CA^{2-} dianion [4], demonstrating that the bridging ligand in (9) has the same bond delocalization as is illustrated in Figure 5.10. The chloranilate linker doesn't show any specific structural feature for the reduced radical (cat,sq) or catecholate (cat,cat) form (Figure 3.2), which would present longer $C - O$ bonds with the more single bond character and nearly equidistant aromatic $C - C$ bond lengths close to those of a phenyl ring [49, 46, 78, 77]; instead it still remains the semiquinone form which precludes any reduction by the Cu(I) ion. Comparing to the Cu(II) analogues, the less electronegative Cu(I) ion with valence d^{10} configuration allows the donating electrons of CA^{2-} are of more ligand property rather than delocalizing deeply into the metal's orbitals, leading to the sufficient charge delocalization of the linking ligand just as what's in its free dianion. The longer $Cu - O$ bonds in comparison to those of Cu(II) tetraoxolene compounds [104, 40, 41, 13] also support this deduction. Although Cu(I) ion appears to be more electron-rich from its oxidation state, however, its full-filled d-orbitals provide predominant stability for electrons which makes the energy gap between the ground state and the excited state, where d-electrons populate the anti-bonding orbital of general bridging ligand character, too large to access valence tautomerism easily. Consequently, long distance electronic communication would happen difficultly for the $[Cu^I] - (sq, sq)^{2-} - [Cu^I]$ configuration under normal conditions.

The large energetic gap between bonding and anti-bonding orbitals of the bridge is also illustrated in the UV-vis spectrum of the compound. Both $\pi - \pi^*$ and $n - \pi^*$ transitions of the ligand are blue-shifted to higher energies comparing to those of free chloranilate acid (Table 5.6). This observation can be interpreted that coordination to a metal ion results in an increase in the bonding orbital to anti-bonding orbital gap of the dianion of the chloranilate ligand. No metal-ligand charge transfer band is observed for the complex which probably arises from a large discrepancy in energies between the HOMO and LUMO of the complex, which may be a consequence of the extra stability of the Cu(I) d^{10} configuration. It is generally considered that the intramolecular charge transfer of the tetraoxolene bridged complexes is due to the effective orbital overlap of the metal $d(\pi)$ and the bridging ligand π^* orbitals that are comparable in their energy

| Compound | Wavenumber (nm) | Absorbance (arbitrary unit) |
|-------------|-----------------|-----------------------------|
| Complex (9) | 294.8 | 2.373 |
| | 480.8 | 0.989 |
| H_2CA | 303.2 | 2.201 |
| | 527.6 | 0.105 |

Table 5.6.: Spectra parameters for the UV-vis absorption (in arbitrary unit) of (9) and H_2CA .

levels. [118, 49, 46, 21, 27, 5, 72, 47] The low energy levels of the fully occupied d orbitals of Cu(I) ion might result in a relatively large energy difference between the $d(\pi)$ orbitals of Cu and the π^* orbitals of chloranilate, which encumbers the effective orbital recombination. Therefore, the absorption for intramolecular charge transfer within (9) is not in presence.

Since both the dppf ligand and the Cu centers would take part in the electron transfer during the cyclic voltammogram of (9), it is challenging to interpret the diagram through assigning each wave unambiguously to a specific redox process. Nevertheless, the wave at 0.719 V of large peak current can be undoubtedly attributed to the simultaneous Fe^{2+}/Fe^{3+} oxidation of the two terminal dppf groups, which do not undergo electronic communication because of their very long intramolecular distance (15.702 Å), comparing with the Fe^{2+}/Fe^{3+} redox couple at 0.723 V for the free dppf molecule [82] and with a value of 0.70 V and 0.68 V for dppf-Cu(I) containing complexes (dppf)Cu(L1) (L1 = N,N'-di-n-butyl-2-amino-5-alcoholate-1,4-benzoquinonemonoiminium) and (dppf)Cu(L2) (L2 = N,N'-diisopropyl-2-amino-5-alcoholate-1,4-benzoquinonemonoiminium), respectively [11]. The peak at 0.929 V in the anodic region can be assigned to a Cu^+/Cu^{2+} oxidation of the two copper centers through a two-electron transfer process. Both of the two oxidations are irreversible without the consequent reduction peak. The sample started to decompose just after the first two-electron reduction process at -0.987 V, and yellow depositions on the electrode surface were observed during the measuring, which were main obstacles for reversible electrode reactions. According to the results of the previous electrochemical measurements for Cu(I) and chloranilate dianion [115, 120], both could undergo a reduction giving the first reductive peak at -0.987 V. As the Cu(I) acceptor with full-filled d^{10} electronic configuration is less electronegative than its chloranilate donor, this peak is assigned to a two-electron reduction of the ligand from CA^{2-} to CA^{4-} , whereas the other two reductive peaks at -1.737 and -2.031 V are impossible to interpret. The complex underwent an ECE process during the cyclic voltammetry measurement, which gives rise to the observed complexity of the redox properties of tetranuclear complex (9).

6 Summary and conclusions

6.1 Complexes with tris(pyrazolyl)borate ligands

The coordination ability for design and building transition metal complexes of the first generation of tris(pyrazolyl)borate chelating ligands (Tp and Tp^*) were successfully extended through isolation and structural determination of several unprecedented cobalt complexes, with mono or multi-nuclear frameworks supported by the tridentate facially coordinated Tp and Tp^* ligands. The findings are beyond the limitation of the strong tendency towards formation of octahedral Tp_2^xM type complexes that usually result from Tp and Tp^* associated reactions.

The tri-nuclear Co complex $Tp_2Co_2(Hpz)_2Br_2(CoBr_2)$ (**1**) was prepared from reaction of TpK and $CoBr_2$, and is the first multinuclear Co(II) complex with $TpCo^+$ building blocks reported. Its molecular structure determined through single crystal X-ray diffraction comprises two Co(II) centers, which both are octahedrally coordinated by a Tp ligand, a pyrazole, and two bromides, and are linked by a $[Co^{II}]$ unit via $Co - Br$ bridges. The intramolecular neighboring $Co \cdots Co$ distance is 3.472 Å. The compound is extremely air-sensitive and can be easily transformed into an ionic Co(III) compound $(Tp_2Co^{III})_2(Co_2^{II}Br_6)$ (**2**). The isolation of (**2**) in addition to the formation of (**1**) may be ascribed to trace amounts of water and dioxygen dissolved in solvent that participated in the reaction. Meanwhile, a side-product with the molecular formula $H(Hpz)B(pz)_2CoBr_2$ (**3**) was isolated from the reaction, in which Co^{2+} is coordinated by a protonated tris(pyrazolyl)borate unit in an unusual dipodal manner.

Studying the influence of methyl substituents on 3- and 5-positions of the pyrazolyl ring of Tp ligands towards its coordination behavior was performed through a comparable reaction of tris(3,5-dimethyl-pyrazolyl)borate anion (Tp^*) and $CoBr_2$, from which a mono-nuclear tetrahedral coordinated Tp^*CoBr (**4**) was obtained and structurally characterized. In addition, a byproduct $H(Hpz^*)B(pz^*)_2CoBr_2$ (**5**) that is analogous to (**3**) was obtained from the previous reaction. Experimental results could manifest that the inductive effects of methyl groups increase the electron density on the pyrazolyl nitrogen donors, favoring their stronger affinity to metal ion. A comparison among structural features of various Tp and Tp^* related complexes discloses a nonnegligible affection of the steric hindrance and shielding effect of the substituents on the coordination of the Co centers to the Tp ligands. These effects underline that Tp^*CoBr would be an appropriate precursor for synthesizing further structurally demanding Tp^*

compounds, as formation of Tp_2^*Co , which is typically the main product of reactions involving the Tp^* structure, could be retarded due to steric impediment arising from the methyl substituents. (4) can be oxidized in solution giving a Co(III) containing compound $(Tp_2^*Co)(CoBr_3pz^*)$ (6), in which Co(III) (low spin) has a large octahedral ligand field splitting. A Co^{2+} induced $B - N$ cleavage reaction of Tp^*CoBr was found to be a side reaction.

Reaction of complex (4) with $LiSPh$ gave the thiophenolato complex Tp^*CoSPh (7) whose crystal structure was determined. The crystallographic parameters demonstrate that the ligand SPh^- leads to a large distorted tetrahedral geometry about the Co(II) center where tripodal Tp^* coordinates to the metal center in manner of bearing a resemblance to that for half-sandwich $Cp^xM - L$ complexes, due to interaction of the ligand's π^* orbital and d orbitals of the metal.

A very rare, linked dinuclear cobalt complex (8) supported by the first generation scorpionate Tp^* ligand was synthesized from a controlled reaction of $CoBr_2$, Tp^* , and Li^+pz^- . The molecular structure of (8) shows that two Tp^*Co building blocks are bridged by two pyrazolyl anions and a dioxygen molecule, where both the cobalt centers are octahedrally coordinated being separated from each other in a distance of 3.591 Å. NMR spectra indicate that the complex is diamagnetic. A reasonable explanation for that is both of the copper centers are oxidized to +3 state by dioxygen and in the low spin d^6 electron configuration, whereas the bridging $[O_2]$ unit is a peroxide O^{2-} dianion, which is consistent with strong peroxide $O - O$ stretching observed in IR spectrum. Particular $Co - O$ bonds of great covalent nature are found existing within the complex, based on its structural parameters.

The new complexes discovered, further expand the chemistry concerned with homoscorpionates of the first generation, exhibiting their potential for building complicated structures embracing various metal centers. Although a large amount of new types of scorpionates ligands having sophisticated molecular extensions have been developed since the 70's, the first generation homoscorpionates just as Tp and Tp^* are still of unique importance, due to their easy accessibility. The possibility of stabilizing more complicated molecules containing Tp and Tp^* provides new route to design and study modern materials, catalysts, and molecular devices.

6.2 Cu(I) complex of the chloranilate dianion

An unprecedented tetranuclear complex (9) containing Cu(I) centers bridged by chloranilate dianion (CA^{2-}) and two dppf ancillary ligands was successfully prepared and characterized. At ambient temperature, two $(dppf)Cu^+$ have been linked by

the bidentate chelating chloranilate ligand resulting in the formation of the complex $(dppf)_2Cu_2^I(CA)$. A single crystal X-ray study confirmed its tetranuclear molecular structure, in which the two Cu(I) centers are tetrahedrally coordinated by two oxygen donors of the CA^{2-} ligand as well as two phosphorus atoms from each dppf ligand. The two copper centers are connected by the tetraoxolene ligand with a separation of 7.940 Å. The bond lengths point toward the fact that the bridging dianion is of the bis-semiquinone type, comprising highly delocalized $O - C - C - C - O$ moieties. Because of the remarkable stability of d^{10} electron configuration of the copper ion, the redox active chloranilate ligand preserves its semiquinone dianion state. Neither structural feature of CA^{3-} radical nor hint of valence tautomerism relating to metal-ligand electron redistribution was observed.

The energy difference between the ligand's HOMO and LUMO obviously becomes larger after coordination to the copper center, which manifests itself by the blue-shift of the $\pi - \pi^*$ absorption of the bridged chloranilate ligand in UV-Vis spectrum comparing to that of free chloranilate dianion. These results express a quite complicate intramolecular interaction involving both redox active metal centers and ligand concerned with metal-metal electronic communication, metal-ligand valence tautomerization, and non-innocent ligand related oxidation or reduction. Elaborate manipulation of each oxidation state on the premise of preserving the coordination pattern and valence delocalization of chloranilate ligand and its derivatives, as well as appropriate metal ions with proper spins are thus vital considerations held in further development of such kind of compounds, which are potentially of enormous importance for researches of new materials, molecular devices, and bioinorganic chemistry.

Part IV.

Supplement

7 Experimental part

7.1 General description

All chemicals were purchased as reagent grade from commercial suppliers and used without further purification unless otherwise noted. Solvents were purchased from either Merck KGaA or Aldrich Chemical Co. All solvents applied for water and oxygen free reactions were predried with molecular sieve (0.4 nm) for a week. THF was refluxed under argon atmosphere over K metal for 3 days and freshly distilled prior to use; diethyl ether was refluxed over Na metal/benzophenone for 3 days and freshly distilled prior to use; dichloromethane was refluxed over CaH_2 for 3 days and freshly distilled prior to use; toluene was refluxed over Na metal for a week and freshly distilled prior to use; petroleum ether was refluxed over Na/K alloy for a week and distilled prior to use; acetonitrile was refluxed over P_2O_5 for 1 day and freshly distilled prior to use. All reactions involving air-sensitive species were carried out under Ar using standard Schlenk techniques [73].

7.2 Analytical methods

NMR spectra were recorded on Bruker ARX 300 and Bruker DRX 500 spectrometers. Chemical shifts (δ) were given in ppm with TMS as reference. IR spectra were obtained on Nicolet Impact 400 and Nicolet 6700 FT-IR spectrometers. Samples were prepared as KBr pellets or directly mounted on an ATR unit of the spectrometer. Single crystal X-ray diffraction was performed on STOE, STADI 4 X-ray diffractometer and ENRAF-NONIUS, CAD4 X-ray diffractometer in Material Science department at TU Darmstadt or on ENRAF-NONIUS, CAD4 X-ray diffractometer in Max-Planck-Institut für Kohlenforschung, in Mülheim an der Ruhr, using graphite-monochromated $Mo K\alpha$ radiation; the structures were calculated with SHELXS-97 and SHELXS-97 packages [97] and displayed with the crystal structure visualisation software “Mercury” [51]. Cyclic voltammograms were recorded on an Amel potentiostat in DME with 0.1 M [nBu_4N][BF_4] as supporting electrolyte; a platinum working electrode and an aqueous saturated calomel reference electrode (SCE) were used for the measurement, and the voltage scan rate is 100 mV/s. Elemental analysis to identify C, H, N compositions was obtained in the microanalytical laboratory of TU Darmstadt. UV-Vis spectra were recorded on Perkin Elmer, Lambda 900 spectrometer.

7.3 Preparation of starting materials

7.3.1 Sodium 3,5-dimethylpyrazolide

1.07 g *NaH* (43.6 mmol) was suspended in toluene. A solution of 4.27 g of 3,5-dimethylpyrazole (44.5 mmol) in toluene was dropped into this suspension at room temperature with stirring. Vigorous gas evolution was observed. The mixture was refluxed for 12 h and then cooled down to room temperature. A white precipitate was formed, which were filtered off under Ar atmosphere, washed two times with toluene followed by two times with petroleum ether, and finally dried under vacuum. The crude product was extracted with hot THF and filtered. Removal of the solvent of the filtrate gave white crystals that were dried under vacuum. Yield: 95 %

7.3.2 $[(\text{CH}_3\text{CN})_4\text{Cu}](\text{BF}_4)$

The compound was prepared according to previously described procedures developed by Kubas. [64]

7.3.3 $[(\text{dppf})\text{Cu}(\text{NCCH}_3)_2](\text{BF}_4)$

The compound was prepared according to the published procedures from Diez et al. [33]. 0.378 g $[(\text{CH}_3\text{CN})_4\text{Cu}](\text{BF}_4)$ (1.2 mmol) was dissolved in 40 ml of acetonitrile and 0.665 g of dppf (1.2 mmol) was added to the solution. 30 ml of dichloromethane was then added. The resulting solution was stirred at room temperature for 20 h and then concentrated. 30 ml of diethyl ether was added, resulting in a small amount of precipitate. The mixture was filtered, concentrated to ca. 30 ml, and then stored at -28 °C. After 24 h yellow crystals were obtained. Yield: 50 - 60 %

7.4 Preparation of ligands

7.4.1 Potassium hydrotris(pyrazolyl)borate (TpK)

A 250 ml three-neck flask was equipped with an air-condenser connected to a gas volume gauge. 50 mmol of KBH_4 (2.7 g) and 200 mmol of pyrazole (13.6 g) are mixed together and put into the flask together with a magnetic stirring bar. A Quickfit adapter

with a thermometer was mounted on the flask through one of its three necks. The mixture was heated with stirring to 90 °C. The powder melted and H₂ evolution started. The melt temperature was increased gradually along with the gas evolution to 180 °C, until a total volume of 3.75 l of H₂ (150 mmol) had been released. The reaction mixture was cooled down to 150 °C and poured into 30 ml of toluene with vigorous stirring. After 5 min, the mixture was filtered, washed with 10 ml of hot toluene for 2 times, and then with 10 ml of hexane for another 2 times. The resulting white crystals were air-dried and recrystallized from anisole.

Yield: 9.6 g (76 %)

¹H NMR (d⁶-DMSO, 300 MHz, 25 °C): δ = 5.98 (s, C⁴ – H, 3H), 7.29 (s, C³ – H, 3H), 7.31 (s, C⁵ – H, 3H) ppm. IR (KBr, 4000 – 400 cm⁻¹): $\tilde{\nu}$ = 3121 (w, ν (C – H)), 2436 (m, ν (B – H)), 1639 (w, ν (C = C)), 1504 (m, ν (C = C)), 1417 (m, ν (N = N)), 1388 (s, ν (N = N)), 1292 (s, ν (C = N)), 1213 (s, δ (C – H)), 1117 (s, δ (C – H)), 1044 (s, ν (B – N)), 963 (m, ring breathing), 777 (s, γ (C – H)), 732 (s, γ (C – H)), 672 (w), 625 (w) cm⁻¹. **Elemental analysis** (for C₉H₁₀N₆BK, M = 251.9 g/mol): calculated C 42.86, H 3.97, N 33.33; found C 42.29, H 4.08, N 32.26.

7.4.2 Potassium hydrotris(3,5-dimethyl-pyrazolyl)borate (Tp^{*} K)

The reaction was performed using a similar procedure as described for TpK. In a three-neck flask equipped with an air-condenser and a thermometer, 9.6 g of 3,5-dimethyl-pyrazole (0.1 mol) and 1.35 g of KBH₄ (25 mmol) were heated together to melt while 1875 ml of hydrogen gas (75 mmol) were released. The final reaction temperature of the liquid melt was 240 °C. The mixture was then poured under stirring into 50 ml of toluene and filtered after cooling down to room temperature. The final white crystals were filtered off, washed three times with 10 ml of hot toluene followed by two times of washing with 10 ml of hexane. The crude product was recrystallized from anisole.

Yield: 6.02 g, 1.79 mmol (72 %)

¹H NMR (D₂O, 300 MHz, 25 °C): δ = 2.15 (s, CH₃, 18H), 5.88 (s, C⁴ – H, 3H) ppm. ¹³C NMR (D₂O, 75.5 MHz, 25 °C): 103.90 (CH₃), 146.08 (–CH–) ppm. IR (KBr, 4000 – 400 cm⁻¹): 3121 (w, ν (C – H)), 2925 (m, ν (H₂C – H)), 2438 (m, ν (B – H)), 1538 (s, ν (C = C)), 1416 (s, ν (C = N)), 1349 (m, δ (CH₃)), 1191 (s, δ (CH₃)), 1071 (s, ν (B – N)), 812 (m, γ (C – H)) cm⁻¹.

7.5 Synthesis of new complexes

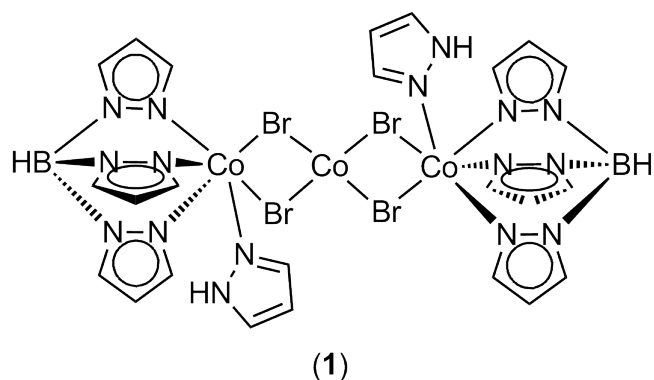


Figure 7.1.: $[\text{HB}(\text{pz})_3\text{Co}(\text{Hpz})]_2(\mu\text{-Br})_4\text{Co}$

7.5.1 $[\text{HB}(\text{pz})_3\text{Co}(\text{Hpz})]_2(\mu\text{-Br})_4\text{Co}$ (1)

To a THF (40 ml) solution of CoBr_2 (0.39 g, 1.78 mmol), 0.4 g of *TpK* (1.6 mmol) was added at room temperature. A white precipitate formed immediately and the whole mixture was stirred overnight. All of the solvent was then evaporated through a vacuum line, and the residue was extracted with CH_2Cl_2 and filtered. The filtrate was concentrated to 5 ml and layered with petroleum ether. After 24 hours purple crystals of (1) were collected which are highly air-sensitive. (Figure 7.1)

Molar mass: 1058.22 g/mol

Yield: ca. 0.06 g, 0.06 mmol (10 %)

IR (KBr, 4000 – 400 cm^{-1}): 3419 (m, $\nu(\text{N-H})$), 3112 (w, $\nu(\text{C-H})$), 2477 (m, $\nu(\text{B-H})$), 1633 (w, $\nu(\text{C=C})$), 1503 (m, $\nu(\text{C=C})$), 1405 (s, $\nu(\text{N=N})$), 1308 (s, $\nu(\text{C=N})$), 1212 (m, $\delta(\text{C-H})$), 1114 (m, $\delta(\text{C-H})$), 1047 (s, $\nu(\text{B-N})$), 980 (m), 766 (s, $\gamma(\text{C-H})$), 716 (s, $\gamma(\text{C-H})$), 461 (w, $\nu(\text{Co-N})$) cm^{-1} .

Atomic coordinates ($\times 10^4$) and equivalent isotropic displacement parameters ($\text{Å}^2 \times 10^3$) for complex (1)

| | x | y | z | U (eq) |
|-------|---------|---------|---------|--------|
| Br(1) | 1508(1) | 2423(1) | 2441(1) | 91(1) |
| Br(2) | 123(1) | 4095(1) | 1455(1) | 71(1) |
| Co(1) | 1786(1) | 3165(1) | 1192(1) | 56(1) |
| Co(2) | 0 | 3277(1) | 2500 | 63(1) |
| N(1) | 3087(6) | 2438(6) | 1031(5) | 68(3) |
| N(2) | 3251(6) | 2104(5) | 384(5) | 58(2) |
| N(3) | 997(6) | 2195(5) | 684(4) | 52(2) |

| | | | | |
|--------|----------|----------|----------|---------|
| N(4) | 1425(6) | 1870(5) | 88(4) | 57(2) |
| N(5) | 1997(6) | 3739(6) | 221(4) | 56(2) |
| N(6) | 2295(5) | 3203(6) | -297(4) | 53(2) |
| N(7A) | 2744(14) | 4018(13) | 1742(10) | 54(5) |
| N(8A) | 2532(15) | 4454(16) | 2417(9) | 79(5) |
| C(1) | 3878(9) | 2198(8) | 1406(7) | 80(4) |
| C(2) | 4540(9) | 1719(9) | 1025(8) | 87(4) |
| C(3) | 4133(8) | 1673(7) | 378(7) | 75(4) |
| C(4) | 138(8) | 1785(7) | 766(6) | 60(3) |
| C(5) | -25(8) | 1190(8) | 258(7) | 73(3) |
| C(6) | 815(8) | 1250(7) | -165(6) | 67(3) |
| C(7) | 1890(7) | 4517(7) | -52(6) | 63(3) |
| C(8) | 2118(7) | 4491(8) | -743(6) | 67(3) |
| C(9) | 2358(7) | 3651(8) | -882(6) | 60(3) |
| C(10A) | 3625(17) | 4399(15) | 1470(13) | 63(6) |
| C(11A) | 4175(19) | 4786(16) | 1945(11) | 82(9) |
| C(12A) | 3491(17) | 4742(19) | 2578(12) | 85(7) |
| B(1) | 2450(9) | 2212(8) | -177(7) | 56(3) |
| N(7B) | 2506(13) | 4268(13) | 1616(9) | 48(4) |
| N(8B) | 2290(30) | 4910(20) | 2185(17) | 172(14) |
| C(10B) | 3330(19) | 4700(20) | 1318(14) | 85(9) |
| C(11B) | 3580(30) | 5290(20) | 1759(17) | 147(15) |
| C(12B) | 3100(30) | 5280(30) | 2471(18) | 141(14) |

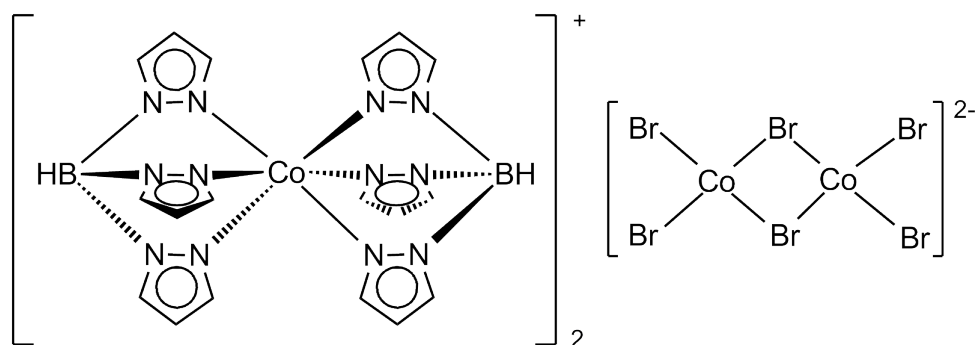
7.5.2 $\{[\text{HB}(\text{pz})_3]_2\text{Co}\}_2(\text{Co}_2\text{Br}_6)$ (2)

After separation of (1), the mother liquid from the crystallization of (1) was further stored in the air. Green crystals appeared after another 24 hours. (Figure 7.2)

Molar mass: 1082.02 g/mol

Yield: ca. 0.08 g, 0.07 mmol (18 %)

IR (KBr, 4000 – 400 cm^{-1}): 3102 (m, $\nu(\text{C} - \text{H})$), 2532 (m, $\nu(\text{B} - \text{H})$), 1623 (w, $\nu(\text{C} = \text{C})$), 1502 (m, $\nu(\text{C} = \text{C})$), 1410 (s, $\nu(\text{N} = \text{N})$), 1397 (m, $\nu(\text{N} = \text{N})$), 1326 (s, $\nu(\text{C} = \text{N})$), 1223 (s, $\delta(\text{C} - \text{H})$), 1119 (m, $\delta(\text{C} - \text{H})$), 1053 (s, $\nu(\text{B} - \text{N})$), 997 (w, ring breathing), 777 (m, $\gamma(\text{C} - \text{H})$), 461 (w, $\nu(\text{Co} - \text{N})$), 421 (w, $\nu(\text{Co} - \text{N})$) cm^{-1} .



(2)

Figure 7.2.: $\{[\text{HB}(\text{pz})_3]_2\text{Co}\}_2(\text{Co}_2\text{Br}_6)$

Atomic coordinates ($\times 10^4$) and equivalent isotropic displacement parameters ($\text{\AA}^2 \times 10^3$) for complex (2)

| | x | y | z | U (eq) |
|-------|---------|---------|----------|--------|
| Co(1) | 5000 | 5000 | 0 | 38(1) |
| N(1) | 6542(4) | 5330(3) | -672(3) | 47(1) |
| N(2) | 7526(3) | 4688(4) | -563(3) | 46(1) |
| N(3) | 4987(3) | 3282(3) | -442(3) | 44(1) |
| N(4) | 6097(3) | 2829(3) | -366(3) | 47(1) |
| N(5) | 6077(4) | 4987(3) | 1178(3) | 46(1) |
| N(6) | 7095(4) | 4370(4) | 1103(3) | 48(1) |
| C(1) | 6954(5) | 6177(4) | -1184(4) | 53(1) |
| C(2) | 8204(5) | 6093(5) | -1421(4) | 57(1) |
| C(3) | 8520(5) | 5158(5) | -1013(4) | 51(1) |
| C(4) | 4051(5) | 2353(4) | -851(4) | 54(1) |
| C(5) | 4554(5) | 1282(5) | -1029(5) | 65(2) |
| C(6) | 5830(5) | 1627(5) | -725(5) | 62(2) |
| C(7) | 6094(5) | 5522(5) | 2145(4) | 60(1) |
| C(8) | 7123(6) | 5262(6) | 2681(5) | 75(2) |
| C(9) | 7714(5) | 4548(6) | 2007(5) | 66(2) |
| B(1) | 7338(5) | 3709(5) | 66(5) | 49(2) |
| Co(2) | 5000 | 0 | 5000 | 36(1) |
| N(7) | 5944(3) | 1414(3) | 5903(3) | 42(1) |
| N(8) | 6892(4) | 1289(3) | 6569(3) | 43(1) |

| | | | | |
|-------|----------|----------|----------|---------|
| N(9) | 6598(3) | -568(4) | 4740(3) | 43(1) |
| N(10) | 7493(3) | -526(4) | 5520(3) | 44(1) |
| N(11) | 4848(3) | -834(3) | 6097(3) | 40(1) |
| N(12) | 5900(4) | -747(4) | 6752(3) | 43(1) |
| C(10) | 5872(5) | 2586(5) | 6028(4) | 53(1) |
| C(11) | 6782(6) | 3261(5) | 6799(4) | 65(2) |
| C(12) | 7403(5) | 2404(5) | 7111(4) | 60(2) |
| C(13) | 7098(5) | -1036(5) | 3910(4) | 53(1) |
| C(14) | 8299(5) | -1299(5) | 4138(5) | 66(2) |
| C(15) | 8523(5) | -947(5) | 5181(4) | 56(1) |
| C(16) | 3861(5) | -1500(5) | 6407(4) | 52(1) |
| C(17) | 4279(6) | -1866(5) | 7273(4) | 66(2) |
| C(18) | 5585(5) | -1363(5) | 7450(4) | 54(1) |
| B(2) | 7183(5) | 8(5) | 6588(4) | 46(1) |
| Br(1) | -518(1) | 7759(1) | 1491(1) | 58(1) |
| Br(2) | -777(1) | 11314(1) | 2397(1) | 79(1) |
| Br(3) | 1696(1) | 10391(1) | 445(1) | 51(1) |
| Co(3) | -350(1) | 9736(1) | 1130(1) | 44(1) |
| O(1) | 4459(9) | 4469(9) | 4511(7) | 191(3) |
| C(19) | 3272(10) | 3782(9) | 4372(7) | 134(3) |
| O(2) | 346(18) | 6023(16) | 4799(14) | 413(10) |

7.5.3 HB(pz)₂(Hpz)CoBr₂ (3)

Blue crystals of the side product (3) from the reaction for preparation of (1) was isolated from the crystallization mother liquid of (1). (Figure 7.3)

Molar mass: 432.61 g/mol

Yield: ca. 0.03 g, 0.07 mmol (4.3 %)

Atomic coordinates ($\times 10^4$) and equivalent isotropic displacement parameters ($\text{Å}^2 \times 10^3$) for complex (3)

| | x | y | z | U (eq) |
|------|----------|----------|---------|--------|
| C(1) | 10239(5) | -1363(3) | 3501(5) | 43(1) |

| | | | | |
|-------|----------|----------|----------|-------|
| C(2) | 11028(6) | -2100(4) | 3302(5) | 53(2) |
| C(3) | 10204(5) | -2487(3) | 2238(5) | 47(1) |
| C(4) | 4506(5) | -1783(3) | 2010(5) | 41(1) |
| C(5) | 4079(5) | -2586(3) | 1452(5) | 43(1) |
| C(6) | 5179(5) | -2814(3) | 848(4) | 39(1) |
| C(7) | 6890(6) | -606(3) | -2045(5) | 48(1) |
| C(8) | 8400(6) | -542(3) | -1782(5) | 53(2) |
| C(9) | 8877(5) | -1053(3) | -713(5) | 42(1) |
| N(1) | 8997(4) | -1303(2) | 2598(4) | 32(1) |
| N(2) | 8982(4) | -2010(2) | 1805(4) | 34(1) |
| N(3) | 5797(4) | -1526(2) | 1768(4) | 33(1) |
| N(4) | 6206(4) | -2176(2) | 1032(3) | 32(1) |
| N(5) | 6521(4) | -1125(3) | -1176(4) | 40(1) |
| N(6) | 7735(4) | -1414(2) | -323(3) | 32(1) |
| B(1) | 7718(6) | -2189(4) | 656(5) | 35(1) |
| Co(1) | 7197(1) | -540(1) | 2442(1) | 32(1) |
| Br(1) | 6913(1) | -69(1) | 4502(1) | 49(1) |
| Br(2) | 7089(1) | 711(1) | 1082(1) | 41(1) |

7.5.4 HB(3,5-Me₂-pz)₃CoBr (4)

1.14 g of *CoBr*₂ (5.3 mmol) was dissolved in 20 ml of THF in a 100 ml Schlenk flask. Under stirring, a solution of *KTp** (1.6 g, 4.76 mmol) in THF was added dropwise, and the mixture was stirred at R.T. for 1 hour. The mixture was filtered and the residue was washed with THF until the eluent became colorless. The blue filtrate was evaporated under vacuum to dryness. The residue was redissolved in 10 ml of *CH*₂*Cl*₂ and stored at -28 °C. After 12 hours the first crop of blue crystals were collected and then 10 ml of petroleum ether was added to the mother liquid, affording the second crop of crystals after being stored at -28 °C for another 48 hours. Single crystals suitable for X-ray crystal structure determination were grown by layering a concentrated *CH*₂*Cl*₂ solution of (4) with pentane at room temperature. (Figure 7.4)

Molar mass: 435.6 g/mol

Yield: 0.96 g, 2.2 mmol (46 %)

IR (KBr, 4000 – 400 cm⁻¹): 3121 (w, $\nu(=C-H)$), 2927 (w, $\nu(H_2C-H)$), 2541 (m, $\nu(B-H)$), 1540 (s, $\nu(C=C)$), 1447 (s, $\nu(C=N)$), 1419 (m, $\nu(N=N)$), 1346 (m,

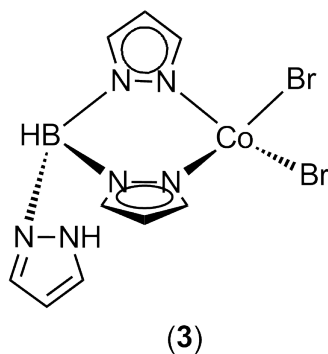


Figure 7.3.: $\text{HB}(\text{pz})_2(\text{Hpz})\text{CoBr}_2$

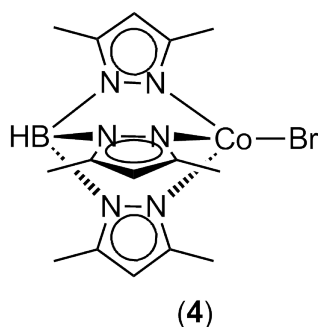


Figure 7.4.: $\text{HB}(3,5\text{-Me}_2\text{-pz})_3\text{CoBr}$

$\delta(\text{CH}_3)$, 1172 (s, $\delta(\text{C} - \text{H})$), 1064 (s, $\nu(\text{B} - \text{N})$), 982 (w, ring breathing), 800 (s, $\gamma(\text{C} - \text{H})$), 689 (w), 638 (w), 464 (w, $\nu(\text{Co} - \text{N})$) cm^{-1} . **MS** (EI): $m/z = 435 (\text{M}^+)$, 356 ($[\text{M} - \text{Br}]^+$), 340 ($[\text{M} - \text{pz}^*]^+$). **$^1\text{H NMR}$** (CDCl_3 , 300 MHz, 25 °C): $\delta = 80.30$ (s, $\text{C} - \text{H}$, 3H), 13.06 (s, $\text{C}^5 - \text{CH}_3$, 9H), 13.60 (s, $\text{C}^3 - \text{CH}_3$, 9H), -39.74 (w, $\text{B} - \text{H}$, 1H) ppm.

Atomic coordinates ($\times 10^4$) and equivalent isotropic displacement parameters ($\text{\AA}^2 \times 10^3$) for complex (4)

| | x | y | z | U (eq) |
|-------|---------|----------|---------|--------|
| C(1) | 1969(3) | 4525(5) | 2317(3) | 42(1) |
| C(2) | 2429(4) | 3760(6) | 1699(4) | 49(1) |
| C(3) | 1793(4) | 3946(6) | 1097(3) | 44(1) |
| C(4) | 0 | 9720(9) | 1425(5) | 51(2) |
| C(5) | 0 | 9881(10) | 649(6) | 61(2) |
| C(6) | 0 | 8365(10) | 341(5) | 50(2) |
| C(7) | 2322(4) | 4690(7) | 3105(4) | 54(1) |
| C(8) | 1920(4) | 3399(8) | 299(3) | 63(2) |
| C(9) | 0 | 10956(9) | 2038(6) | 64(3) |
| C(10) | 0 | 7831(13) | -481(5) | 75(3) |

| | | | | |
|-------|---------|----------|---------|-------|
| B(1) | 0 | 5355(11) | 912(6) | 43(2) |
| Br(1) | 0 | 7622(1) | 3724(1) | 59(1) |
| Co(1) | 0 | 6605(1) | 2487(1) | 35(1) |
| N(1) | 1092(3) | 5149(4) | 2089(2) | 37(1) |
| N(2) | 962(3) | 4781(4) | 1339(2) | 36(1) |
| N(3) | 0 | 8106(7) | 1586(4) | 43(2) |
| N(4) | 0 | 7287(8) | 920(4) | 44(2) |
| C(11) | 3039(4) | 132(6) | 3165(4) | 54(2) |
| C(12) | 2614(4) | 239(7) | 3871(4) | 60(2) |
| C(13) | 3243(4) | 1183(7) | 4308(3) | 52(1) |
| C(14) | 5000 | 5501(8) | 2449(5) | 47(2) |
| C(15) | 5000 | 6644(9) | 3030(5) | 50(2) |
| C(16) | 5000 | 5798(9) | 3696(6) | 49(2) |
| C(17) | 2684(4) | -726(7) | 2463(5) | 75(2) |
| C(18) | 3125(5) | 1734(9) | 5100(4) | 77(2) |
| C(19) | 5000 | 5749(11) | 1632(6) | 73(3) |
| C(20) | 5000 | 6441(13) | 4502(6) | 75(3) |
| B(2) | 5000 | 2644(11) | 4043(6) | 46(3) |
| Br(2) | 5000 | 966(1) | 1164(1) | 71(1) |
| Co(2) | 5000 | 1641(1) | 2443(1) | 41(1) |
| N(5) | 3904(3) | 963(5) | 3157(3) | 45(1) |
| N(6) | 4035(3) | 1606(5) | 3868(2) | 45(1) |
| N(7) | 5000 | 4013(6) | 2760(4) | 44(2) |
| N(8) | 5000 | 4184(7) | 3532(4) | 40(2) |

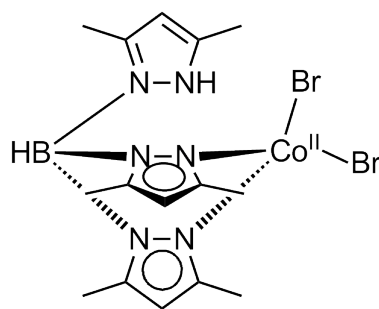
7.5.5 HB[(3,5-Me₂-pz)₂H(3,5-Me₂-pz)]CoBr₂ (5)

Crystals of (5) were collected from the crystallization mother liquid of (4) as a side-product with a light blue color distinct from the dark blue crystals of (4). (Figure 7.5)

Molar mass: 516.6 g/mol

Yield: ca. 0.21 g, 0.4 mmol (8.5 %)

IR (KBr, 4000 – 400 cm⁻¹): 3349 (vs, $\nu(N-H)$), 2923 (w, $\nu(H_2C-H)$), 2507 (m, $\nu(B-H)$), 1630 (s, $\nu(C=C)$ (Hpz^{*})), 1568 (vs, $\nu(C=C)$ (Hpz^{*})), 1542 (s, $\nu(C=C)$), 1444 (s, $\nu(C=N)$), 1415 (m, $\nu(N=N)$), 1379 (m, $\delta(CH_3)$), 1184 (s, $\delta(C-H)$), 1047



(5)

Figure 7.5.: $\text{HB}[(3,5\text{-Me}_2\text{-pz})_2\text{H}(3,5\text{-Me}_2\text{-pz})]\text{CoBr}_2$

(vs, $\nu(B - N)$), 982 (w, ring breathing), 806 (s, $\gamma(C - H)$), 652 (s), 566 (m), 465 (w, $\nu(\text{Co} - \text{N})$), 428 (w, $\nu(\text{Co} - \text{N})$) cm^{-1} .

Atomic coordinates ($\times 10^4$) and equivalent isotropic displacement parameters ($\text{\AA}^2 \times 10^3$) for complex (5)

| | x | y | z | U (eq) |
|-------|----------|---------|---------|--------|
| C(1) | 4597(6) | 2756(5) | 5934(5) | 40(2) |
| C(2) | 5065(7) | 2862(5) | 5080(5) | 46(2) |
| C(3) | 6263(6) | 2532(5) | 5295(4) | 38(2) |
| C(4) | 9461(6) | 3311(5) | 7526(5) | 39(2) |
| C(5) | 9575(7) | 4018(5) | 8213(5) | 46(2) |
| C(6) | 8567(6) | 3977(5) | 8663(5) | 41(2) |
| C(7) | 8638(7) | 488(5) | 7914(6) | 48(2) |
| C(8) | 8302(7) | -6(5) | 8689(6) | 55(2) |
| C(9) | 7194(7) | 367(5) | 8839(5) | 46(2) |
| C(10) | 3338(7) | 3021(6) | 6118(7) | 61(2) |
| C(11) | 7184(7) | 2479(7) | 4638(5) | 59(2) |
| C(12) | 10332(7) | 3053(6) | 6861(6) | 54(2) |
| C(13) | 8220(8) | 4523(6) | 9491(6) | 60(2) |
| C(14) | 9766(8) | 374(7) | 7467(8) | 72(3) |
| C(15) | 6414(9) | 99(6) | 9557(6) | 64(2) |
| N(1) | 5467(5) | 2371(4) | 6657(4) | 36(1) |
| N(2) | 6516(4) | 2227(4) | 6255(4) | 33(1) |
| N(3) | 8390(4) | 2840(4) | 7534(4) | 33(1) |
| N(4) | 7866(5) | 3258(4) | 8235(4) | 36(1) |

| | | | | |
|-------|---------|---------|---------|-------|
| N(5) | 7745(5) | 1144(4) | 7617(4) | 36(1) |
| N(6) | 6849(5) | 1071(4) | 8188(4) | 37(1) |
| Co(1) | 5212(1) | 1759(1) | 7916(1) | 38(1) |
| Br(1) | 5299(1) | 2933(1) | 9148(1) | 73(1) |
| Br(2) | 3386(1) | 829(1) | 7651(1) | 68(1) |
| B(1) | 7794(7) | 1960(5) | 6901(5) | 35(2) |

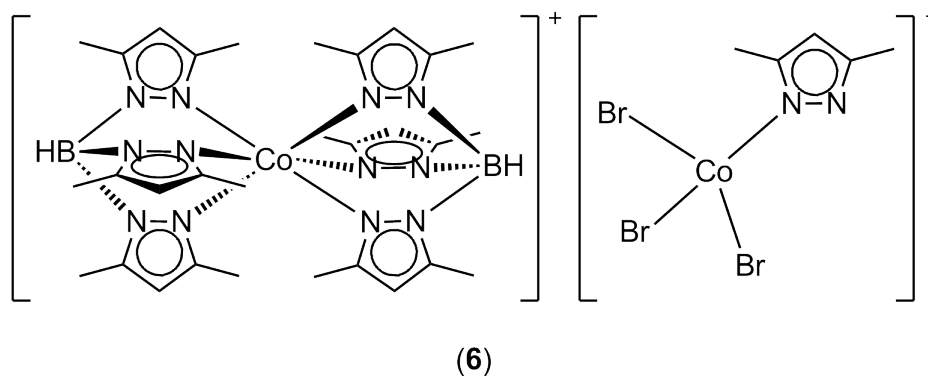


Figure 7.6.: $\{[\text{HB}(3,5\text{-Me}_2\text{-pz})_3]_2\text{Co}\}[(3,5\text{-Me}_2\text{-pz})\text{CoBr}_3]$

7.5.6 $\{[\text{HB}(3,5\text{-Me}_2\text{-pz})_3]_2\text{Co}\}[(3,5\text{-Me}_2\text{-pz})\text{CoBr}_3]$ (6)

0.44 g of crystals of (4) (1 mmol) were dissolved in 10 ml of CH_2Cl_2 , and the resulting solution was slowly evaporated in the air at room temperature. Green needle-like crystals were obtained, whose quality was sufficient for X-ray single crystal diffraction and other spectroscopic measurements. (Figure 7.6)

Molar mass: 1046.3 g/mol

Yield: 0.95 g, 0.9 mmol (90 %)

IR (KBr, 4000 – 400 cm^{-1}): 3301 (w), 3116 (m, $\nu(=C-H)$), 2926 (m, $\nu(\text{H}_2\text{C}-H)$), 2551 (m, $\nu(B-H)$), 1567 (m, $\nu(C=C)$), 1542 (s, $\nu(C=C)$), 1447 (s, $\nu(C=N)$), 1416 (s, $\nu(N=N)$), 1384 (s), 1362 (s, $\delta(\text{CH}_3)$), 1213 (s), 1190 (s, $\delta(C-H)$), 1069 (s, $\nu(B-N)$), 819 (s, $\gamma(C-H)$), 588 (w, $\nu(\text{Co}-N)$), 504 (w, $\nu(\text{Co}-N)$) cm^{-1} . **$^1\text{H NMR}$** (CDCl_3 , 300 MHz, 25 °C): 0.492 (s, C^5-CH_3 , 18H), 0.853 (s, C^3-CH_3 , 3H), 1.254 (s, C^5-CH_3 , 3H), 2.372 (s, C^3-CH_3 , 18H), 5.292 (s, C^4H , 1H), 5.607 (s, C^4H , 6H) ppm. **$^{13}\text{C NMR}$** (CDCl_3 , 75.5 MHz, 25 °C): 12.15 (C^5-CH_3), 13.74 (C^3-CH_3), 96.15 (C^3), 110.65 (C^4), 154.95 (C^5) ppm.

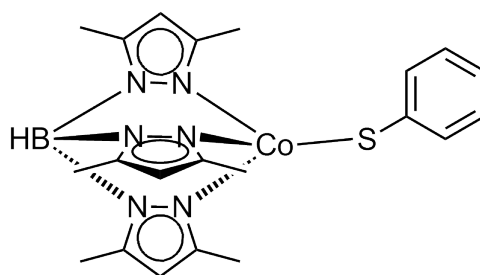
Atomic coordinates ($\times 10^4$) and equivalent isotropic displacement parameters ($\text{Å}^2 \times 10^3$) for complex (6)

| | x | y | z | U (eq) |
|------|---------|---------|---------|--------|
| C(1) | 7092(6) | 1268(2) | 5547(5) | 37(1) |
| C(2) | 7065(6) | 1318(2) | 4255(5) | 41(1) |
| C(3) | 8010(6) | 908(2) | 3796(5) | 36(1) |
| C(4) | 8168(6) | -908(2) | 6275(5) | 33(1) |
| C(5) | 7202(6) | -923(2) | 7278(5) | 39(1) |

| | | | | |
|-------|-----------|----------|-----------|--------|
| C(6) | 7144(5) | -389(2) | 7758(5) | 35(1) |
| C(7) | 12482(6) | 480(2) | 6764(5) | 34(1) |
| C(8) | 12517(6) | 754(2) | 7926(5) | 42(1) |
| C(9) | 11064(6) | 812(2) | 8274(5) | 38(1) |
| C(10) | 1184(13) | 2500 | -556(12) | 70(3) |
| C(11) | -299(11) | 2500 | -193(13) | 72(3) |
| C(12) | -243(10) | 2500 | 1117(12) | 62(3) |
| C(13) | 6313(7) | 1610(3) | 6508(6) | 58(2) |
| C(14) | 8344(7) | 811(3) | 2431(5) | 48(2) |
| C(15) | 8579(7) | -1394(2) | 5476(6) | 46(2) |
| C(16) | 6304(7) | -166(3) | 8854(5) | 51(2) |
| C(17) | 13805(6) | 308(3) | 6020(5) | 46(2) |
| C(18) | 10464(7) | 1042(3) | 9468(6) | 60(2) |
| C(19) | 1804(15) | 2500 | -1857(12) | 105(4) |
| C(20) | -1436(11) | 2500 | 2063(12) | 87(4) |
| B(1) | 8444(6) | 558(3) | 7154(5) | 29(1) |
| Br(1) | 5452(1) | 1657(1) | 39(1) | 63(1) |
| Br(2) | 4362(1) | 2500 | 3120(1) | 47(1) |
| Co(1) | 10000 | 0 | 5000 | 22(1) |
| Co(2) | 4380(1) | 2500 | 808(1) | 43(1) |
| N(1) | 8014(4) | 835(2) | 5868(4) | 30(1) |
| N(2) | 8578(4) | 614(2) | 4788(4) | 26(1) |
| N(3) | 8682(4) | -381(2) | 6147(3) | 26(1) |
| N(4) | 8034(4) | -63(2) | 7060(4) | 29(1) |
| N(5) | 11027(4) | 382(2) | 6412(4) | 27(1) |
| N(6) | 10167(4) | 591(2) | 7343(4) | 28(1) |
| N(7) | 2112(8) | 2500 | 444(8) | 56(2) |
| N(8) | 1217(8) | 2500 | 1473(8) | 57(2) |

7.5.7 HB(3,5-Me₂-pz)₃Co(SPh) (7)

Preparation of lithium benzothiolate (PhSLi): In a Schlenk flask, 0.09 ml of PhSH (0.88 mmol) was dissolved in 20 ml of THF. The solution was cooled down to -78 °C and at this temperature 0.55 ml (0.88 mmol) of 1.6 M *n*BuLi in hexane was slowly added. The mixture was stirred at -78 °C for 30 min and warmed to room temperature.



(7)

Figure 7.7.: $\text{HB}(3,5\text{-Me}_2\text{-pz})_3\text{Co}(\text{SPh})$

0.185 g (0.846 mmol) of CoBr_2 was dissolved in 30 ml of THF. To this blue solution, 0.26 g (0.774 mmol) of KTP^* was added, and the mixture was stirred at R.T. for 30 min. The freshly prepared PhSLi solution was then dropped into the reaction mixture, which turned dark green immediately. After stirring for 2 hours, all volatiles were removed under high vacuum, and the residue was extracted with CH_2Cl_2 and filtered. The filtrate was concentrated to 10 ml and kept at $-30\text{ }^\circ\text{C}$. Green needle-like crystals were isolated from the mother liquid, which were highly air-sensitive. (Figure 7.7)

Molar mass: 464.7 g/mol

Yield: 0.22 g, 0.47 mmol (62 %)

IR (KBr, $4000 - 400\text{ cm}^{-1}$): 3064 (w, $\nu(\text{C} - \text{H})$), 2960, 2924 (w, $\nu(\text{H}_2\text{C} - \text{H})$), 2542 (w, $\nu(\text{B} - \text{H})$), 1642 (m, $\nu(\text{C} = \text{C})$ Ph), 1576 (m, $\nu(\text{C} = \text{C})$ Ph), 1542 (m, $\nu(\text{C} = \text{C})$), 1474 (m, $\nu(\text{N} = \text{C})$), 1450 (m, $\nu(\text{N} = \text{N})$), 1180 (s, $\delta(\text{C} - \text{H})$), 1062 (s, $\nu(\text{B} - \text{N})$), 803 (s, $\gamma(\text{C} - \text{H})$), 738 (s, $\nu(\text{S} - \text{C})$), 691 (s, $\gamma(\text{C} - \text{H})$), 464 (w, $\nu(\text{N} - \text{Co})$) cm^{-1} .

Atomic coordinates ($\times 10^4$) and equivalent isotropic displacement parameters ($\text{Å}^2 \times 10^3$) for complex (7)

| | x | y | z | U (eq) |
|------|-----------|---------|----------|--------|
| N(1) | -9653(2) | 1260(7) | -4408(3) | 37(6) |
| N(2) | -9431(2) | 1272(7) | -3799(3) | 28(5) |
| N(3) | -10087(2) | 3992(7) | -4363(3) | 17(4) |
| N(4) | -9973(2) | 4326(7) | -3716(3) | 24(4) |
| N(5) | -10477(2) | 1208(7) | -4133(3) | 37(5) |
| N(6) | -10443(2) | 1320(7) | -3459(3) | 40(6) |
| C(1) | -8979(2) | 464(7) | -3856(3) | 58(8) |
| C(2) | -8922(2) | -48(7) | -4500(3) | 51(8) |
| C(3) | -9338(2) | 444(7) | -4842(3) | 41(6) |

| | | | | |
|-------|------------|-----------|-----------|---------|
| C(4) | -9930(2) | 6104(7) | -3641(3) | 24(6) |
| C(5) | -10016(2) | 6869(7) | -4243(3) | 47(7) |
| C(6) | -10114(2) | 5563(7) | -4689(3) | 38(6) |
| C(7) | -10829(2) | 395(7) | -3191(3) | 52(8) |
| C(8) | -11103(2) | -289(7) | -3700(3) | 48(8) |
| C(9) | -10886(2) | 214(7) | -4282(3) | 67(10) |
| C(10) | -9265(2) | 1383(7) | -1895(3) | 69(10) |
| C(11) | -8820(2) | 1941(7) | -1685(3) | 70(9) |
| C(12) | -8479(2) | 779(7) | -1483(3) | 92(12) |
| C(13) | -8582(2) | -940(7) | -1491(3) | 102(14) |
| C(14) | -9027(2) | -1498(7) | -1701(3) | 70(10) |
| C(15) | -9368(2) | -337(7) | -1904(3) | 66(9) |
| C(16) | -8708(8) | 50(20) | -3424(10) | 20(5) |
| C(17) | -9468(17) | 390(50) | -5520(20) | 106(15) |
| C(18) | -9790(5) | 7707(18) | -3188(9) | 0(3) |
| C(19) | -10200(10) | 5350(30) | -5463(13) | 44(7) |
| C(20) | -10833(15) | 110(40) | -2438(18) | 83(12) |
| C(21) | -11151(13) | 210(40) | -4808(17) | 83(11) |
| Co(1) | -7615(1) | -2609(4) | -4768(2) | 45(1) |
| S(1) | -7800(4) | -1961(12) | -5765(5) | 87(3) |
| B(1) | -7314(7) | -2970(20) | -3390(10) | 3(4) |
| N(7) | -6952(5) | -3771(16) | -3891(7) | 4(3) |
| N(8) | -7028(6) | -3897(19) | -4513(7) | 14(4) |
| N(9) | -7795(6) | -3680(20) | -3453(8) | 22(4) |
| N(10) | -8008(7) | -3750(20) | -4006(9) | 33(5) |
| N(11) | -7374(7) | -1030(20) | -3664(10) | 37(5) |
| N(12) | -7448(7) | -610(20) | -4209(9) | 26(5) |
| C(22) | -6662(7) | -4790(20) | -4727(9) | 11(4) |
| C(23) | -6335(3) | -5269(8) | -4317(3) | 33(6) |
| C(24) | -6526(3) | -4627(8) | -3738(3) | 21(5) |
| C(25) | -8470(3) | -4619(8) | -3959(3) | 14(5) |
| C(26) | -8503(3) | -5047(8) | -3303(3) | 23(5) |
| C(27) | -8080(3) | -4473(8) | -2996(3) | 35(6) |
| C(28) | -7492(3) | 1202(8) | -4218(3) | 48(7) |

| | | | | |
|-------|------------|-----------|-----------|---------|
| C(29) | -7408(3) | 1704(8) | -3578(3) | 35(6) |
| C(30) | -7326(3) | 223(8) | -3211(3) | 41(6) |
| C(31) | -8147(3) | -3591(8) | -6076(3) | 34(6) |
| C(32) | -8012(3) | -5282(8) | -6062(3) | 46(7) |
| C(33) | -8338(3) | -6532(8) | -6232(3) | 69(10) |
| C(34) | -8799(3) | -6090(8) | -6416(3) | 80(11) |
| C(35) | -8935(3) | -4399(8) | -6429(3) | 123(16) |
| C(36) | -8609(3) | -3149(8) | -6259(3) | 89(12) |
| C(37) | -6666(13) | -4990(30) | -5424(16) | 63(10) |
| C(38) | -6372(9) | -4730(30) | -2993(11) | 30(6) |
| C(39) | -8829(11) | -4650(30) | -4638(14) | 54(8) |
| C(40) | -7948(11) | -4660(30) | -2368(13) | 49(8) |
| C(41) | -7593(6) | 2167(18) | -4822(9) | 0(4) |
| C(42) | -7221(12) | 380(40) | -2599(15) | 66(9) |
| Co(2) | -9824(1) | 2368(4) | -3164(2) | 46(1) |
| S(2) | -9628(4) | 3117(11) | -2161(5) | 79(3) |
| B(2) | -10112(15) | 2190(50) | -4476(19) | 62(10) |

7.5.8 [HB(3,5-Me₂-pz)₃Co]₂(μ-pz)₂(μ-O₂) (8)

In a 100 ml Schlenk flask, 0.033 g (0.48 mmol) pyrazole was dissolved in 10 ml of THF to give a colorless solution. Then 0.3 ml (0.48 mmol) 1.6 M *n*BuLi in hexane was added and the colorless solution turned yellow quickly. The resulting solution was stirred for 20 min at R.T., and 0.16 g (0.48 mmol) of *KTp*^{*} was added into the solution of the deprotonated pyrazole, resulting in a white suspension. To a solution of 0.106 g (0.48 mmol) of *CoBr*₂ in 20 ml of THF the pre-prepared suspension was slowly added at room temperature, and the whole mixture was stirred for 12 hours, during which it gradually turned violet. After that the solvent was removed under vacuum and 40 ml of toluene was added for extraction of product. The mixture was filtered, washed with toluene, and the filtrate was again evacuated to dryness. The residue was redissolved in 10 ml of *CH*₂*Cl*₂ giving a red purple solution, which was stored at -30 °C for crystallization. After 3 days, brown crystals were isolated from the mother liquid. The single crystals for X-ray crystallography were grown through diffusion of petroleum ether vapor into a saturated solution of the product. (Figure 7.8)

Molar mass: 877.6 g/mol

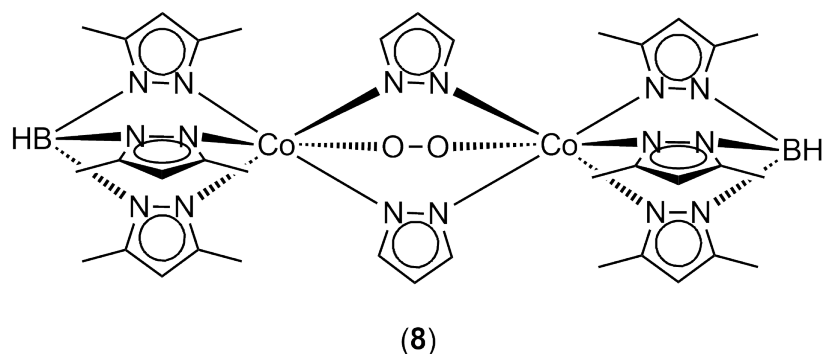


Figure 7.8.: $[\text{HB}(3,5\text{-Me}_2\text{-pz})_3\text{Co}]_2(\mu\text{-pz})_2(\mu\text{-O}_2)$

Yield: 0.11g, 0.13 mmol (52 %)

IR (KBr, 4000 – 400 cm^{-1}): 3123 (w, $\nu(\text{C} - \text{H})$), 2958 (m, $\nu(\text{C} - \text{H})$), 2827 (m, $\nu(\text{C} - \text{H})$), 2521 (m, $\nu(\text{B} - \text{H})$), 1550 (s, $\nu(\text{C} = \text{C})$), 1457 (s, $\nu(\text{C} = \text{N})$), 1421 (s, $\nu(\text{N} = \text{N})$), 1384 (s, $\delta(\text{CH}_3)$), 1215 (s, $\delta(\text{C} - \text{H})$ (pz)), 1191 (m, $\delta(\text{C} - \text{H})$ (pz^{*})), 1062 (s, $\nu(\text{B} - \text{N})$), 866 (m, $\nu(\text{O} - \text{O})$), 845 (m, $\nu(\text{O} - \text{O})$), 776 (m, $\gamma(\text{C} - \text{H})$), 747 (m, $\gamma(\text{C} - \text{H})$), 484 (w, $\nu(\text{Co} - \text{N})$) cm^{-1} . **¹H NMR** (CDCl_3 , 300 MHz, 25 °C): 1.59 (s, $\text{C}^5 - \text{CH}_3$, 12H), 1.67 (s, $\text{C}^5 - \text{CH}_3$, 6H), 2.78 (s, $\text{C}^3 - \text{CH}_3$, 6H), 2.86 (s, $\text{C}^3 - \text{CH}_3$, 12H), 6.03 (s, C^4H , 2H), 6.10 (s, C^4H , 4H), 6.67 (s, C^4H , 2H), 6.99 (s, C^3H , 4H) ppm. **MS** (EI): $m/z = 356$ ($[\text{Tp}^*\text{Co}]^+$).

Atomic coordinates ($\times 10^4$) and equivalent isotropic displacement parameters ($\text{Å}^2 \times 10^3$) for complex (8)

| | x | y | z | U (eq) |
|-------|----------|----------|---------|--------|
| Co(1) | 2065(2) | 6825(2) | 1449(1) | 36(1) |
| Co(2) | 2094(2) | 7143(2) | 3527(1) | 40(1) |
| N(1) | 2836(12) | 5356(11) | 1174(7) | 43(3) |
| N(2) | 2855(12) | 5477(10) | 311(7) | 44(3) |
| N(3) | 2895(12) | 7687(11) | 312(8) | 45(3) |
| N(4) | 2618(12) | 7580(11) | -449(8) | 47(3) |
| N(5) | 485(12) | 7093(11) | 699(7) | 43(3) |
| N(6) | 715(12) | 6780(10) | -36(7) | 41(3) |
| N(7) | 1364(11) | 8252(10) | 1675(7) | 38(3) |
| N(8) | 1343(13) | 8357(10) | 2451(7) | 47(3) |
| N(9) | 1280(12) | 5989(10) | 2530(7) | 38(3) |
| N(10) | 1322(10) | 6086(9) | 3313(6) | 30(3) |
| O(1) | 3516(11) | 6499(10) | 2170(7) | 61(3) |

| | | | | |
|-------|-----------|-----------|-----------|---------|
| O(2) | 3504(13) | 6715(12) | 2846(9) | 84(4) |
| N(11) | 2936(17) | 8181(15) | 3788(9) | 79(6) |
| N(12) | 2895(14) | 8159(12) | 4636(8) | 55(4) |
| N(13) | 497(13) | 7661(11) | 4260(7) | 46(3) |
| N(14) | 732(14) | 7882(11) | 4988(8) | 54(4) |
| N(15) | 2850(12) | 5892(11) | 4673(7) | 44(3) |
| N(16) | 2620(12) | 6205(11) | 5425(7) | 43(3) |
| C(1) | 3447(17) | 4236(15) | 1633(11) | 56(4) |
| C(2) | 3937(17) | 3713(16) | 986(12) | 61(5) |
| C(3) | 3560(15) | 4495(14) | 188(10) | 48(4) |
| C(4) | 3720(20) | 3781(15) | 2575(10) | 72(6) |
| C(5) | 3796(18) | 4398(16) | -680(11) | 63(5) |
| C(6) | -768(16) | 7353(15) | 797(10) | 51(4) |
| C(7) | -1357(17) | 7211(14) | 139(11) | 57(4) |
| C(8) | -387(17) | 6869(14) | -383(10) | 54(4) |
| C(9) | -1470(17) | 7755(18) | 1496(12) | 74(6) |
| C(10) | -430(20) | 6568(19) | -1185(11) | 83(6) |
| C(11) | 3470(20) | 8557(17) | 37(12) | 75(6) |
| C(12) | 3600(20) | 8982(17) | -865(13) | 86(7) |
| C(13) | 3091(17) | 8344(14) | -1138(11) | 55(5) |
| C(14) | 3950(30) | 8940(20) | 649(18) | 132(10) |
| C(15) | 2940(20) | 8474(17) | -2088(10) | 82(6) |
| C(16) | 799(14) | 9269(13) | 1080(10) | 45(4) |
| C(17) | 397(16) | 10087(14) | 1466(10) | 53(4) |
| C(18) | 776(19) | 9488(17) | 2329(12) | 73(5) |
| C(19) | 649(17) | 5188(13) | 2642(11) | 54(4) |
| C(20) | 295(15) | 4765(13) | 3509(10) | 50(4) |
| C(21) | 775(15) | 5331(13) | 3910(9) | 45(4) |
| C(22) | 3550(30) | 8970(20) | 3367(17) | 107(8) |
| C(23) | 4120(30) | 9260(20) | 3958(16) | 106(8) |
| C(24) | 3610(20) | 8800(18) | 4736(11) | 73(6) |
| C(25) | 4080(40) | 9170(30) | 2390(20) | 189(15) |
| C(26) | 3840(20) | 8892(16) | 5573(11) | 74(6) |
| C(27) | -737(17) | 7974(14) | 4181(11) | 56(4) |

| | | | | |
|-------|-----------|----------|----------|-------|
| C(28) | -1330(20) | 8383(15) | 4831(12) | 71(6) |
| C(29) | -335(19) | 8269(15) | 5357(10) | 58(5) |
| C(30) | -1437(19) | 7910(18) | 3461(11) | 77(6) |
| C(31) | -460(20) | 8644(19) | 6128(12) | 90(7) |
| C(32) | 3430(16) | 4788(16) | 4940(11) | 57(5) |
| C(33) | 3610(18) | 4347(16) | 5851(11) | 65(5) |
| C(34) | 3127(16) | 5237(14) | 6121(10) | 49(4) |
| C(35) | 3880(20) | 4138(17) | 4347(12) | 84(7) |
| C(36) | 3062(19) | 5266(18) | 7046(10) | 72(6) |
| B(1) | 2080(18) | 6576(15) | -374(11) | 43(4) |
| B(2) | 2120(20) | 7444(17) | 5338(11) | 50(5) |

7.5.9 (dppf)₂Cu₂(μ -CA) (9)

40 ml of EtOH was bubbled with Ar for 15 min to expel any trace of oxygen gas. Into this solvent, 35 mg of chloranilic acid (0.16 mmol) was added and dissolved at R.T. 0.06 ml of triethylamine (0.4 mmol) was then added to the solution. The former red solution turned purple immediately. 0.27 g (*dppf*)Cu(CH₃CN)₂(BF₄) (0.338 mmol) was added to the purple solution, and the mixture was stirred for 14 hours at room temperature. Reddish-brown precipitate separated from the solution, leaving an almost colorless mother liquid. The precipitated crystals were filtered off and washed three times with ethanol, and dried in a vacuum desiccator. Single crystals were grown by layering with petroleum ether in a solution of dichloromethane. After 24 hours, red crystals suitable for X-ray diffraction were isolated. (Figure 7.9)

Molar mass: 1441.7 g/mol

Yield: 0.21 g, 0.15 mmol (91%)

IR (KBr, 4000 – 400 cm⁻¹): 3070, 3048 (m, ν (= C – H)), 1573 (m, ν (C = C)), 1508 (vs, ν (C – O)), 1480, 1435 (s, ν (C = C), Ph), 1365 (m, ν (C – C), CA), 1165 (m, δ (C – H)), 1096, 1029 (m, δ (C – H)), 998 (w, ring breathing), 840 (s, ν (C – Cl)), 747 (s, γ (C – H)), 693 (s, γ (C – H)), 486 (s, ν (C – P)) cm⁻¹. **¹H NMR** (CDCl₃, 500 MHz, 25 °C): 4.22 (s, C₅H₄–, 8H), 4.24 (s, C₅H₄–, 8H), 7.19 - 7.52 (m, C₆H₅–, 40H) ppm. **¹³C NMR** (CDCl₃, 125 MHz, 25 °C): 73.98 (C₅H₄–, C³), 76.35 (C₅H₄–, C²), 106.97 (C – Cl), 130.88 (*p*-C, Ph), 132.20 (*m*-C, Ph), 136.14 (*i*-C, Ph), 136.38 (*o*-C, Ph), 175.17 (C – O) ppm.

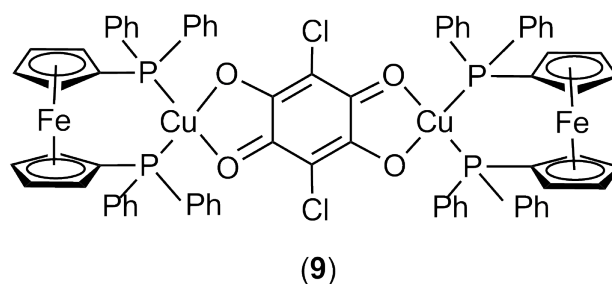


Figure 7.9.: (dppf)₂Cu₂(CA)

Atomic coordinates ($\times 10^4$) and equivalent isotropic displacement parameters ($\text{\AA}^2 \times 10^3$) for complex (9)

| | x | y | z | U (eq) |
|--------|------------|-----------|-----------|----------|
| Cu(1) | 0.2164(1) | 0.7624(1) | 0.6715(1) | 0.018(1) |
| Fe(1) | -0.1159(1) | 1.0448(1) | 0.7591(1) | 0.014(1) |
| Cl(1) | 0.4151(1) | 0.6309(1) | 0.3123(1) | 0.022(1) |
| Cl(2A) | -0.3655(2) | 1.4751(2) | 0.9262(2) | 0.048(1) |
| Cl(2B) | -0.3541(2) | 1.4481(2) | 0.9671(2) | 0.042(1) |
| P(1) | 0.2224(1) | 0.9372(1) | 0.7175(1) | 0.015(1) |
| P(2) | 0.0141(1) | 0.7375(1) | 0.7351(1) | 0.015(1) |
| O(1) | 0.2985(2) | 0.7120(2) | 0.5235(2) | 0.018(1) |
| O(2) | 0.3729(2) | 0.6043(2) | 0.6784(2) | 0.020(1) |
| C(1) | 0.3927(2) | 0.6134(2) | 0.5073(2) | 0.016(1) |
| C(2) | 0.4355(2) | 0.5514(2) | 0.5974(2) | 0.016(1) |
| C(3) | 0.4594(3) | 0.5588(2) | 0.4154(2) | 0.017(1) |
| C(4) | 0.0608(3) | 1.0447(2) | 0.7752(2) | 0.016(1) |
| C(5) | 0.0011(3) | 1.1571(2) | 0.7317(2) | 0.019(1) |
| C(6) | -0.1263(3) | 1.2144(2) | 0.7981(2) | 0.020(1) |
| C(7) | -0.1457(3) | 1.1376(2) | 0.8829(2) | 0.019(1) |
| C(8) | -0.0316(3) | 1.0324(2) | 0.8696(2) | 0.017(1) |
| C(9) | -0.1091(3) | 0.8789(2) | 0.7189(2) | 0.015(1) |
| C(10) | -0.0838(3) | 0.9567(2) | 0.6337(2) | 0.018(1) |
| C(11) | -0.1969(3) | 1.0628(3) | 0.6451(2) | 0.022(1) |
| C(12) | -0.2920(3) | 1.0510(2) | 0.7368(2) | 0.021(1) |
| C(13) | -0.2394(3) | 0.9385(2) | 0.7828(2) | 0.018(1) |
| C(14) | 0.2960(3) | 1.0376(2) | 0.6243(2) | 0.018(1) |

| | | | | |
|-------|------------|-----------|-----------|----------|
| C(15) | 0.3093(3) | 1.0231(3) | 0.5259(2) | 0.021(1) |
| C(16) | 0.3587(3) | 1.1010(3) | 0.4532(2) | 0.025(1) |
| C(17) | 0.3967(3) | 1.1927(3) | 0.4785(2) | 0.026(1) |
| C(18) | 0.3856(3) | 1.2072(3) | 0.5755(3) | 0.029(1) |
| C(19) | 0.3346(3) | 1.1309(3) | 0.6488(2) | 0.025(1) |
| C(20) | 0.3090(3) | 0.9174(3) | 0.8101(2) | 0.021(1) |
| C(21) | 0.2801(3) | 1.0094(3) | 0.8773(2) | 0.028(1) |
| C(22) | 0.3538(4) | 0.9918(4) | 0.9422(3) | 0.039(1) |
| C(23) | 0.4545(4) | 0.8837(5) | 0.9429(3) | 0.045(1) |
| C(24) | 0.4827(3) | 0.7922(4) | 0.8779(3) | 0.039(1) |
| C(25) | 0.4099(3) | 0.8084(3) | 0.8117(2) | 0.028(1) |
| C(26) | -0.0278(3) | 0.6240(2) | 0.6834(2) | 0.017(1) |
| C(27) | -0.1552(3) | 0.6410(3) | 0.6776(2) | 0.023(1) |
| C(28) | -0.1829(3) | 0.5483(3) | 0.6417(2) | 0.027(1) |
| C(29) | -0.0830(3) | 0.4400(3) | 0.6105(2) | 0.027(1) |
| C(30) | 0.0444(3) | 0.4232(3) | 0.6142(2) | 0.025(1) |
| C(31) | 0.0723(3) | 0.5148(2) | 0.6508(2) | 0.022(1) |
| C(32) | -0.0355(3) | 0.7031(2) | 0.8678(2) | 0.021(1) |
| C(33) | 0.0477(3) | 0.7033(3) | 0.9227(3) | 0.028(1) |
| C(34) | 0.0154(5) | 0.6764(3) | 1.0231(3) | 0.041(1) |
| C(35) | -0.1018(5) | 0.6492(3) | 1.0703(3) | 0.042(1) |
| C(36) | -0.1861(4) | 0.6480(3) | 1.0170(3) | 0.038(1) |
| C(37) | -0.1524(3) | 0.6736(3) | 0.9164(2) | 0.027(1) |
| C(99) | -0.4771(8) | 1.5176(8) | 1.0720(6) | 0.045(2) |

Bibliography

- [1] ALVARADO, Y., BOUTRY, O., GUTIERREZ, E., MONGE, A., NICASIO, M. C., POVEDA, M. L., PEREZ, P. J., RUIZ, C., BIANCHINI, C., AND CARMONA, E. *Chem. Eur. J.* **3**, 6 (1997), 860–873.
- [2] ALVARADO, Y., BUSOLO, M., AND LAPEZ-LINARES, F. *J. Mol. Catal. A* **142**, 2 (1999), 163 – 167.
- [3] ANDERSEN, E. K. *Acta Cryst.* **22** (1967), 196.
- [4] ANDERSEN, E. K. *Acta Cryst.* **22** (1967), 191.
- [5] AUBURN, P. R., DODSWORTH, E. S., HAGA, M., LIU, W., NEVIN, W. A., AND LEVER, A. B. P. *Inorg. Chem.* **30**, 18 (1991), 3502–3512.
- [6] BARRACLOUGH, C. G., LAWRENCE, G. A., AND LAY, P. A. *Inorg. Chem.* **17**, 12 (1978), 3317–3322.
- [7] BERTOLACINI, R. J., AND BARNEY, J. E. *Anal. Chem.* **30**, 2 (1958), 202–205.
- [8] BLOSCH, L. L., ABOUD, K., AND BONCELLA, J. M. *J. Am. Chem. Soc.* **113**, 18 (1991), 7066–7068.
- [9] BLOSCH, L. L., GAMBLE, A. S., ABOUD, K., AND BONCELLA, J. M. *Organometallics* **11**, 7 (1992), 2342–2344.
- [10] BRAUDE, E. A. *J. Chem. Soc.* (1945), 490.
- [11] BRAUNSTEIN, P., BUBRIN, D., AND SARKAR, B. *Inorg. Chem.* **48**, 6 (2009), 2534–2540. PMID: 19226148.
- [12] BRUCE, M. I., AND OSTAZEWSKI, A. P. P. *J. Chem. Soc., Dalton Trans.* (1973), 2433–2436.
- [13] BRUIJNINCX, P. C. A., VICIANO-CHUMILLAS, M., LUTZ, M., SPEK, A. L., REEDIJK, J., VAN KOTEN, G., AND GEBBINK, R. J. M. K. *Chem. Eur. J.* **14**, 18 (2008), 5567–5576.
- [14] CALVO, M. A., LANFREDI, A. M. M., ORO, L. A., PINILLOS, M. T., TEJEL, C., TIRIPICCHIO, A., AND UGOZZOLI, F. *Inorg. Chem.* **32**, 7 (1993), 1147–1152.
- [15] CARONERA, C., DEI, A., LATARD, J.-F., SANGREGORIO, C., AND SORACE, L. *Angew. Chem., Int. Ed.* **43**, 24 (2004), 3136–3138.
- [16] CHAUDHURI, P., AND ODER, K. *J. Chem. Soc., Dalton Trans.* (1990), 1597.
- [17] CHERNYAEV, I. I. *Ann. Inst. Platine USSR* **246**, 4 (1926), 261.

-
- [18] CHURCHILL, M. R., DEBOER, B. G., ROTELLA, F. J., ABU SALAH, O. M., AND BRUCE, M. I. *Inorg. Chem.* 14, 9 (1975), 2051–2056.
- [19] CHURCHILL, M. R., GOLD, K., AND MAW, C. E. *Inorg. Chem.* 9, 7 (1970), 1597–1604.
- [20] COE, B. J., AND GLENWRIGHT, S. J. *Coord. Chem. Rev.* 203, 1 (2000), 5 – 80.
- [21] COTTON, F. A., MURILLO, C. A., VILLAGRAN, D., AND YU, R. *J. Am. Chem. Soc.* 128, 10 (2006), 3281–3290.
- [22] CREUTZ, C., AND TAUBE, H. *J. Am. Chem. Soc.* 95, 4 (1973), 1086–1094.
- [23] CURNOW, O. J., AND NICHOLSON, B. K. *J. Organomet. Chem.* 267, 3 (1984), 257 – 263.
- [24] CURNOW, O. J., NICHOLSON, B. K., AND SEVERINSEN, M. J. *J. Organomet. Chem.* 388, 3 (1990), 379 – 390.
- [25] CURTIS, M. D., SHIU, K. B., AND BUTLER, W. M. *Organometallics* 2 (1983), 1475.
- [26] CURTIS, M. D., SHIU, K. B., AND BUTLER, W. M. *J. Am. Chem. Soc.* 108 (1986), 1550.
- [27] DA SILVA, R. S., GORELSKY, S. I., DODSWORTH, E. S., TFOUNI, E., AND LEVER, A. B. P. *J. Chem. Soc., Dalton Trans.* (2000), 4078 – 4088.
- [28] DE ALWIS, D. C. L., AND SCHULTZ, F. A. *Inorg. Chem.* 42, 11 (2003), 3616–3622. PMID: 12767201.
- [29] DEL, A., GATTESCHI, D., PARDI, L., AND RUSSO, U. *Inorg. Chem.* 30, 12 (1991), 2589–2594.
- [30] DEL, A., GATTESCHI, D., SANGREGORIO, C., AND SORACE, L. *Acc. Chem. Res.* 37, 11 (2004), 827–835. PMID: 15612672.
- [31] DIAZ-REQUEJO, M. M., BELDERRAIN, T. R., NICASIO, M. C., TROFIMENKO, S., AND PEREZ, P. J. *J. Am. Chem. Soc.* 125, 40 (2003), 12078–12079. PMID: 14518978.
- [32] DIAZ-REQUEJO, M. M., CABALLERO, A., BELDERRAIN, T. R., NICASIO, M. C., TROFIMENKO, S., AND PEREZ, P. J. *J. Am. Chem. Soc.* 124, 6 (2002), 978–983. PMID: 11829605.
- [33] DIEZ, J., GAMASA, M. P., GIMENO, J., AGUIRRE, A., GARCIA-GRANDA, S., HOLUBOVA, J., AND FALVELLO, L. R. *Organometallics* 18, 4 (1999), 662–669.
- [34] FABRIZI DE BIANI, F., JAEKLE, F., SPIEGLER, M., WAGNER, M., AND ZANELLO, P. *Inorg. Chem.* 36, 10 (1997), 2103–2111.
- [35] FOLEY, T. J., HARRISON, B. S., KNEFELY, A. S., ABBOUD, K. A., REYNOLDS, J. R., SCHANZE, K. S., AND BONCELLA, J. M. *Inorg. Chem.* 42, 16 (2003), 5023–5032.

-
- [36] FOLGADO, J. V., ESCRIVA, E., BELTRAN-PORTER, A., AND BELTRAN-PORTER, D. *Trans. Met. Chem.* 12 (1987), 306–310. 10.1007/BF01024019.
- [37] FOLGADO, J. V., IBANEZ, R., CORONADO, E., BELTRAN, D., SAVARIAULT, J. M., AND GALY, J. *Inorg. Chem.* 27, 1 (1988), 19–26.
- [38] FONER, S. N., AND HUDSON, R. L. *J. Chem. Phys.* 36, 10 (1962), 2676–2680.
- [39] FUJIHARA, T., SCHÄNHERR, T., AND KAIZAKI, S. *Inorg. Chim. Acta* 249, 2 (1996), 135 – 141.
- [40] FUJII, C., MITSUMI, M., KODERA, M., MOTODA, K.-I., OHBA, M., MATSUMOTO, N., AND OKAWA, H. *Polyhedron* 13 (1994), 933 – 938.
- [41] GALLERT, S., WEYHERMUELLER, T., WIEGHARDT, K., AND CHAUDHURI, P. *Inorg. Chim. Acta* 274, 1 (1998), 111 – 114.
- [42] GEMEL, C., TRIMMEL, G., SLUGOVIC, C., KREMEL, S., MEREITER, K., SCHMID, R., AND KIRCHNER, K. *Organometallics* 15, 19 (1996), 3998–4004.
- [43] GENTILE, P., AND SHANKOFF, T. *Journal of Inorganic and Nuclear Chemistry* 28, 5 (1966), 1283 – 1289.
- [44] GHOSH, C. K., AND GRAHAM, W. A. G. *J. Am. Chem. Soc.* 109, 15 (1987), 4726–4727.
- [45] GUO, D., AND MCCUSKER, J. K. *Inorg. Chem.* 46, 8 (2007), 3257–3274.
- [46] GUPTA, P., DAS, A., BASULI, F., CASTINEIRAS, A., SHELDRIK, W. S., MAYER-FIGGE, H., AND BHATTACHARYA, S. *Inorg. Chem.* 44, 6 (2005), 2081–2088.
- [47] HAGA, M., DODSWORTH, E. S., AND LEVER, A. B. P. *Inorg. Chem.* 25, 4 (1986), 447–453.
- [48] HAYASHI, A., NAKAJIMA, K., AND NONOYAMA, M. *Polyhedron* 16, 23 (1997), 4087 – 4095.
- [49] HEINZE, K., HUTTNER, G., ZSOLNAI, L., JACOBI, A., AND SCHOBER, P. *Chem. Eur. J.* 3, 5 (1997), 732–743.
- [50] HIKICHI, S., YOSHIZAWA, M., SASAKURA, Y., KOMATSUZAKI, H., MORO-OKA, Y., AND AKITA, M. *Chem. Eur. J.* 7, 23 (2001), 5011–5028.
- [51] [HTTP://WWW.CCDC.CAM.AC.UK/PRODUCTS/MERCURY/](http://www.ccdc.cam.ac.uk/products/mercury/).
- [52] ILKHECHI, A. H., GUO, S., BOLTE, M., AND WAGNER, M. *Dalton Trans.* (2003), 2303 – 2307.
- [53] JACOBSON, R. R., TYEKLAR, Z., FAROOQ, A., KARLIN, K. D., LIU, S., AND ZUBIETA, J. *J. Am. Chem. Soc.* 110, 11 (1988), 3690–3692.

-
- [54] JAEKLE, F., POLBORN, K., AND WAGNER, M. *Chem. Ber.* 129, 6 (1996), 603–606.
- [55] JANIAK, C. *Coord. Chem. Rev.* 163, 0 (1997), 107.
- [56] JENKINS, D. M., AND PETERS, J. C. *J. Am. Chem. Soc.* 127, 19 (2005), 7148–7165.
PMID: 15884957.
- [57] JONES, R. D., SUMMERVILLE, D. A., AND BASOLO, F. *Chem. Rev.* 79, 2 (1979), 139–179.
- [58] KATAYAMA, H., YAMAMURA, K., MIYAKI, Y., AND OZAWA, F. *Organometallics* 16, 20 (1997), 4497–4500.
- [59] KAUFFMAN, G. B. *J. Chem. Educ.* 54, 2 (1977), 86.
- [60] KAWAHARA, M., KABIR, M. K., YAMADA, K., ADACHI, K., KUMAGAI, H., NARUMI, Y., KINDO, K., KITAGAWA, S., AND KAWATA, S. *Inorg. Chem.* 43, 1 (2004), 92–100.
PMID: 14704057.
- [61] KITAGAWA, S., AND KAWATA, S. *Coord. Chem. Rev.* 224 (2002), 11 – 34.
- [62] KITAJIMA, N., KODA, T., HASHIMOTO, S., KITAGAWA, T., AND MOROOKA, Y. *J. Am. Chem. Soc.* 113, 15 (1991), 5664–5671.
- [63] KITAJIMA, N., AND TOLMAN, W. B. *Prog. Inorg. Chem.* 43 (1995), 419.
- [64] KUBAS, G. J. *Inorg. Synth.* 119 (1979), 90.
- [65] KUNZ, K., BOLTE, M., LERNER, H.-W., AND WAGNER, M. *Organometallics* 28, 10 (2009), 3079–3087.
- [66] LI, D., RUSCHMAN, C., PARKIN, S., CLÄ©RAC, R., AND HOLMS, S. M. *Chem Commun* (2006), 4036–4038.
- [67] LIDE, D. R. *Handbook of Chemistry and Physics*, 87 ed. Boca Raton, FL: CRC Press, 1998.
- [68] LLORET, F., JULVE, M., FAUS, J., SOLANS, X., JOURNAUX, Y., AND MORGENSTERN-BADARAU, I. *Inorg. Chem.* 29, 12 (1990), 2232–2237.
- [69] LONG, D. P., AND BIANCONI, P. A. *J. Am. Chem. Soc.* 118, 49 (1996), 12453–12454.
- [70] LUO, T.-T., LIU, Y.-H., TSAI, H.-L., SU, C.-C., UENG, C.-H., AND LU, K.-L. *Eur. J. Inorg. Chem.* 2004, 21 (2004), 4253–4258.
- [71] MARSH, R. E., AND SCHAEFER, W. P. *Acta Crystallographica Section B* 24, 2 (Feb 1968), 246–251.
- [72] MASUI, H., LEVER, A. B. P., AND AUBURN, P. R. *Inorg. Chem.* 30, 10 (1991), 2402–2410.

-
- [73] McNALLY, J. P., S., L., AND COOPER, N. J. *Experimental Organometallic Chemistry*. American Chemical Society: Washington, DC, 1987.
- [74] MEALLI, C., ARCUS, C. S., WILKINSON, J. L., MARKS, T. J., AND IBERS, J. A. *J. Am. Chem. Soc.* 98, 3 (1976), 711–718.
- [75] MILLER, J. S., AND MIN, K. S. *Angew. Chem., Int. Ed.* 48, 2 (2009), 262–272.
- [76] MIN, K. S., DiPASQUALE, A., RHEINGOLD, A. L., AND MILLER, J. S. *Inorg. Chem.* 46, 4 (2007), 1048–1050.
- [77] MIN, K. S., DiPASQUALE, A. G., GOLEN, J. A., RHEINGOLD, A. L., AND MILLER, J. S. *J. Am. Chem. Soc.* 129, 8 (2007), 2360–2368. PMID: 17269771.
- [78] MIN, K. S., RHEINGOLD, A. L., DiPASQUALE, A., AND MILLER, J. S. *Inorg. Chem.* 45, 16 (2006), 6135–6137. PMID: 16878921.
- [79] MURTUZA, S., CASAGRANDE, O. L., AND JORDAN, R. F. *Organometallics* 21, 9 (2002), 1882–1890.
- [80] MYERS, W. K., DUESLER, E. N., AND TIERNEY, D. L. *Inorg. Chem.* 47, 15 (2008), 6701–6710. PMID: 18605690.
- [81] NAKAZAWA, H., IKAI, S., IMAOKA, K., KAI, Y., AND YANO, T. *J. Mol. Catal. A* 132, 1 (1998), 33 – 41.
- [82] PAIM, L. A., BATISTA, A. A., DIAS, F. M., GOLFETO, C. C., ELLENA, J., SIEBALD, H. G. L., AND ARDISSON, J. D. *Trans. Met. Chem.* 34 (2009), 949.
- [83] PARETZKI, A., DAS, H. S., WEISSER, F., SCHERER, T., BUBRIN, D., FIEDLER, J., NYCZ, J. E., AND SARKAR, B. *Eur. J. Inorg. Chem.* 2011, 15 (2011), 2413–2421.
- [84] PATNAIK, P. *Handbook of Inorganic Chemical Compounds*. McGraw-Hill Professional, 2003.
- [85] PETTINARY, C. *Scorpionates Two: Chelating Borate Ligands*. College Press, London, 2008.
- [86] PIERPONT, C. G., FRANCESCONI, L. C., AND HENDRICKSON, D. N. *Inorg. Chem.* 16, 9 (1977), 2367–2376.
- [87] REYNOLDS, S. J., SMITH, C. E., JONES, C. J., AND McCLEVERTY, J. A. *Inorg. Synth.* 23 (1985), 4.
- [88] RHEINGOLD, A. L., OSTRANDER, R. L., HAGGERTY, B. S., AND TROFIMENKO, S. *Inorg. Chem.* 33, 17 (1994), 3666–3676.
- [89] ROBIN, M. B., AND DAY, P. Mixed valence chemistry-a survey and classification. vol. 10 of *Advances in Inorganic Chemistry and Radiochemistry*. Academic Press, 1968, pp. 247 – 422.

-
- [90] ROUNDHILL, S. G. N., ROUNDHILL, D. M., BLOOMQUIST, D. R., LANDEE, C., WILLETT, R. D., DOOLEY, D. M., AND GRAY, H. B. *Inorg. Chem.* 18, 3 (1979), 831–835.
- [91] ROY, S., SARKAR, B., BUBRIN, D., NIEMEYER, M., ZALIS, S., LAHIRI, G. K., AND KAIM, W. *J. Am. Chem. Soc.* 130, 46 (2008), 15230–15231. PMID: 18954055.
- [92] ROY, S., SARKAR, B., DUBOC, C., FIEDLER, J., SARPER, O., LISSNER, F., MOBIN, S., LAHIRI, G., AND KAIM, W. *Chem. Eur. J.* 15, 28 (2009), 6932–6939.
- [93] ROY, S., SIEGER, M., SARKAR, B., SCHWEDERSKI, B., LISSNER, F., SCHLEID, T., FIEDLER, J., AND KAIM, W. *Angew. Chem., Int. Ed.* 47, 33 (2008), 6192–6194.
- [94] RUGGIERO, C. E., CARRIER, S. M., ANTHOLINE, W. E., WHITTAKER, J. W., CRAMER, C. J., AND TOLMAN, W. B. *J. Am. Chem. Soc.* 115, 24 (1993), 11285–11298.
- [95] SANFORD, M. S., HENLING, L. M., AND GRUBBS, R. H. *Organometallics* 17, 24 (1998), 5384–5389.
- [96] SCHAEFER, W. P. *Inorg. Chem.* 7, 4 (1968), 725–731.
- [97] SHELDRIK, G. M. *SHELXL97, Program for the Crystal Structure Refinement*. University of Goettingen, Germany, 1997.
- [98] SLUGOVIC, C., SCHMID, R., AND KIRCHNER, K. *Coord. Chem. Rev.* 185 - 186, 0 (1999), 109 – 126.
- [99] SLUGOVIC, C., WIEDE, P., MEREITER, K., SCHMID, R., AND KIRCHNER, K. *Organometallics* 16, 13 (1997), 2768–2769.
- [100] SUN, Y.-J., ZHANG, L. Z., CHENG, P., LIN, H.-K., YAN, S.-P., LIAO, D.-Z., JIANG, Z.-H., AND SHEN, P.-W. *J. Mol. Catal. A* 208 (2004), 83–90.
- [101] TAO, J., MARUYAMA, H., AND SATO, O. *J. Am. Chem. Soc.* 128, 6 (2006), 1790–1791. PMID: 16464068.
- [102] THOMPSON, J. S., MARKS, T. J., AND IBERS, J. A. *J. Am. Chem. Soc.* 101, 15 (1979), 4180–4192.
- [103] THOMPSON, J. S., SORRELL, T., MARKS, T. J., AND IBERS, J. A. *J. Am. Chem. Soc.* 101, 15 (1979), 4193–4200.
- [104] TINTI, F., VERDAGUER, M., KAHN, O., AND SAVARIAULT, J. M. *Inorg. Chem.* 26, 15 (1987), 2380–2384.
- [105] TOLMAN, C. A. *J. Am. Chem. Soc.* 92 (10) (1970), 2956.
- [106] TOMSON, N. C., CRIMMIN, M. R., PETRENKO, T., ROSEBRUGH, L. E., SPROULES, S., BOYD, W. C., BERGMAN, R. G., DEBEER, S., TOSTE, F. D., AND WIEGHARDT, K. *J. Am. Chem. Soc.* 133, 46 (2011), 18785–18801.

-
- [107] TROFIMENKO, S. *J. Am. Chem. Soc.* **89**, 13 (1967), 3170–3177.
- [108] TROFIMENKO, S. *Chem. Rev.* **93**, 3 (1993), 943–980.
- [109] TROFIMENKO, S., CALABRESE, J. C., DOMAILLE, P. J., AND THOMPSON, J. S. *Inorg. Chem.* **28**, 6 (1989), 1091–1101.
- [110] TROFIMENKO, S., CALABRESE, J. C., AND THOMPSON, J. S. *Inorg. Chem.* **26**, 10 (1987), 1507–1514.
- [111] TROMMSDORF, H. P. *J. Chem. Phys.* **56** (1972), 5358.
- [112] TROST, B. M., DYKER, G., AND KULAWIEC, R. J. *J. Am. Chem. Soc.* **112**, 21 (1990), 7809–7811.
- [113] TROST, B. M., AND KULAWIEC, R. J. *J. Am. Chem. Soc.* **114**, 14 (1992), 5579–5584.
- [114] TROST, B. M., MARTINEZ, J. A., KULAWIEC, R. J., AND INDOLESE, A. F. *J. Am. Chem. Soc.* **115**, 22 (1993), 10402–10403.
- [115] TSIAMIS, C. *Inorg. Chim. Acta* **198 - 200**, 0 (1992), 651 – 661.
- [116] VAIRA, M. D., AND MANI, F. *Inorg. Chim. Acta* **70**, 0 (1983), 99 – 105.
- [117] VAUGHAN, W. M., ABBOUD, K. A., AND BONCELLA, J. M. *Organometallics* **14**, 4 (1995), 1567–1577.
- [118] WARD, M. D. *Inorg. Chem.* **35**, 6 (1996), 1712–1714.
- [119] YE, S., SARKAR, B., LISSNER, F., SCHLEID, T., VAN SLAGEREN, J., FIEDLER, J., AND KAIM, W. *Angew. Chem., Int. Ed.* **44**, 14 (2005), 2103–2106.
- [120] YOSHINO, A., MATSUDAIRA, H., ASATO, E., KOIKAWA, M., SHIGA, T., MASAOKI, O., AND OKAWAC, H. *Chem. Commun.* (2002), 1258.

Lebenslauf

Persönliche Angaben

Name, Vorname **Zhang, Baoxin**
Adresse Bismarckstr. 70, App. 52
 64293 Darmstadt
Geburtsdatum, -ort 01.12.1982 Jinan
Nationalität chinesisch
Familienstand verheiratet seit 30. Oktober 2009

Promotion

Seit 08/2008 **Doktorarbeit (Voraussichtlicher Abschluss als Dr. rer. nat. im 04/2013)**
 Technische Universität Darmstadt, Deutschland
 Schwerpunkt: Herstellung und Charakterisierung neuartiger
 Übergangsmetallkomplexe

Studium

10/2005 - 07/2007 **Master of Science im Studiengang „Advanced Materials“**
 Universität Ulm, Deutschland
 Schwerpunkt: Nanomaterialien
09/2001 - 07/2005 **Bachelor of Science im Fachgebiet „Chemie“**
 Shandong University, VR China

Baoxin Zhang, Darmstadt, 11.03.2013